NTNU – Trondheim
Norwegian University of
Science and Technology

Fatigue Loads on Large Diameter Monopile Foundations of Offshore Wind Turbines

Tine Louise Trøen

Marine Technology
Submission date: June 2014
Supervisor: Sverre Steen, IMT

Norwegian University of Science and Technology
Department of Marine Technology

NTNU – Trondheim
Norwegian University of
Science and Technology

Fatigue Loads on Large Diameter Monopile Foundations of Offshore Wind Turbines in Shallow Water

Tine Louise Trøen

June 2014

MASTER THESIS
Department of Marine Technology
Norwegian University of Science and Technology

Supervisor 1: Professor II Jørgen Ranum Krokstad

NTNU Trondheim
Norges teknisk-naturvitenskapelige universitet
Institutt for marin teknikk

MASTER THESIS

for

Stud. tech. Tine Louise Trøen

Fatigue Loads on Large Diameter Monopile Foundations of Offshore Wind Turbines in Shallow Waters

Utmattingslaster på stordiameter monopelfundamenter for offshore vindturbiner på grunt vann

The background for this project is related to the development of the Doggerbank offshore wind park in the British part of the North Sea. The project is in the early design phase and different kinds of monopile foundations are being considered. Among the main issues in the design of offshore wind turbines are fatigue loads on the substructure. As the size of wind turbines for offshore use is increasing on a general basis, the structure is subjected to larger fatigue loads. This results in a demand for more accurate load prediction. The misalignment of wind and wave forces also results in a decrease in damping effects from the turbine, which may be critical for the design of the foundation of offshore wind turbines. Additionally, the effects of springing on fatigue and the lifetime of large diameter foundations have not been well documented, and may have a significant contribution to the fatigue loads. Relevant standards often only require evaluation of the worst load cases in terms of misalignment of wind and waves. This may result in overestimation of the fatigue life. For large diameter foundations this will have a significant impact on the installation and building costs of the foundation and accurate prediction of fatigue loads thus become more important. In light of these conditions the master thesis will focus on the following points:

1. Review of load cases relevant for the fatigue limit state of offshore wind turbine foundations recommended in relevant standards and design of foundations.
2. Assessment of the effect of variable misalignment of wind and wave loads on the fatigue life of foundations for offshore wind turbines, and investigation of the sensitivity of the fatigue life due to this misalignment.
3. Investigate aerodynamic damping effects relevant for fatigue life assessments.
4. Investigation and numerical prediction of the sensitivity of fatigue life to second order loads by comparison of results obtained from finite element software code

The above points will be applied to a mass dominated large diameter suction bucket foundation, and examplified through coupled finite element analysis of the structure. The study will require aero-elastic damping to include correct damping level for the structure.

The work scope may prove to be larger than initially anticipated. Subject to approval from the supervisors, topics may be deleted from the list above or reduced in extent.

In the thesis the candidate shall present his personal contribution to the resolution of problems within the scope of the thesis work

Theories and conclusions should be based on mathematical derivations and/or logic reasoning identifying the various steps in the deduction.

The candidate should utilise the existing possibilities for obtaining relevant literature.

Thesis format
The thesis should be organised in a rational manner to give a clear exposition of results, assessments, and conclusions. The text should be brief and to the point, with a clear language. Telegraphic language should be avoided.

The thesis shall contain the following elements: A text defining the scope, preface, list of contents, summary, main body of thesis, conclusions with recommendations for further work, list of symbols and acronyms, references and (optional) appendices. All figures, tables and equations shall be numerated.

The supervisors may require that the candidate, in an early stage of the work, presents a written plan for the completion of the work.

The original contribution of the candidate and material taken from other sources shall be clearly defined. Work from other sources shall be properly referenced using an acknowledged referencing system.

The report shall be submitted in two copies:
- Signed by the candidate
- The text defining the scope included
- In bound volume(s)
- Drawings and/or computer prints which cannot be bound should be organised in a separate folder.

Ownership
NTNU has according to the present rules the ownership of the thesis. Any use of the thesis has to be approved by NTNU (or external partner when this applies). The department has the right to use the thesis as if the work was carried out by a NTNU employee, if nothing else has been agreed in advance.

Thesis supervisors:

Jørgen R. Krokstad (principal research engineer Statkraft– professor II)

Deadline: June 10, 2014
Submitted: January 14, 2014

Preface

This master thesis has been prepared at the Department of Marine Technology at the Norwegian University of Science and Technology during the spring semester of 2014. The thesis is a requirement for completing the degree of Master of Science.

The thesis has been related to Statkraft's offshore wind developments, and has been inspired by some of the challenges met during the design process of foundations for offshore wind turbines. This real-life coupling to the thesis has been an extra motivational factor throughout the process. A personal motivational factor for writing this thesis has been a strong interest in offshore wind energy, especially in terms of its potential to increase the share of renewable energy in the World's energy mix.

I would like to take advantage of this opportunity to thank my supervisor Prof. II Jørgen Krokstad for his guidance and advice throughout the semester, for providing inspiration and motivation throughout the process of writing this thesis and for giving me hands-on experience of the dynamics of an onshore wind turbine by arranging an excursion to he wind farm at Smøla. The experience of standing at the top off a wind turbine and feeling the dynamic response when stopping the turbine will not be easily forgotten. I would also like to thank Lene Eliassen and Loup Suja Thauvin for their introduction to the field of aerodynamics and wind turbines, and especially for their help solving software problems that appeared along the way. In addition, I would like to express my deep gratitude to Lene for helping me update my results after a significant error was discovered in the model used for the analyses. The error was discovered only a few days before the submission date, and without her help and the computational strength of Statkraft's server I would not have gotten the correct results in time to update them in this thesis.

Finally, I would like to thank my fellow students at NTNU for interesting discussions on the topic of offshore wind turbines and my friends at NTNU for keeping up motivation through the semester.

Trondheim, 2014-06-16

Tine Louise Trøen

Abstract

The objective of this master thesis is to investigate the fatigue loading on an offshore wind turbine located in a waterdepth of 45 m. Offshore wind turbines are especially prone to fatigue due to variable environmental loading from wind and waves. The thesis is focused on the effect of misaligned wind and waves and second order wave loading on the fatigue life of the offshore wind turbine. The effect of second order loading is investigated in terms of the resonant phenomena of springing, as the natural frequency of bottom mounted wind turbines are in the frequency range where the second harmonic wave load has its maximum. The damping of the offshore wind turbine is important as the dynamic response of the offshore wind turbine is dependent on the level of damping. In terms of springing and misalignment, the aerodynamic damping is especially important as this is the main source of damping in the fore-aft direction of the offshore wind turbine in operation. Hence, also the aerodynamic damping is investigated to evaluate the results from the simulations in with a reference to the damping of the offshore wind turbine.

The overall damping, aerodynamic damping and overall damping in the absence of wind is determined by means of analyses of the free vibrations of the tower top when subjected to a step pulse loading. The overall damping in the absence of wind is determined from an analysis of the decay of the free vibrations of the tower top induced by the step pulse loading and a turbulent wind field. The deterministic part of the response is the part of the response used for calculation of the damping ratio.

Simulations with waves coming from angles of 15°, 30°, 45° and 90° relative to the wind direction are performed to investigate the effect of misalignment on the fatigue damage. As a reference load case one simulation with codirectional wind and waves is performed as well. As the aerodynamic damping is reduced for increasing misalignment up to 90°, an investigation of the effect of springing on the wind turbine is also performed. Hence, the simulations are firstly perfomed with Morison's equation for the computation of wave loads and then with the first two terms of the FNV-method to include second order loading.

An investigation of the effect of second order loading in terms of springing is also conducted. For this investigation twelve load cases have been chosen in order to investigate how the response to the second order loading is affected by overall damping, steepness of the waves and the peak period of the wave spectrum. The simulations are performed separately with Morison's equation and the two first terms of the FNV-method.

The damping of the offshore wind turbine is found to be in correspondence with the applied damping for the elements of the substructure in the model. As the soil damping applied is very low, an additional simulation with increased damping is performed to investigate the effect

of increased soil damping on the total damping. The increased soil damping does have an effect on the overall damping in the absence of wind, which is increased from 0.75% to 1.75%. The computed aerodynamic and overall damping including the aerodynamic contribution does however not give the expected results as it does not follow the shape of the thrust curve.

The second order FNV-method is found to be overconservative for the load cases investigated in this thesis. The mudline moment and the standard deviation of the mudline moment is larger for all load cases, even those that are expected to be dominated by linear loading. The overconservatism is partly due to the constant diameter assumption of the FNV-formulation and its application in this thesis. As the mudline diameter is used for the computation of the wave loads, the resulting load from the first term of the FNV-method is higher than the load computed with Morison's equation which takes the changes of the cross section into account.

The effect of misalignment between wind and waves is significant for angles above the 15° bin. The largest fatigue damage is seen for the load case with a 90° angle of misalignment. Due to the low damping in the side-side direction the response to second order loading, also when taking the overprediction of the FNV-method into account, is larger in this direction than the other ones. Correspondingly the fatigue damage is also larger for this load case for the simulations with the FNV method.

The investigation of the effect of springing shows the largest effect of second order loading for the load cases with a peak period that is twice the natural period of the first mode. The largest effect is found for H_S = 2.5 and U_{hub} = 13.9 m/s. However, this simulation is characterised with two peaks in the response spectrum for the combined first and second order wave load, that cannot be explained in terms of the natural frequencies of the structure. Hence, the results for this load case is biased by these peaks. The second largest effect is found for the same peak period and significant wave heigth and no wind applied. This is in correspondence with the expected response.

The conclusive remarks to the investigations performed is that the misalignment of wind and waves does have an impact on the fatigue life of the offshore wind turbine when only the single environmental state is considered. Taking the probabilities of occurrence into account however, the impact becomes smaller. The load case with the largest fatigue damage for the misaligned load cases does in fact not occur, meaning that from a realistic point of view this will not have a significance for the total fatigue life. In addition the damping of the offshore wind turbine is seen to have an effect in the significance of the second order loading for the total response. This is seen both for the misaligned load cases and the load cases for investigation of springing, as the ratio between the standard deviations computed for the two different wave load models is larger when the damping is low. Finally, a remark to the conservatism in the wave loads computed by the FNV-method is made. As the loads predicted with this method are larger for the linear wave loading as well, the results are more difficult to interpret as the overprediction compared to the

results from simulations with Morison's equation must be taken into account when analysing the results. An improvement to the method of investigation applied in this thesis will be to calculate the wave loading with an equivalent diameter that will give the same linear loading as Morison's equation for the linear wave loads, when using the second order FNV-method.

Sammendrag

Målet i denne masteroppgaven er å undersøke utmattingslaster på en offshore vinturbin med et sugebøttefundament på 45 meters vanndyp. Offshore vindturbiner er spesielt utsatt for utmatting ettersom de utsettes for variable miljølaster i form av vind og bølger. Denne oppgaven fokuserer på effekten av retningsforskyvning mellom vind og bølger på levetiden til vindturbinen, og effekten andreordens bølgelaster har på levetiden. Effekten av andreordens bølgelaster undersøkes ved å se på resonansfenomenet springing, ettersom egenfrekvensen for første moden til bunnmoterte offshore vindturbiner ligger i samme frekvensområde som den andreharmoniske bølgelasten har sitt maksimum. Dempningen av vindturbinen er viktig for den dynamiske responsen siden responsen er avhengig av nivået av dempning i systemet. I forhold til retningsforksyvning mellom vind og bølger og spriging, er aerodynamisk dempning spesielt viktig etter som dette er hovedkilden til dempningen av vindturbinen i vindens retning når turbinen er operativ. På grunn av dette undersøkes også den aerodynamiske dempningen av vindturbinen for å kunne evaluere resultatene med hensyn på dempningen.

Den totale dempningen, aerodynamisk dempning og total dempning uten aerodynamisk dempning beregnes ved å analysere de frie vibrasjonene i toppen av turbintårnet etter at vindturbinen har blitt påført en firkantet pulslast med start ved simuleringens start og som settes lik null etter 100 sekunder. Den totale dempningen av vindturbinens respons bestemmes ved ulike vindhatisgheter ved å påføre et turbulent vindfelt i tillegg til pulslasten. Dempningsforholdet beregnes deretter fra den deterministiske delen av forskyvningen i toppen av tårnet.

Simuleringer med inkommende bølger fra vinkler på 15°, 30°, 45° og 90° utføres for å undesøke effekten av retningsforskyvning mellom vind og bølger. En simulering hvor vind og bølger har samme retning utføres også for å ha et sammenligningsgrunnlag for effekten av ulik retning på vind og bølger på levetiden til vindturbinen. Ettersom den aerodynamiske dempningen for bølgene minker med økende vinkel mellom vind og bølger beregnes også bølgelastene ved de to første leddene i FNV-metoden for å undersøke om springing vil ha noen effekt for disse last tilfellene.

Effekten av andreordenslaster i form av springing undersøkes også. Her simuleres tolv lasttilfeller som er for å undersøke hvordan effekten av andreordenslaster påvirkes av total dempning, steilhet på bølgene og topp perioden for bølgespekteret. Simuleringene utføres både med de to første leddene i FNV-metoden og Morisons ligning.

Den beregnede dempningen for vindturbinen er funnet å være tilsvarende dempningen som er påført for hvert element i modellen. Ettersom dempningen i havbunnen er lav, utføres også en ekstra simulering for å undersøke hvorden den totale dempningen uten aerodynamisk

dempning påvirkes økt dempning i sjøbunnen. Den økte jorddempningen fører til en økt total dempning for vindturbinen ved fraværende vind, og øker fra 0.75% til 1.75%. Den beregnede aerodynamiske og totale dempningen inkludert det aerodynamiske bidraget gir imidlertid ikke resultater som stemmer overens med det forventede resultatet ettersom dempningen ikke følger formen på thrustkurven.

Beregningen av laster med de to første leddene i FNV-metoden gir overkonservative resultater for alle lasttilfellene som undersøkes i denne oppgaven. Mudlinemomentet og standardavviket for momentet er større enn ved beregning med Morisons ligning for alle lasttilfelle, inkludert de som er forventet å være dominert av lineære bølgelaster. Denne overkonservativiteten skyldes delvis antagelsen om konstant diameter i FNV-metoden og at det er diameteren ved sjøbunnen som er brukt i utregningene for FNV-metoden i denne oppgaven. Dette fører til at den lineære lasten som beregnes i det første leddet i FNV-metoden er større enn den lineære lasten beregnet ved hjelp av Morisons ligning, som tar hensyn til den varierende diameteren.

Effekten av forskjellig retning på vind og bølger er signifikant for vinkler med størrelse som er større enn de som inkluderes 15° intervallet. Lasttilfellet med 90° vinkel mellom vind og bølger har den største utmattingsskaden. På grunn av den lave dempningen perpendikulært på vindretningen er responsen som følge av andreordens laster større for dette lasttilfellet enn for de andre lasttilfellene, også når man tar hensyn til at FNV-metoden er for konservativ slik den brukes i denne oppgaven. Tilsvarende er også utmattingsskaden større for dette lasttilfellet ved bruk av FNV-metoden enn for de resterende lasttilfellene.

For undersøkelsene av effekten av springing på utmattingsskaden på vindturbinen viser at andreordenslastene har størst effekt for lasttilfellene hvor topp perioden på bølgespekteret er det dobbelte av egenperioden til vindturbinens første mode. Den største effekten er funne for lasttilfellet med H_S = 2.5 and U_{hub} = 13.9 m/s. Resultatene fra denne simuleringen viser imidlertid to distinkte topper i responsspekteret for den kombinerte første- og andreordenslasten beregnet med FNV-metoden. Disse toppene er vanskelige å forklare ut i fra egenfrekvensene til strukturen og det antas at disse toppene påvirker resultatet slik at en ukorrekt fremstilling av effekten av andreordenslaster blir gitt. Den største effekten av andreordens laster hvor disse distinkte toppene ikke er til stede i responsspekteret er funnet for lasttilfellet med samme topp periode og bølgehøyde, og med vinshastighet lik null. Dette lasttilfellet vil ha lavere dempning enn tilsvarende lasttilfeller hvor vind er påført, og en større effekt av andreordenslaster for dette lasttilfellet samsvarer dermed med den forventede responsen. Dempningen av vindturbinen er

Man kan konkludere med at forskjellig retning på vind og bølger vil ha en effekt på utmattingslivet til vindturbinen når man kun ser på en enkelt miljøtilstand. Dersom man tar hensyn til sannsynligheten for de forskjellige lasttilfellene vil effekten bli mindre for det totale utmattingslivet. Lasttilfellet hvor den største utmattingsskaden oppnås for lasttilfellene med

ulik retning på vind og bølger forekommer ikke i dataene fra NORA10 databasen, og vil dermed ikke ha noen effekt på det totale utmattingslivet i en realistisk analyse. I tillegg har dempningen av vindturbinen vist seg å påvirke viktigheten av andreordenslaster i den totale responsen til vindturbinen. Dette er observert for både lasttilfellene som er simulert for å undersøke effekten av springing og for lasttilfellene for forskjellig retning på vind og bølger, ved at forholdet mellom standardavviket for mudlinemomentet ved simuleringer med Morisons ligning og med FNV-metoden er større når dempningen i systemet er lav. Til slutt kan det også påpekes at konservativiteten i bølgelastene som beregned med FNV-metoden fører til at resultatene er vanskeligere å tolke ettersom man også må ta hensyn til at FNV-metoden også beregner større lineære bølgelaster enn Morisons ligning. Et forbedringspunkt for bruken av FNV-metoden for beregning av første- og andreordenslaster er å bruke en ekvivalent diameter som gir den samme lineære bølgelasten for FNV-metoden som for Morisons ligning.

Contents

List of Tables

List of Figures

Nomenclature

Abbreviations

FLS	Fatigue Limit State
FNV	Faltinsen-Newman-Vinje wave load model
$JONSWAP$	Joint North Sea Wave Analysis Project
$NORA10$	Norwegian Reanalysis 10 km
NSS	Normal Sea State
NTM	Normal Turbulence Model
NWP	Normal Wind Profile
RNA	Rotor Nacelle Assembly

Roman Symbols

m_{1b}	First order (static) moment of the area of the chord along the blade
Δt	Time step
$\overline{U}$	Mean wind speed
A	Wave amplitude, FNV-model
a	Radius of cylinder, FNV-model
c	Chord of turbine blade
$c_{damping}$	Damping coefficient, aerodynamic damping
$C_{L\alpha}$	Lift coefficient
D	Accumulated damage, Miner sum
dV_d	Change in wind speed perpendicular to rotor plane

f	Frequency
H_S	Significant wave height
I	Turbulence intensity
k	Thickness exponent on fatigue strength
L_k	Scale parameter for (Kaimal) wind spectrum
$log\bar{a}$	Intercept of log N axis
m	Negative inverse slope og the S-N curve
M_0	Modal mass
N	Total number of measurements or time steps
n	Indice of time steps
n	Number of amplitudes for calculation of logarithmic decrement
N_i	Total number of cycles to failure for stress range i
n_i	Number of cycles for stress range i
r	Radius rotor
$S(f)$	Response spectrum
$S_U(f)$	Spectral density of wind speed
T	Total length of time series
t	Thickness
T_p	Spectral peak period
t_{ref}	Reference thickness
T'	Change in thrust force with time
$U(t)$	Wind speed at time instant t

U_{10}	10-minute mean wind speed
U_{hub}	Wind speed at hub height
$U_m(t)$	Mean wind speed component at time instant t
$U_t(t)$	Turbulence component of wind speed at time instant t
V_0	Wind speed
$X(\omega)$	Response
x_0	Amplitude of first oscillation for calculation of logarithmic decrement

Greek Symbols

α	Shape parameter for high frequency range of the JONSWAP spectrum
δ	Logarithmic decrement
$\Delta\sigma$	Stress range
γ	Peakedness parameter, JONSWAP spectrum
λ	Wavelength
Ω	Angular velocity of rotor
ω	Angular frequency, wave frequency
ω_n	Natural frequency
ρ	Density of air, density of water
σ	Standard deviation of the wind velocity
$\sigma, \sigma_a, \sigma_b$	Standard deviation, width parameter JONSWAP spectrum
σ_U	Standard deviation of wind speed
ξ	Damping ratio
ξ_{aero}	Logarithmic decrement of aerodynamic damping

ζ	TWave elevation
f	Wave frequency
f_p	Peak frequency for wave spectrum
x_n	Amplitude of last included oscillation in calculation of logarithmic decrement

Chapter 1

Introduction

For the past decade, the offshore wind energy industry has expanded greatly in order to comply with the need for an energy mix based on a larger percentage of renewable energy sources. Both the number of installed wind turbines and the sizes of the wind turbines are increasing. The general trend in the industry is a shift towards larger generators, rotors and correspondingly higher hub heights and larger foundations for support. Due to a correlation between operation and maintenance costs and number of offshore wind turbines in a wind farm, there is an economical incentive for increasing the size of wind turbines that are installed offshore. Today, some of the largest wind turbines installed offshore have turbines with a rated energy output of 5MW. In order to reduce the cost of energy, i.e. the cost of each MW produced, and take advantage of the benefits of the correlation between number of wind turbines and operation and maintenance costs, turbine sizes are expected to increase in the years to come. Turbines with a rated output of 6 and 7 MW have recently been installed offshore off the coast of Belgium and Scotland respectively, and the sizes are expected to increase up to 20MW if proven economically and technically feasible[1] (Sieros et al., 2012).

Due to the dynamic complexity of offshore wind turbines and their exposure to aerodynamic, hydrodynamic and mechanical loading, offshore wind turbines are especially prone to fatigue damages. Hence fatigue is an important design driver for the support structure and is typically governing for the design together with the stiffness of the structure. In addition, it is essential that the natural frequency of the structure as well as the rotational frequency of the rotor do not coincide, and that the natural frequency is well outside the range of wave excitation frequencies in order to ensure the integrity of the structure throughout its lifetime.

The damping of the offshore wind turbine is an important parameter in terms of fatigue. The damping will have an effect of the magnitude of the response of the structure and is important to model correctly to obtain accurate results for the fatigue damage. For offshore wind turbines, the aerodynamic damping is the most important damping effect when the turbine is in operation. The aerodynamic damping is caused by the changes in thrust force on the rotor when the relative wind speed on the turbine blades changes, and will result in a force that is directed oppositely to the excitation force (Cerda and van der Tempel, 2005). This will result in a damping effect on the motions of the turbine.

[1] The objective of the Upwind project, supported by the EU, is to investigate the barriers for increasing the turbine size up to 20MW.

Another important factor that may affect the fatigue life of an offshore wind turbine is the relative angle, the misalignment, between incoming waves and wind. In a production state, aerodynamic damping from the turbine will contribute to the overall damping of the dynamic system. However, both wind and waves vary in magnitude and direction and will in many cases not be co-directional. This misalignment between wind and waves will decrease the damping effect from the aerodynamic damping and evidently fatigue will be increased.

Vibrations caused by second order hydrodynamic loading is also a concern for the design of offshore wind turbines. These vibrations occur when the structure is exited by second order wave loading from waves with a period twice the natural period of the structure. This phenomenon is often referres to as springing or sum-frequency effects. The natural frequency of offshore wind turbines are designed to lie outside the range of frequencies where first order wave excitation has the highest energy content, however the maximum spectral values of second order loads occur at the double frequency of the first order peak frequency. Thus, a resonance condition may arise from second order loading, and the structure is subjected to springing.

In the commercial software Fedem Windpower, the second order loading is calculated according to the FNV-model presented by Faltinsen et al. (1995), due to its simple implementation in the source code. This load model uses Airy-approximation to extend the second order loading to the surface level. Although the model has been extended to include finite water depths by Newman (1996), the fact that Airy theory is not valid in shallow to intermediate water depths raises a question whether this theory is accurate enough for application in this range of water depths.

1.1 Background and Motivation

The motivation behind this thesis is based on the need for more accurate fatigue prediction in order to develop more cost effective designs for support structures for offshore wind turbines. Fatigue is one of the most important design drivers for the support structure. As the support structure is one of the main contributors to the total cost of an installed offshore wind turbine, the potential of reducing cost by optimizing the design with regard to fatigue damages is large.

In addition, the trend within the industry is that offshore wind turbines are increasing in size and moving into deeper waters. The trend of increased in sizes of turbines and the Rotor Nacelle Assembly (RNA) originated from the cost of energy. Thus there is an economic advantage in increasing the sizes of the turbines, especially if the increased production and installation costs can be kept down. This development also involves a higher focus on prediction of fatigue loads. Larger turbines and RNAs will lead to a larger mass on top of the tower and will shift the natural frequency of the structure towards the range of frequencies where the structure is excited by

linear wave loading and probability of resonance increases. Thus the demand to accurately predict fatigue loads on the structure increases as this will have an impact on the resulting design.

As most offshore wind turbines are situated in intermediate to shallow water, nonlinearities in the waves will be more pronounced and need to be considered when performing analyses on offshore wind turbines. From a fatigue perspective, the sum-frequency effects from second order loading will have the most impact as the structure is excited at resonance by frequencies in the range of linear wave loading. The sum-frequency effects may give a considerably lower fatigue life if this should occur, and must be taken into account for accurate predictions of the fatigue life. This also means that the software used for such calculations must be able to model this effect correctly, without over- or underestimating the accumulated fatigue damage from sum-frequency effects.

Fatigue loading due to misalignment and sum-frequency effects is highly dependent on the damping of the system. Herein, the aerodynamic damping plays a vital role, as this damping effect only contributes to damping in the fore-aft direction. Thus incoming waves that are perpendicular to the wind will have negligible damping contribution from the aerodynamic damping. This also means that springing loads will be less damped and that large responses may occur if the second order loading has a sum-frequency close to the natural frequency. For an accurate prediction of fatigue loads it is thus important that the overall damping, including both structural and soil damping, as well as aerodynamic damping is modeled correctly.

1.1.1 Problem Formulation and Objectives

Fatigue loads are one of the dominating design drivers for support structures for offshore wind turbines. In order to achieve a more cost efficient design of support structures, accurate prediction of these fatigue loads is crucial. More accurate and reliable fatigue calculations are important for the foundation designers to obtain an optimal design, and this will be even more important when turbine sizes increase and offshore wind turbines are installed in deeper waters.

Misalignment between wind and waves is one of the sources of uncertainty in the prediction of the fatigue life. In order to find an accurate fatigue life, the variability in the relative angle between the wind and wave direction should be included in the simulations. This is necessary to account for the decreased damping level experienced when the wave direction deviates from the wind direction. Due to the computational effort required to carry out a sufficient number of simulations this is normally not accounted for, and the conservative load cases are used for fatigue calculations.

The objective of this thesis is to look closer into the fatigue loads that support structures for offshore wind turbines, with a suction bucket foundation, are subjected to. The effect of misalignment between wind and waves on the fatigue loading on the support structure will be investigated, focusing on the relative angle between wind and waves. This effect will be assessed and compared to the results of analyses where the misalignment has not been accounted for. In addition to this the load cases that are relevant for the fatigue limit state will be reviewed in terms of the ability to predict a correct fatigue life when using these load cases. The review will be based on the load cases recommended in DNV (2010a).

As the damping level of offshore wind turbines are very important for the fatigue damage accumulated over the structure's lifetime, the relevant damping effects for fatigue life assessment will also be investigated. As aerodynamic damping is one of the main contributors to the overall damping of the structure, this will be the main focus of the investigation.

Additionally, an investigation of the sensitivity of the fatigue life to second order loads will be conducted, in order to determine whether sum-frequency effects has a significant effect/impact on the fatigue life. Numerical predictions of the fatigue life for the support structure when subjected to second order loading will be performed to evaluate the sensitivity.

1.2 Approach

The investigation of the effect of misalignment and sum-frequency effects on the fatigue life will be conducted by performing dynamic simulations in the finite element software Fedem Windpower. This software code is especially developed for wind turbines both onshore and offshore. A finite element model of the turbine, provided by Statkraft, will be used for the analyses. The soil and suction bucket is also modeled by a finite element model, incorporating both the properties of the soil and the foundation.

Damping effects will be investigated by performing logarithmic decay tests in Fedem Windpower where the transient decay of the free vibrations of the tower top is analysed. This is done by calculating the logarithmic decrement for deterministic part of the response due to a turbulent wind field and a constant step pulse loading. By performing this test with different wind speeds the total damping including aerodynamic damping can be predicted. The change in overall damping with changing wind speed will be predicted by performing logarithmic decay test for a range of turbulent wind speeds.

The investigation of the effect of misaligned wind and waves will be conducted by comparing a series of simulations for selected environmental states, with different significant wave height, peak period, mean wind speed and directions. The selected simulations will also include

simulations with a 90°angle between wind and waves to demonstrate the worst case scenario in terms of misalignment. The probability of occurrence of the selected environmental states will also be taken into account when evaluating the effect of misalignment, as this will also be a factor in the total impact misalignment has on the fatigue life of offshore wind turbines.

The effect of second order loading will be investigated in a similar manner as the misalignment effect. Simulations will be performed for selected environmental states and wave loading will be calculated using Morison's equation and the second order load term from the FNV-model. The results from simulations using only Morison's equation and simulations using the first two terms of the FNV-load model, i.e. the sum of loading from Morison's equation and the second order load term of the FNV-model, will then be compared to investigate the sensitivity of the fatigue life to second order loading. As non-linearities are more pronounced for sea states with a high steepness of the waves, these sea states will be investigated in particular. The probability of occurrence for each of the selected environmental states will also be taken into account to determine the total impact on the fatigue life.

1.3 Structure of the Report

The following chapters of the thesis are structured as follows. In Chapter 2 the current research on misalignment, springing and the load models used to predict springing are discussed, and the scope and limitations to the objectives in the thesis are given. Herein the dimensions and concepts used for the offshore wind turbine used in the simulations, is described as well. Chapter 3 presents relevant background information needed for a complete understanding of the thesis, including metocean design basis, integrated analysis, damping and damping effects, springing and nonlinear load models for calculation of second order loads on vertical cylinders. Chapter 4 will review the recommended load cases that are currently used for prediction of fatigue loading on the support structure to give the reader a deeper understanding about the challenges in predicting these loads through simulations. In Chapter 5 the methods and models used for prediction of fatigue loads due to misalignment and sum-frequency effects are described, as well as how the relevant damping effects will be investigated. The results from the simulations are presented in chapter 6 and discussed in terms of the objectives of the thesis in chapter 7. In Chapter 8 conclusions regarding the obtained results and suggestions for further work are given.

Chapter 2

Scope and Limitations

2.1 System Definitions

2.1.1 Terminology

Before describing the scope of the thesis more in depth, it is useful to clarify the terminology that is used in the rest of the thesis. As some of the terminology for the different parts of offshore wind turbines are used differently in literature, the terms that will be used for the different parts of the structure in this thesis are specified. The terms referring to the verious parts of the offshore wind turbine are defined in Figure 2.1.

In addition, as the excitation will be investigated in a three dimensional environment, the motions and mode shapes of the offshore wind turbine will be referred to as in the fore-aft direction and the side-side direction. The fore-aft direction corredsponds to motion in parallell to the wind direction, while the side-side direction is the direction perpendicular to the wind direction. As the wind direction regarded is the same for the purpose of this thesis, the fore-aft direction corresponds to motion or response along the x-axis of the model, and side-side to motion along the y-axis.

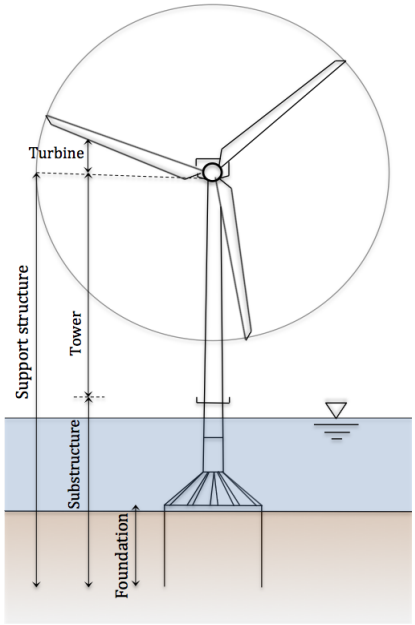

Figure 2.1: Terminology for the different parts of an offshore wind turbine to be used in the rest of the thesis. Reproduced from Marino (2010).

2.1.2 Dimensions and Model Specifications

In the following thesis an offshore wind turbine equipped with the 5MW NREL turbine (Jonkman et al., 2009) will be used for the simulations. A support structure model provided by Statkraft will be used for analyses. The geometry of this wind turbine model is shown in Figure 2.2. The offshore wind turbine is situated at a location with a water depth of 45 m at Doggerbank. It has a hub height of 98.1 m taken from the mean sea level, giving a total height of the tower and support structure from the seabed of 143.1 m. The remaining dimensions and wind turbine characteristics are given in Table 2.1.

A tower, substructure and a suction bucket foundation constitute the support structure of the turbine. The suction bucket is based on the concept developed by Universal Foundation, and secures the turbine and tower to the seabed by means of the total weight of the structure and suction that is applied during installation (Houlsby et al., 2005). The bucket has a diameter of 20 m and a skirt length of 14 m. These dimensions have been supplied by Statkraft. The tower is connected to the bucket by means of a interface made up by triangular flanges welded to the bucket and the submerged part of the support structure. The dimensions of the relevant the parts of the support structure are summarized in Table 2.2. Note that the inner dimensions are given including grouting.

Table 2.1: Properties of the 5MW NREL wind turbine (Jonkman et al., 2009), and tower dimensions.

Wind Turbine Properties	
Rating	5 MW
Rotor Orientation, Configuration	Upwind, 3 blades
Control	Variable speed, Collective Pitch
Drivetrain	High Speed, Multiple-stage Gearbox
Rotor, Hub Diameter	125.8 m, 3.0 m
Hub Height	98.1 m
Cut-in, Rated, Cut-out Wind Speed	3 m/s, 11.4 m/s, 25 m/s
Cut-in, Rated Rotor Speed	6.9 rpm, 12.1 rpm
Rated Tip Speed	80 m/s
Overhang, Shaft Tilt, Precone	5 m, 5°, 2.5°
Rotor Mass	110 000 kg
Nacelle Mass	240 042 kg
Tower Mass	907 519 kg
Substructure Mass (excluding bucket)	2 374 005 kg

2.1.3 Metocean and Environmental Conditions

The metocean data used for determining the metocean conditions for the analyses are taken from the NORA10 database. Due to the background of this thesis connecting the investigations that will be performed to the Doggerbank field, site-specific hindcast data are used. The hindcast data correspond to a location of 54.87°latitude and 1.79°longitude.

The NORA10 database has been developed by the Norwegian Meteorological Institute and contains high resolution hindcast data for the Norwegian Sea and the Barents Sea in addition

Table 2.2: Dimensions of the support structure

Support structure dimensions	
Total height of tower from seabed	143.1 m
Height of submerged tower, seabed to MSL	45.0 m
Height of grouted part of tower	65.0 m
Outer diameter of substructure at mudline	8.0 m
Inner diameter of substructure at mudline	5.84 m
Outer diameter of substructure at MSL	6.37 m
Inner diameter of substructure at MSL	5.84 m
Diameter of bucket	20 m
Skirt length of bucket	14 m

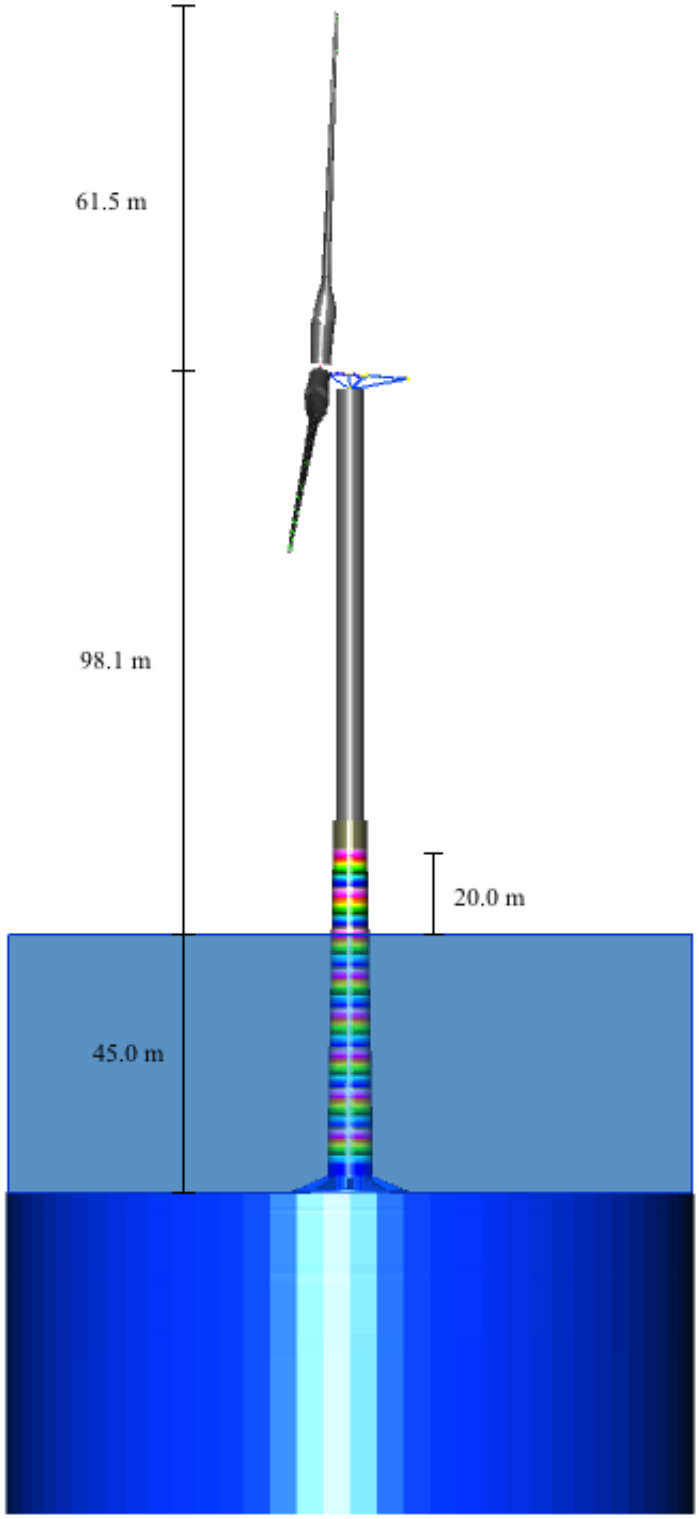

Figure 2.2: Dimensions of the offshore wind turbine.

to the North Sea (Reistad et al., 2011). The data that are used in this thesis spans from 1957 until 2010. The hindcast data are based on atmospheric reanalyses from the European

Reanalysis project, ERA40, for which Reistad et al. (2011) applied a high-resolution numerical weather prediction model to obtain a resolution of 10km. A 50km model for the North Atlantic was also used to obtain hindcast wave data and the waves were forced with winds from ERA-40 reanalysis. Additionally, the bottom topography has been taken into account in the data, so that the wave heights represent the actual wave height at the specific location.

2.1.4 Wave Load Regime

The hydrodynamic load regime of marine structures can be described as either inertia, diffraction or drag dominated, meaning that either mass, diffraction or drag forces dominate the hydrodynamic loading on the structure. Which load regime that dominates is determined by calculation of the ratio between the wave height, H and the diameter of the cylinder, D, and the ratio between the wavelength, λ and the diameter of the cylinder. The load regime can then be found by comparing the values to the diagram in Figure 2.3, which shows the relative importance of inertia, wave and drag wave loads on a vertical cylinder. The offshore wind turbine used in this thesis is assumed to be inertia dominated. Knowing that the diameter of the substructure is varies from 8.0 meters at the mudline to 6.0 meters at the interface with the tower one can estimate the whiether this assumption can be valid or not. As the ratio between the wave height and the diameter must be above 10 for drag forces to be dominating, one can quickly eliminate this load regime. For most wave heights and waves lengths the laoding will in fact be dominated by inertia forces, however for short waves the loading may enter the diffraction dominated region.

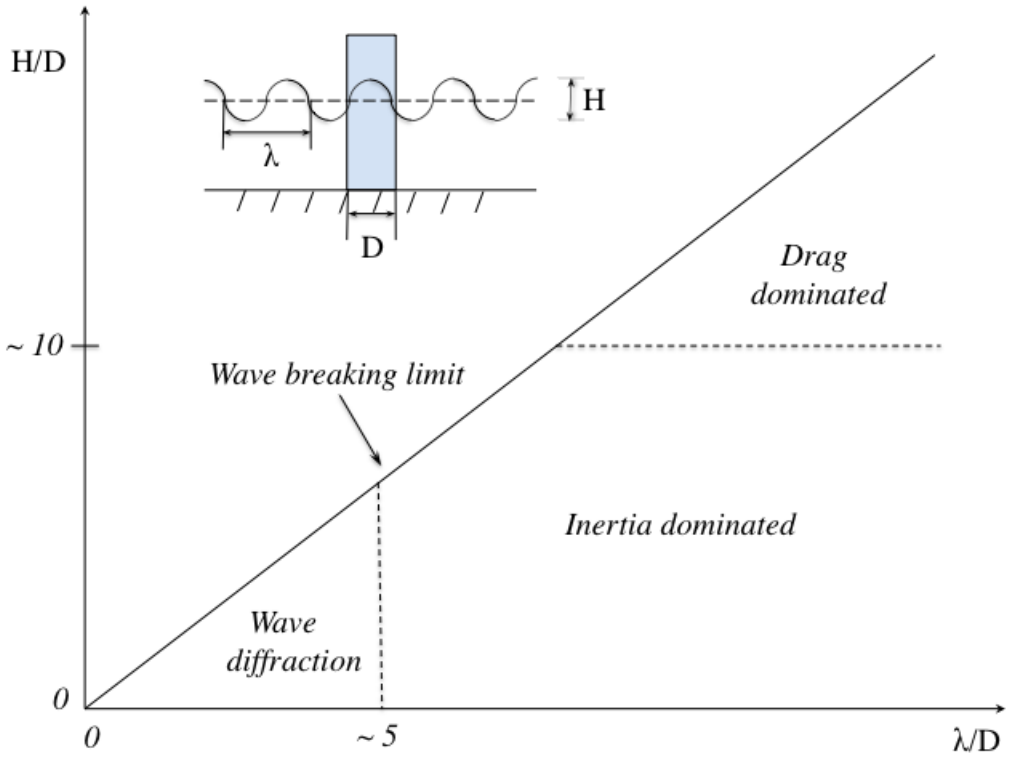

Figure 2.3: Relative importance of the drag, inertia and diffraction wave loads on a vertical cylinder. Reproduced from Faltinsen (1990).

The load regime of the offshore wind turbine can be verified by plotting the ratio between wave height and diameter of the offhore wind turbine against the ratio between the wavelength and the diameter. In Figure 2.4 shows this plot for the offshore wind turbine decribed in this chapter, based on the maximum and minimum values of the significant wave height is the NORA10 data. The wave heights are sorted according to the peak period of the sea state in intervals of 1 second. As seen in Figure 2.4, the assumption of an inertia dominated structure is valid since only the smallest and shortest waves fall within the diffraction dominated wave load regime.

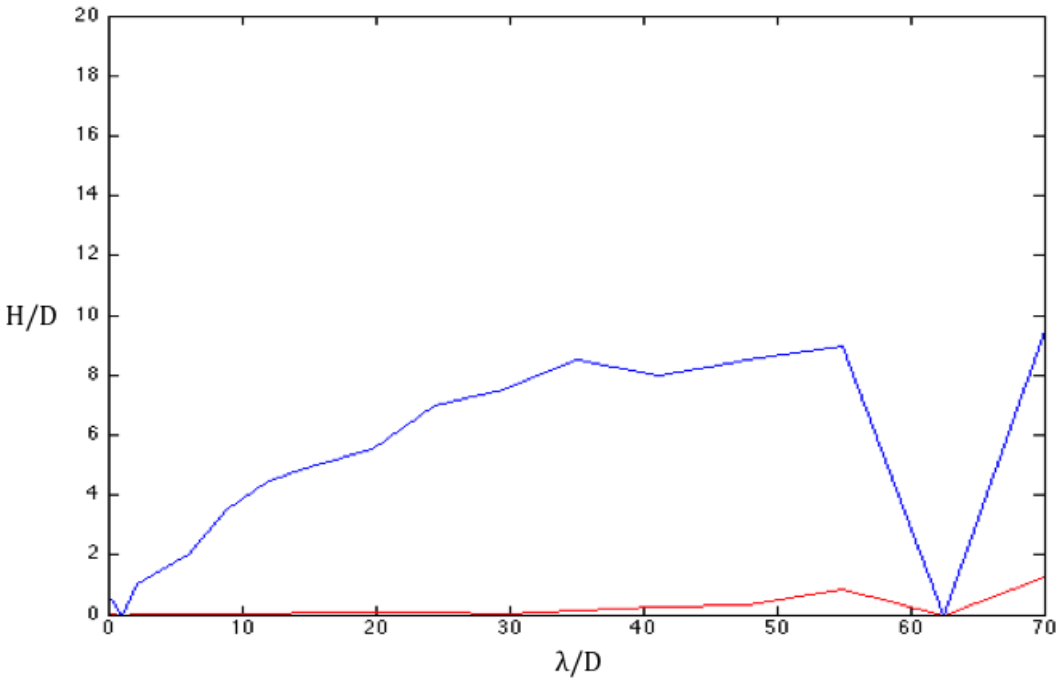

Figure 2.4: Classification of load regime for offshore wind turbine using wave data from NORA10.

2.1.5 Natural Frequencies

The natural frequencies of the different modes are determined in Fedem Windpower once a dynamic analysis is performed. Table 2.3 gives a summary of the natural frequencies for the first ten mode shapes.

The focus of the thesis is on the excitation of the natural frequency of the first mode shape of the structure in the fore-aft and side-side direction, and will be discussed further in the following chapter, Background Knowledge. The first mode shape is illustrated for both the fore-aft direction and side-side direction in Figure 2.4.

Table 2.3: Natural frequency of blade and support structure modes.

Mode	Natural frequency [Hz]
1st fore-aft bending mode	0.2497
1st side-side bending mode	0.2498
1st blade assymetric flapwise	0.6546
1st blade assymetric flapwise	0.6581
1st blade collective flapwise	0.6721
2nd side-side bending mode	0.8631
2nd fore-aft bending mode	0.9128

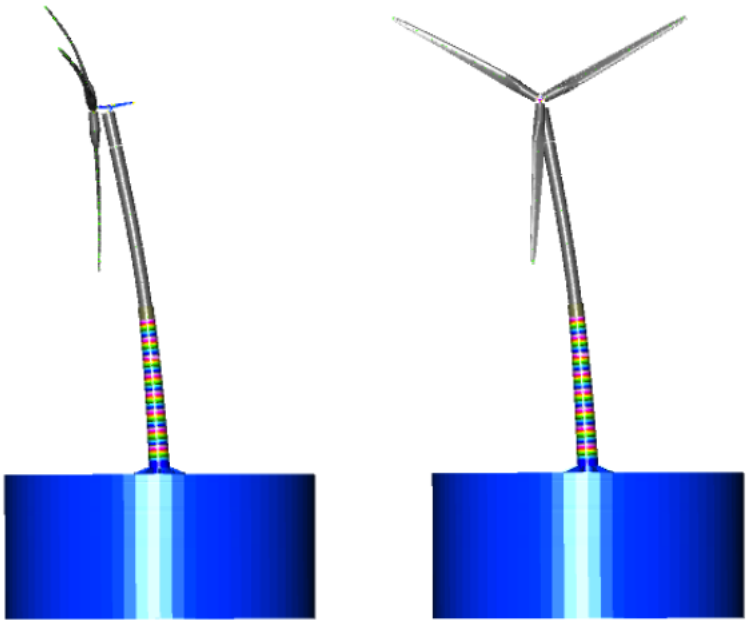

Figure 2.5: llustration of the first mode shape of the support structure in the fore-aft direction (right) and side-side direction (left).

2.2 Limitations

Although current and tidal variations are present at the Doggerbank field, the current loading and variations in mean sea level will not be taken into account in the analyses. The variations in mean sea level are not regarded to have any significant effect on the fatigue loading and are thus omitted. Current loading may have an effect on the fatigue life due to variability in the loading. However, the objective of the thesis is to investigate load effects due to second order wave loading and misaligned wind and waves, and for simplicity current loading is neglected. In addition to the above limitations, seasonal changes will not be taken into account.

The NORA 10 data used for analyses in the thesis are taken from a location corresponding to a water depth of 20.9 m. The offshore wind turbine investigated in this thesis is modeled for a water depth of 45 m, a water depth that is more than the double of the water depth for the location where the data is provided from. The wave height will increase with decreasing water depth as until the waves brake. Thus using waves from a location with a smaller water depth, especially when using wave data from the sea states with the most steep waves, the wave heights used may be higher than the waves that are actually generated at a water depth of 45 m.

Due to the large number of analyses required to determine the fatigue from all combined sea and wind states, and the even larger number required when misalignment is taken into account, only some specifically chosen cases will be analysed in this thesis. These cases will be carefully chosen based on their ability to demonstrate the effects and responses due to second order load effects and misalignment. This means that a full fatigue analysis of the structure is not performed, but rather an investigation of how the fagtigue damage in the chosen sea states is affected by misalignment, damping effects and second order loading in terms of sum-frequency effects. In order to demonstrate the effects of sum-frequency effects, some of the less occurring combinations of sea states with a high steepness and their corresponding wind speeds will be chosen. The reason for this is that these sea states will contain larger nonlinearities. In addition sea states that will trigger response at the eigenfrequency of the first mode are investigated as these are assumed to have the largest effect from the sum-frequency loading. From a dynamics and fatigue point of view, these sea states are interesting to investigate due to the dynamic amplification in this range and the larger fatigue damage that will occur when the structure is excited by waves within this frequency range.

The offshore wind turbine is assumed to be inertia dominated for all sea states. Thus the drag term in Morison's equation will not be included in the wave load calculations. In addition, diffraction of waves will not be considered in the thesis. This may have an impact on the results as diffraction will decrase the mass coefficient in Morison's equation, leading to reduced loads.

Chapter 3

Background Knowledge

In the following chapter relevant background theory for the scope of this thesis will be presented. The infomation included will give the neccessary background to give a good understanding of the objectives that will be investigated, the results obtained and the following dicussion of results.

3.1 Fatigue Loading

Fatigue damage is caused by cyclic loading and is an important parameter to consider for the design of offshore wind turbines. The main contributions to fatigue loading for offshore wind turbines are environmental loads, i.e. loads from wind, waves and current. All the loads mentioned are loads that vary with time. It is thus the deviation of these loads from their mean value that is of significance in a fatigue perspective. In addition to this the mean value of the loads also vary with time, and this must be taken into account, particularly for the environmental loads, however for the duration of a wind state or sea state the mean value can be assumed constant. The variability of the loads and stationary conditions for these loads will be further explained in subchapter 3.

3.1.1 Evaluation of Fatigue Damage/Loading

Fatigue damage is determined by calculation of the cumulative damage, which is done by calculation of the Miner sum. The Miner sum is determined from the sum of the damage from each stress range in the stress history.

$$D = \sum_i \frac{n_i}{N_i} \tag{3.1}$$

In the above equation, n_i is the number of cycles for each stress range i, while N_i is the constant amplitude endurance for the given stress range (Berge, 2006). If the Miner sum is above 1, failure due to fatigue will occur for the given stress history. The total number of stress cycles before

failure is obtained from an S-N curve:

$$logN = log\bar{a} - mlog\left(\Delta\sigma\left(\frac{t}{t_{ref}}\right)^{k}\right) \tag{3.2}$$

Equation 3.2 is the mathematical formulation of the S-N curve, and is defined from the intercept with the $logN$-axis, $log\bar{a}$, and the slope of the surve, m, as well as the stress range$\Delta\sigma$ and ratio between the thickness in the expected direction of crack propagation, t, and the reference thickness t_{ref}.

There are several methods for determining the number of stress cycles to be counted from the stress time history. These methods include level crossing counting, peak counting, simple counting and rainflow counting. For information about how these counting methods are performed, reference is made to Almar-Næss (1985). The difference between these methods of cycle counting is of little significance for narrow-banded stress time histories. For wide-banded loading on the other hand, rainflow counting is recommended as inspection has verified that this counting procedure produces the same stress-strain loops as a material undergoing the same loading history (Almar-Næss, 1985). Rainflow is generally considered as the best suitable of these counting methods.

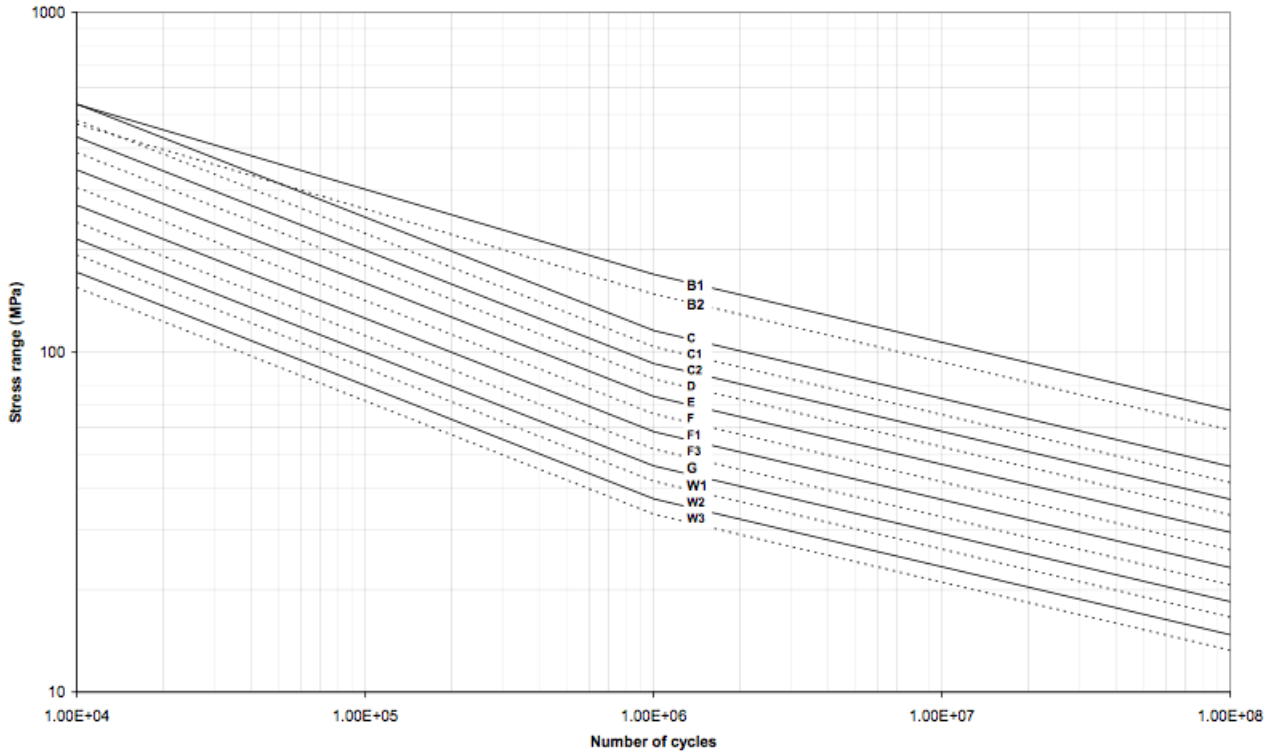

Figure 3.1: SN-curves for welded steel in seawater with cathodic protection (DNV, 2012).

3.2 Stochastic Processes

The generation of wind and waves in real life are stochastic processes. This means that these processes vary with time and cannot easily be reproduced or predicted in advance(Newland, 1993). Both wind and wave processes are assumed stationary over a certain time reference, meaning that over the span of a certain reference period, the statistical parameters remain constant. This assumption enables analysis of the data. The wave process is assumed stationary for a period of three hours. Wind on the other hand is a much more fluctuating process and is only assumed stationary for a period of ten minutes. This difference in reference period for stationarity may be an issue when performing analyses where both of these processes are important for the overall loading and response of a structure. The effect of different reference periods will be discussed further in chapter 3.3, Metocean Design Basis.

In order to understand the dynamics and response of a system, it is useful to study the results both in the time domain and in the frequency domain, as well as understanding the procedure used for transformation between the two domains, the Fourier transformation. This is described in further detail in the following subchapters.

3.2.1 Time and Frequency Domain

Random processes can be analysed in the time domain and in the frequency domain. In the time domain, realizations of the process contain information regarding mean, maximum and minimum values, standard deviation and slow variations of the process. Time realizations are converted to the frequency domain by means of a Fourier transformation. A time domain signal, for instance an irregular wave, can be regarded as a summation of different regular signals, here referred to as harmonic components. A given time signal or time series can be broken down into its harmonic components with a given amplitude, frequency and phase angle. For an irregular wave, this can be expressed as in equation 3.3 below, for both wave frequency ω and frequency f:

$$\zeta(t) = \sum_{i=1}^{n} A_i \sin(\omega_i t - k_i x + \epsilon_i) = \sum_{i=1}^{n} A_i \sin(2\pi f_i t - k_i x + \epsilon_i) \tag{3.3}$$

By means of a Fourier transformation, this sum of regular wave components can be transferred to the frequency domain. By representing the random signal in the time domain as a Fourier series the amplitude, frequency and phase angle of the harmonic components can be reproduced. This is the procedure used in the Fast Fourier Transform (FFT), which is often used to transform time series into spectra. The time series can be taken directly from the time

domain to the frequency domain by applying Equation 3.4.

$$S(f) = \frac{1}{T}\left[\sum_{n=1}^{N} \zeta(n\Delta t)e^{if(n\Delta t)}\Delta t\right]^2 \tag{3.4}$$

Note that in Equation 3.4, it is the power spectral density that is determined per time increment for the wave profile ζ at the time instant $n\Delta t$. This is the usual representation of a time series of the wave elevation in the frequency domain. By performing the inverse operation of Equation 3.4, time signals can be created from the power spectral density. For more details regarding the Fourier Transformation and FFT, reference is made to Chakrabati (1987) and Newland (1993).

In order to obtain a spectrum with sufficient confidence, the total time series is often divided into several segments of equal length, equal number of data points N and a constant time increment Δt. The spectras obtained from these sections are then averaged to obtain the final spectrum (Chakrabati, 1987). For simulation of stochastic processes, a number of realizations with the same input and different seeds are performed and the final spectrum is obtained by averaging the spectras obtained from each of the simulations.

Confidence increases with the number of sections, however for a time series of constant length that is divided into sections, there is a dependency between the parameters used in the FFT method. For a time record that has a finite length, the total length of the record can be expressed as $T = MN\Delta t$. From this relationship it is evident that for a constant time increment Δt, the number of data points for each section will be less, and thus the resolution of the spectrum will decrease so that Δf increases. The result of this is that some important responses/energy contents may not be included in the spectrum. In terms of fatigue, these peaks may indicate large responses and corresponding stress ranges that will have a significant contribution to the fatigue damage. Hence a compromise between the number of sections and data points for each section is needed to obtain a spectrum with sufficient confidence and resolution. Chakrabati (1987) recommends a number of sections larger than, or equal to 8, and a number of data points between 512 and 2048. Additionally, the number of data points should be a power of 2 for to obtain efficient computation, thus limiting the choices of number of data points to 512, 1028 or 2048 for the use of the FFT method on time records.

3.2.2 Nyquist Frequency

The Nyquist frequency, f_N is another important parameter for the spectrum. This is the upper limit of the frequency (Chakrabati, 1987) and is related to the minimum number of data points needed to describe a wave. It is defined in terms of the time increment as:

$$f_N = \frac{1}{2(\Delta t)} \tag{3.5}$$

By setting the Nyquist frequency as the maximum frequency to be included in the Fourier series, the aliasing effect can be avoided. The aliasing effect is a disturbance in the transformed wave components, where waves of higher frequencies than the desired frequency is fitted to the data points used in the transformation (Van der Tempel, 2006). Without applying the Nyquist frequency as the maximum frequency, the spectrum obtained by the Fourier Transformation will have a higher energy content at higher frequencies, and will give an incorrect representation of the spectrum.

3.2.3 Response Spectra

As the loads on an offshore wind turbine vary in time, so does the response. This means that an analysis of the response in the frequency domain may reveal the characteristic responses of the structure. Response spectra are also computed from a time history by the Fourier transform. For a response $x(t)$, the transformation can be expresses as in Equation 3.6, which is the formal definition of the Fourier Transform (Newland, 1993).

$$X(\omega) = \frac{1}{2\pi} \int_{-\frac{T}{2}}^{\frac{T}{2}} x(t) e^{-i\omega t} \mathrm{d}t \tag{3.6}$$

For offshore wind turbines, evaluation of the response in the frequency domain is useful as it will show which frequencies that contain much energy. By comparing the response spectrum to the stectra of the excitation, on can see whether a certain loading will lead to responses at other frequencie and whether structure is excited at resonance. Resonance is seen as spectral density peaks that do not have a linear realtionship to the excitation, as the response is amplified in resonance.

It is important to note that a spectrum representation of the response will not give any information about the nonlinearities of the excitation load. The spectrum only provides a representation of which frequency ranges that contain energy and the magnitude of this energy. Hence, knowledge about the loading process and the expected response in the frequency domain is required to fully utilise the information given in a response spectrum.

3.3 Metocean Design Basis

In the design of offshore wind turbines, metocean data are important for the estimation of environmental loads on the turbine. According to DNV (2010a) these data should ideally

originate from measurements made at the specific site of the offshore wind farm and have a sufficiently large time span. In many cases, such site measurements are not available, and metocean data from hindcast databases are used for estimation of environmental loads. For simplicity, the short term combinations of U_{10}, H_S, and T_p will be referred to as environmental states in the following.

3.3.1 Wind Conditions

For the short term, wind conditions are characterized by the mean wind speed and turbulence, i.e. the fluctuations in wind speed over a relatively short period of time. The total wind speed as a function of time may be expressed in terms of a slowly-varying mean component, $U_m(t)$, and a turbulence component, $U_t(t)$:

$$U(t) = U_m(t) + U_t(t) \tag{3.7}$$

Due to wind shear in the atmospheric boundary layer, the mean wind speed increases with the height above the ground. The mean wind velocity profile is normally represented by the logarithmic profile (Equation 3.8), or by the power law profile (Equation 3.9).

$$U(z) = \frac{u^*}{k_a} ln \frac{z}{z_0} \tag{3.8}$$

where the friction velocity, u^*, is given as

$$u^* = \sqrt{\kappa} U_{10}$$

In Equation 3.8 above, $U(z)$ denotes the wind speed at height z, k_a is von Karman's constant and z_0 is the surface roughness with a value between 0.0001 and 0.01 for open sea with waves (DNV, 2010b). For the definition of the friction velocity, κ denotes the surface friction coefficient and U_{10} is the 10-minute mean wind speed at a heigth of 10 m above the ground.

$$U(z) = U(H) \left(\frac{z}{H} \right)^{\alpha} \tag{3.9}$$

Here $U(H)$ is the wind speed at a given reference height H and α is the power law exponent. α is dependent on the terrain roughness, and has a recommended value of 0.12 for wind profiles over open sea with waves.

These wind velocity profiles differ for different heights, hence care should be taken in the design process to assure that all wind velocities are calculated according to the same wind profile. If a reference height of 10 m is given, the difference between the two wind profiles will increase with height, while if the reference height is the hub height the wind speed will be the same at this height and the difference between the wind profiles will increase with distance from the hub

height. The wind profiles will also give different wind velocities on the rotor disc for different heights. However, when the wind speed at hub height of a wind turbine is known and used to calculate the wind profiles, these differences will cancel over the rotor disc, so that the difference in total loading due to choice of wind profile will be negligible (Van der Tempel, 2006).

Wind conditions are assumed to be stationary over a period of ten minutes, meaning that the mean wind speed and standard deviation due to turbulence are defined over this ten-minute period. The turbulence may be represented by different statistical descriptors(Burton et al., 2011). Turbulence intensity is a simple and common way to describe the overall turbulence, and is defined as:

$$I = \frac{\sigma}{\overline{U}} \tag{3.10}$$

DNV (2010a) recommends the Kaimal turbulence spectrum for representation of the wind speed spectral density, given that the wind data does not indicate that another spectrum is more suitable. The Kaimal spectrum is defined as:

$$S_U(f) = \sigma_U^2 \frac{4\frac{L_k}{U_{10}}}{\left(1+6\frac{fL_k}{U_{10}}\right)} \tag{3.11}$$

3.3.2 Wave Conditions

The short term wave statistics are characterized by the essential parameters H_S and T_p. These parameters are assumed constant over the duration of a sea state. The individual wave heights occurring within a sea state can be modeled by use of a wave spectrum, where the peak of the spectrum will be at the frequency, f_p corresponding to the peak period, T_p. A wave spectrum represents the power spectral density function of the vertical sea surface elevation (DNV, 2010b), i.e. it shows how the total energy of the sea is distributed according to the frequencies of the different wave components present (Michel, 1968). The most commonly used spectrum for North Sea locations is the JONSWAP spectrum. This spectrum describes wind sea conditions and developing sea states that are limited by the fetch length, and is used to produce irregular waves in analyses (DNV, 2010b). The Jonswap spectrum for a sea state with $H_S = 2.5m$ and $T_p = 5.044$ is shown in Figure 3.2.

The mathematical description of the spectum is as follows:

$$S(f) = \alpha \frac{g^2}{(2\pi f)^5} \exp\left[-\frac{5}{4}\left(\frac{f_p}{f}\right)^4\right] \gamma^{\exp\left[-\frac{1}{2}\left(\frac{f-f_p}{\sigma f_p}\right)\right]} \tag{3.12}$$

In this mathematical description, γ is the peakedness parameter and has a mean value of 3.3

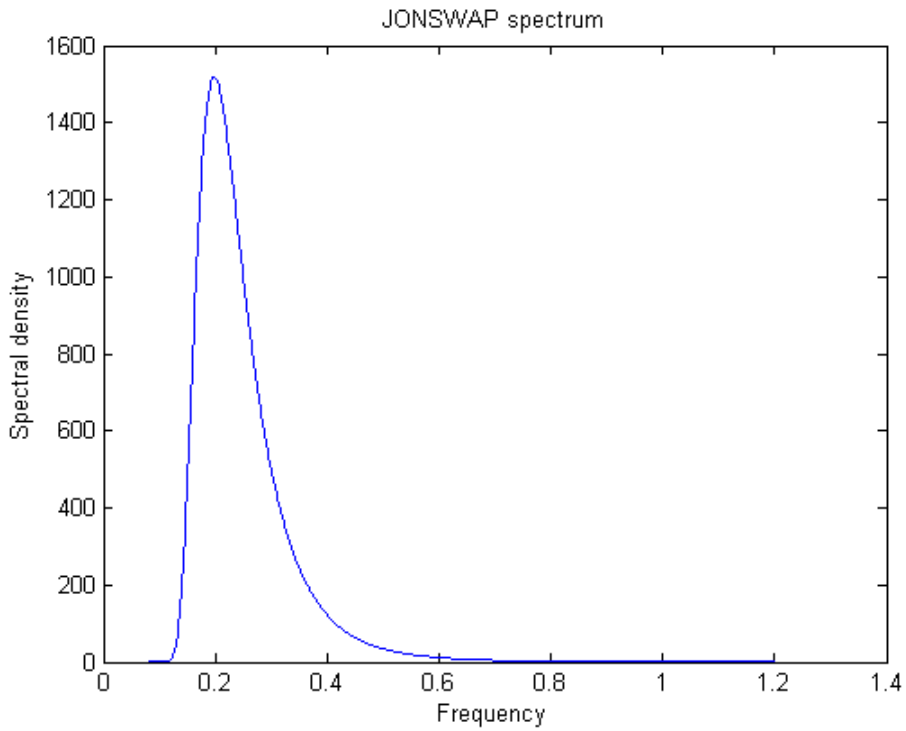

Figure 3.2: JONSWAP spectrum for $H_S = 2.5m$ and $T_p = 5.044$.

(DNV, 2010b). If the peakedness parameter is not given, it may also be determined from the relationships given in Equation 3.13. The peakedness parameter is also important for the bandwidth of the wave process in the frequency domain, which may have an effect on the response of the structure in terms of excitation of the natural frequencies of a structure. If the value of the peakedness parameter is decreased, the bandwidth of the spectrum will increase, and vice versa if the peakedness is increased. The effect of the bandwidth of the response of an offshore wind tubine will be further discussed in 3.6 Natural Frequencies and Dynamic Response.

$$\gamma = \begin{cases} 5 & \text{for } \frac{T_p}{\sqrt{H_S}} \leq 3.6 \\ e^{5.75-1.15\frac{T_p}{\sqrt{H_S}}} & \text{for } 3.6 < \frac{T_p}{\sqrt{H_S}} < 5 \\ 1 & \text{for } 5 \leq \frac{T_p}{\sqrt{H_S}} \end{cases} \tag{3.13}$$

The parameter α is the generalised Phillips' constant and adjusts the shape of the high frequency part of the spectrum. This parameter is dependent on the significant wave height, peak frequency and the peakedness parameter, as shown in Equation 3.14.

$$\alpha = 5\pi^4 \left(\frac{H_S^2 f_p^4}{g^2} \right) (1 - 0.287 ln\gamma) \tag{3.14}$$

The width parameter σ is dependent of the peak frequency so that

$$\sigma = \begin{cases} \sigma_a & \text{for } f \leq f_p \\ \sigma_b & \text{for } f > f_p \end{cases} \tag{3.15}$$

According to DNV (2010b) the value of σ_a should be 0.07 and σ_b taken equal to 0.09.

3.3.3 Probability Density Functions

All environmental states have a certain probability of occurrence. As offshore wind turbines are subjected to wind and waves, the long-term joint probability density function of these environmental parameters is of most interest in a fatigue perspective. The probability of occurrence may be determined by sorting hindcast data or data from measurements into predefined bins, and determining the probability that an environmental state with parameters within that bin will occur.

A more accurate method is to determine the joint probability density function for the environmental parameters. By means of joint probabilities the probability of occurrence of a certain sea state can be estimated and the fatigue life of an offshore wind turbine can be predicted from analysis of a series of environmental states. As wind and wave processes are correlated to some degree, conditional probability functions are needed to represent the long-term probability of occurrence. For codirectional wind and waves, a three parameter probabillity density function, dependent on the significant wave height, spectral peak period and the mean wind speed is needed. Johannessen et al. (2001), suggested a joint probability density function formulated as follows as in Equation 3.16 with the mean wind speed as the primary variable, as this is assumed to be dominating. For the probability function of the wind, Johannessen et al. (2001) used a two-parameter Weibull distribution. This was also used for the wave distribution, whereas the probability of spectral peak period was modeled using a log-normal distribution.

$$f_{W,H_{m0},T_p}(w,h,t) = f_W(w) * f_{H_{m0}|W}(h \mid W) * f_{T_p|H_{m0},W}(t \mid h,w) \tag{3.16}$$

For misaligned wind and waves a fourth parameter is included, which is the angle between the wave direction and the wind direction. This will result in a four-parameter probability distribution.

In a fatigue perspective, the treatment of metocean data may have an effect on the accuracy of the fatigue calculations and hence the final design of the support structure. By fitting the environmental data to probability functions, the probability of a specific environmental state can be determined from the joint probability function given in Equation 3.16. The probability

of an environmental state with arbitrary values for the wind speed, signficant wave height and peak period can then be determined. Another approach to determine the probability of occurrence is to produce scatter diagrams. The probability of occurrence for combinations of the environmental data is then calculated from the number of occurrences of the combination of the peak period, significant wave height and wind speed within set intervals. According to Schløer (2013) the bin sizes are usually set to 0.5 meters for the wave height, 1 second for the peak period and 2 m/s for the wind speed.

3.4 Integrated Analysis

When performing dynamic analyses on offshore wind turbines the structural properties and environmental loading, as well as the systems that may affect the environmental loading should be taken into account in order to obtain accurate results. Most of the available software codes for offshore wind turbines does this by integrated analysis, where the coupled response from hydro- and aerodynamic loading, the dynamics of the structure and the control system of the turbine is calculated (Schløer, 2013).

In DNV (2010a), the loading from wind and waves can be regarded as separate processes that are independent of each other in the short term. Hence, the loading from each of these processes can be calculated separately and added together by superposition to obtain the total environmental loads, and the response is calculated from the total environmental load. This is a conservative approach since coupling of the the response of the aero- and hydrodynamic loading is not accounted for. From a fatigue perspective this may be over-conservative if the applicability of this approach to the load situation is not evaluated. The alternative is to perform an integrated analysis. The loads from wind and waves will be calculated simultaneously and a more correct loading image is obtained, and the coupled response is obtained in stead of the response to the separate excitation loads. As fatigue is an important driver for the design of offshore wind turbines, integrated analysis may contribute to a more cost efficient design as the response to the loading is presicted more accurately.

Another disadvantage using simple superposition of separate loads from waves and wind is that the aerodynamic damping from the turbine at each time instant is not included in the calculations for wave loading (Seidel et al., 2005). The aerodynamic damping will vary with the wind speed and pitch angle of the blades. Thus the aerodynamic damping must be estimated carefully and conservative values must be applied to the calculation of the wave loading when calculating the response of the loading separately. As the aerodynamic damping is a significant part of the overall damping it is evident that the response to the wave loading will be overestimated when conservative damping estimates must be used.

3.5 Damping Effects

The damping ratio of offshore wind turbines is very important in a fatigue perspective, as the amplitude of the response of the structure is dependent on the degree of damping in the system. The damping ratio is inversely proportional to the amplitude of vibrations; hence it is vital to determine a correct damping level in order to obtain accurate lifetime predictions (Devrient et al., 2013). The damping contributions that are relevant for offshore wind purposes are aerodynamic damping, damping devices e.g. a tuned mass damper, vortex shedding damping. In addition, offshore damping, which includes hydrodynamic damping, structural damping and soil damping will be present. The following subchapters will describe aerodynamic, soil and structural damping in more detail.

3.5.1 Aerodynamic Damping

Aerodynamic damping plays a vital role in the dynamics of offshore wind turbines, as it constitutes a significant part of the total damping when the turbine is in operation. The effect of aerodynamic damping is essentially an aerodynamic force counteracting the fore-aft motion of the tower top of an offshore wind turbine. When the tower top moves forward the wind speed experienced by the blades of the turbine will increase slightly. This small increase in wind speed results in a small increase in thrust force on the blades of the turbine. The thrust force acts in the opposite direction of the forward motion of the tower top, and thus decreases the motion, giving a damping effect to the system. For the reverse case, when the tower top has a motion in the aft direction, the wind speed experienced by the turbine blades will be reduced and hence also the thrust force on the blades. This again reduces the motion of the tower top in the aft direction. This counteracting thrust force is related to the velocity term of the system's equation of motion and is thus comparable to damping (Cerda and van der Tempel, 2005).

For a turbine in operation, the aerodynamic loading and also the damping will be dominating for the structural response. Hence the magnitude of the loading and aerodynamic damping will have a significant importance for the structural response to any excitation loads (Schløer, 2013). It is important to note that aerodynamic damping only has an effect for the fore-aft motion of the tower. This means that the damping will decrease when the wind is not acting perpendicular to the rotor plane. However this is seldom the case as the turbine is yawed to face the wind for optimal power production. In misaligned wind and waves on the other hand, the aerodynamic damping will not be give damping to the whole excitation from the waves, only the component acting in the fore-aft direction. This means that the wave excitation will have a larger effect on the fatigue damage due to smaller damping in the side-side direction when operating in this kind of metocean conditions.

For constant speed turbines the aerodynamic damping can be estimated analytically and numerically by a number of different methods. The theoretical maximum value of damping for a given point on the blade can be found from the closed-form formula below:

$$c_{damping} = \frac{1}{2}\rho\Omega r c C_{L\alpha} \tag{3.17}$$

$$\xi_{aero} = \Omega(V_0)\frac{N_b \rho C_{L\alpha} m_{1b}}{4 M_0 \omega_n} \tag{3.18}$$

where

c_{aero} = damping constant for aerodynamic damping
ρ = density of air
Ω = rotational speed of the rotor
r = distance from the hub to the given point on the blade
c = chord of the turbine blade
$C_{L\alpha}$ = lift coefficient
ξ_{aero} = damping ratio for aerodynamic damping
N_b = number of blades on the turbine
$\Omega(V_0)$ = rotational speed as a function of wind speed
m_{1b} = First order (static) moment of the area of the chord along the blade
M_0 = modal mass
ω_n = nartural frequency

Today, most turbines installed offshore are designed according to the principle of optimal tip speed ratio. This means that the rotor speed of this kind of turbines will change according to the change in wind speed to withhold an optimal ratio between rotational speed of the blades and the incoming wind speed. The optimal tip speed ratio is the ratio at which the most power is extracted from the wind. The optimal tip speed ratio is achieved at the rated speed. Below rated speed, the blades will have a constant angle in order to operate as close to the optimal tip speed ratio as possible for the given wind speed. Above rated speed on the other hand, the blades of the turbine are pitched in order to withhold the optimal tip speed ratio. When the blades are pitched, the thrust on the turbine is also decreased, as seen in Figure 3.3, which will lead to a decrease in the aerodynamic damping as well (Van der Tempel, 2006). Hence the aerodynamic damping is very dependent on the control system for the blade pitch and the control strategy applied, making it difficult to determine the aerodynamic damping through calculations(Burton et al., 2011). Although there is no analytical expression for this change, it has been shown that aerodynamic damping is proportional/connected to the change in thrust force.

A theoretical estimate for the aerodynamic damping can be made by applying Van der Tempel's method (Van der Tempel, 2006) to time domain simulation results. From the ratio between the

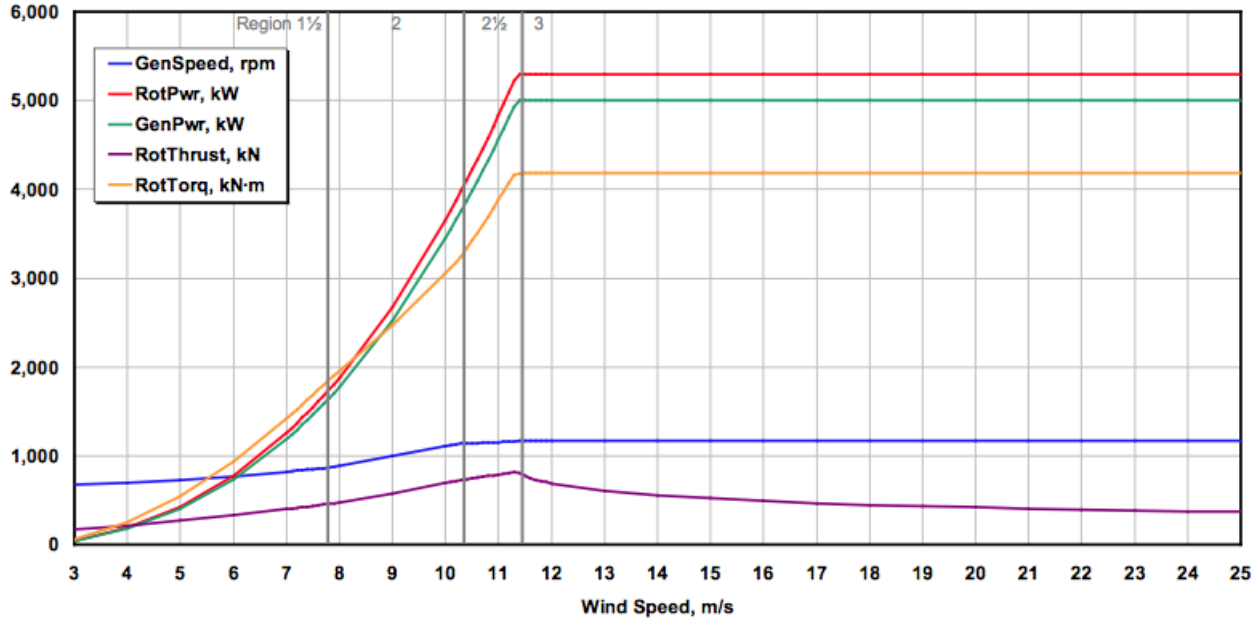

Figure 3.3: The steady state responses of the 5MW NREL reference wind turbine as a function of wind speeds, as presented in Jonkman et al. (2009).

change in thrust force and the change in wind speed normal to the rotor plane one can estimate the size of the aerodynamic damping:

$$c_{damping} = \frac{T'}{dV_d} \tag{3.19}$$

$$\xi_{aero} = \frac{T'}{dV_d}\frac{1}{2M_0\omega_n} \tag{3.20}$$

The aerodynamic damping can be obained more accurately by performing nonlinear time domain simulations in an aero-servo-hydro-elastic software. As described by Kühn (2001), the aerodynamic damping is determined by studying the transient decay of the free vibrations of the tower. By subjecting the wind turbine to loading from a turbulent wind field and a step pulse loading in a simulation, the response of the compined loading in terms of deflection of the tower top is obtained. The results from this simulation influenced by the stochastic nature of the turbulent wind field. In order to derive the damping, the stochastic part of the response must removed. This is done by assuming that linear superposition is valid, and subtracting the response from a simulation with the same wind field but without the step pulse loading from the simulation with the step pulse loading. The remaining part of the original response is regarded at the deterministic part of the response and the combined aerodynamic damping is determined by calculating the logarithmic decrement, δ, of n successive cycles of the

deterministic response according to Equation 3.21. The damping ratio is then derived from Equation 3.22. If the other damping contributions are known, the aerodynamic damping ratio is determined by subtracting these ratios from the total damping ratio.

$$\delta = \frac{1}{n} ln \frac{x_0}{x_n} \tag{3.21}$$

$$\xi = \frac{1}{\sqrt{1 + \left(\frac{2\pi}{\delta}\right)^2}} \tag{3.22}$$

3.5.2 Structural Damping

Structural damping is the damping in the structural material and is connected to the inner friction of the material and gliding within the material. This damping is often expressed in terms of Rayleigh damping (also called proportional damping), where the damping **C** is expressed as a linear combination of the mass and stiffness (Langen and Sigbjörnsson, 1979):

$$\mathbf{C} = \alpha_1 \mathbf{M} + \alpha_2 \mathbf{K} \tag{3.23}$$

Assuming that mass matrix **M** and the stiffness matrix **K** have the orthogonality properties needed for expressing the mass and stiffness in terms of modal mass $\bar{m}_i$ and modal stiffness $\bar{k}_i$, the modal damping coefficient $\bar{c}_i$ is expressed as:

$$\bar{c}_i = \alpha_1 \bar{m}_i + \alpha_2 \bar{k}_i \tag{3.24}$$

This means that the damping ratio λ_i can be expressed in terms of the natural frequencies of the modes of the structure ω_i.

$$\lambda_i = \frac{\bar{c}_i}{2\bar{m}_i\omega_i} = \frac{1}{2}\left(\frac{\alpha_1}{\omega_i} + \alpha_2\omega_i\right) \tag{3.25}$$

From Equation 3.25 it is evident that the Rayleigh damping is dependent on the natural frequency of the modes. Additionally one can see that the mass proportional damping will lead to damping of the lower mode shapes, whereas the stiffness proportional damping will be effective in damping the higher mode shapes. The OC3 project (Jonkman et al., 2007) specifies a structural damping ratio of 1% for offshore wind turbines.

3.5.3 Soil Damping

The dissipation of energy from vibrations into the soil is an important source of damping, and is known as soil damping. Soil damping comprises two types of damping; geometric damping, which is the propagation of wave energy away from the foundation, and inner material damping, which can be described approximately as the same as structural damping (Langen and Sigbjörnsson, 1979). The geometric damping will not be significant for frequencies below 1Hz (Tarp-Johansen et al., 2009). It is common to include the soil damping as Rayleigh damping, which is described in the previous subchapter. According to Langen and Sigbjörnsson (1979), the dissipation factor, giving the relative loss of energy per load cycle, can be estimated to be within the range of 4 - 10% for strucures in the North Sea. This corresponds to an equivalent damping ratio of 2 - 5%.

Although the soil damping may be significant, it is important to note that the effect of the soil damping on the entire structure is dependent on the displacement of the foundation in the surrounding soil (Tarp-Johansen et al., 2009). If the dynamic response in the foundation is insignificant, the damping effect from the soil and foundation will also have an insignificant effect on the total dynamics of the structure.

3.6 Natural Frequencies and Dynamic Response

In order to avoid resonance the natural frequency of the structure should to be outside the frequency range of any significant wave excitation. In addition, the natural frequency of offshore wind turbines cannot be within the range of frequency corresponding to the rotational speed of the blades and the blade passing frequency. These ranges are commonly referred to as 1P and 3P, where 1P, the frequency corresponding to one rotation is three times smaller than the frequency of passing blades, 3P. As the peak frequency of linear wave excitation usually is somewhat below 1P, the natural frequency of the first mode needs to be between the 1P and 3P frequency ranges to avoid resonance, as illustrated in Figure 3.4. The natural frequency of the first mode will stil be excited by waves when located between 1P and 3P, however the degree of excitation is dependent on the peak frequency of the wave spectrum and the bandwidth of the wave spectrum. Assuming the wave height is constant, increasing the peak frequency for the wave spectrum will shift the location of the spectrum closer to the natural frequency of the first mode shape. This will result in more excitation of the structure from linear wave loading as the energy content in the waves will be larger for the frequency corresponding to the natural frequency.

An increase of the bandwith of the wave spectrum will have a similar effect as described for the

increase of the peak frequency, described above. The mean valur of the peakedness parameter, 3.3, is often used for modelling of the wave spectrum DNV (2010b). However, as can be seen from equation 3.13, the value of the parameter is dependent on H_S and T_p, and should be determined for every sea state in order to represent the wave process correctly. This also means that the bandwidth of the spectrum is different for the individual sea states, which may have an impact on the response of the structure excited by these waves. If the peakedness parameter, γ, is decreased, the energy is distributed over a larger range of frequencies. This may result in a larger amount of wave excitation from linear wave loading at the natural frequency of the first mode of the offshore wind tubine, and will have a negative effect on the fatigue life.

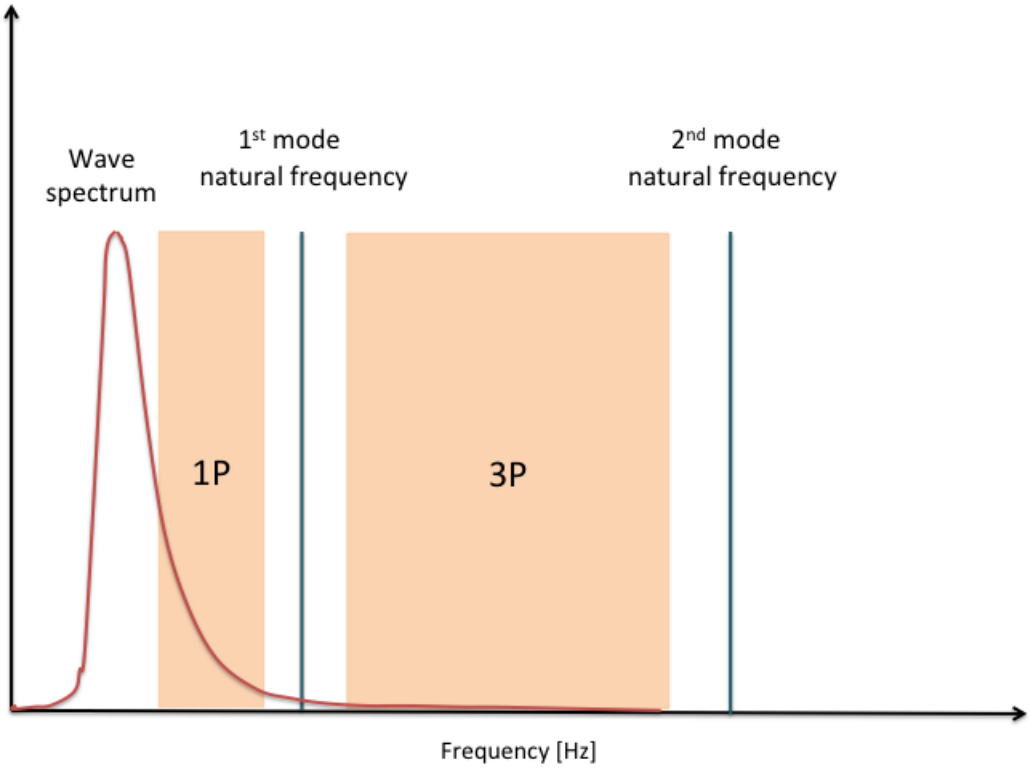

Figure 3.4: Illustration of the ranges of wave, rotation and blade passsing frequencies and the location of the 1^{st} and 2^{nd} mode natural frequencies.

The dynamic transfer function describes the dynamic amplification due to loads with a frequency close to the natural frequency of the structure. Taking the bandwidth of this function into consideration as well, the situation becomes even more complex. As the transfer function spans over a certain range of frequencies close to the natural frequency of the structure, loading within this frequency band will be amplified dynamically. Hence it becomes even harder to avoid dynamic amplification by coincidence with other excitation frequencies, such as 1P and 3P. Although the dynamic amplification of the response is largest at the natural frequency, the excitation forces with frequencies within the bandwidth of the transfer function

will lead to larger accumulated damage to the structure and a corresponding detrimental effect on the fatigue life. Thus, from a fatigue perspective it would be optimal to avoid any dynamic amplification as far as possible. However, this is at the time being not possible with such dynamically complex systems.

Another important issue in terms of the dynamic transfer function is that its bandwidth is dependent on the overall damping of the structure(Burton et al., 2011). Low damping will lead to a transfer function with a smaller bandwidth and a higher peak, causing much higher damage when the offshore wind turbine is excited within this frequency range. High damping has the opposite effect. This will give a dynamic transfer function with a larger bandwidth and a lower peak, so that loading for a wider band of frequencies will excite the structure dynamically but with smaller amplitudes.

Taking second order loading into account, the situation becomes even more complex. The second order loading, taking only sum-frequency effects into account, has its maximum at the frequency corresponding to approximately two times the peak frequency of the wave spectrum. For sea states with a peak frequency that is equal to half the natural frequency of the first mode, this means that the sum-frequency part of the second order loading will excite the offshore wind tubine dynamically. Hence, the effect of the second order loading may have a large impact on the overall response of the structure, and as a result of this the second order loading will also have an impact on the fatigue damage. This is essentially the phenomena of springing.

3.7 Springing

Springing is a non-linear resonance phenomenon that occurs when a structure is exited by wave frequencies. Faltinsen (1990) describes springing as *"... the nonlinear effects due to the quadratic velocity term in Bernoulli's equation that can create excitation forces with higher frequencies than the dominant frequency in a wave spectrum."* In principle this is a sum-frequency effect, meaning that the structure is excited by the second-harmonic of the incident waves. For most marine structures springing will not be a severe problem, as their natural frequencies are outside the ranges where nonlinear loading will be of importance. However for TLPs and bottom mounted offshore wind turbines, springing can be an issue as these structures have relatively high natural frequencies, in the range of 0.25-0.5 Hz (Faltinsen, 1990). This means that the natural frequency is outside the range of linear excitation for most of the time, but within the range of excitation by second order effects, i.e. sum-frequency effects, can occur. Hence, a resonance condition may occur when the natural frequency of the structure is excited by second order wave loads, which can result in a reduced fatigue life.

Figure 3.5 shows a wave spectrum and the corresponding linear and second order loading. As

seen from the figure, the peak of the second order loading as located at a frequency two times larger than the linear loading. It is the loading in this range that is the source of springing for offshore wind turbines.

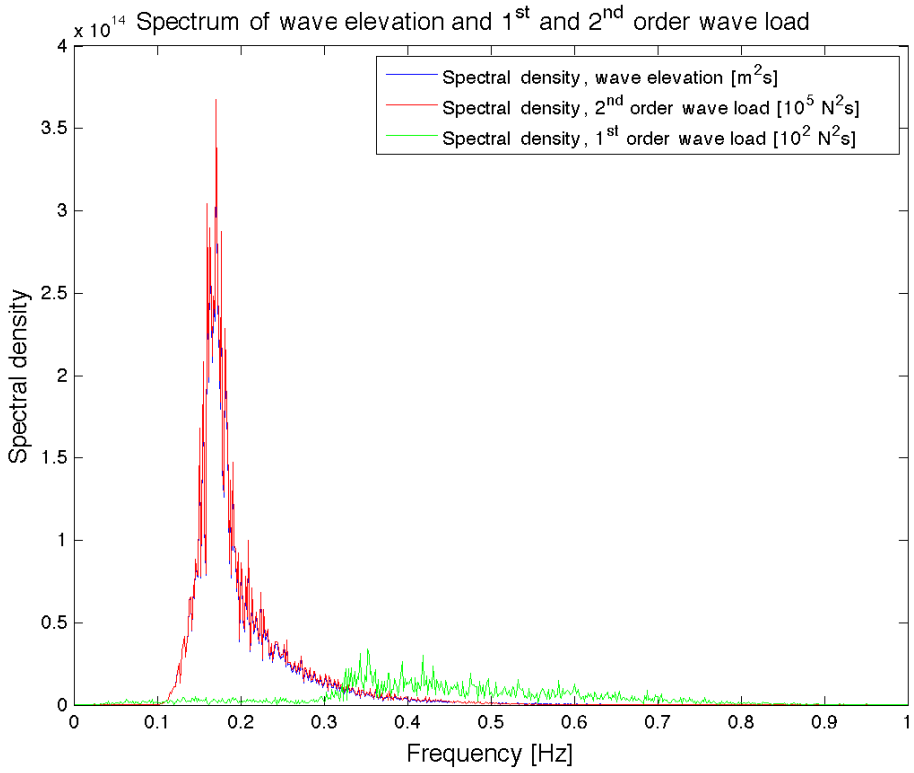

Figure 3.5: Spectra of waves and first and second order loading for $H_S = 1.5$ m and $T_p = 6$ s. Note that the spectral values have been scaled for illustrative purposes.

In the operational state, springing effects will be very small due to the aerodynamic damping (Marino et al., 2013). However, in a parked condition or in misaligned wind and waves, where the aerodynamic damping of wave excitation is small, springing may be more significant as was also shown by Marino et al. (2013). This will lead to a larger dynamic response and a corresponding detrimental effect on the fatigue life of the support structure.

In terms of structural modes of the support structure, second order wave loads are most likely to occur for the first mode natural frequency. The reason for this is that the dominant frequencies of the wave spectrum at periods that occur frequently are approximately half the size of the natural frequency of the first mode, which means that this mode may be excited by the waves in the dominant part of the wave spectrum.

3.7.1 Second Order Load Model - FNV

Morison's equation is the most commonly used formulation for calculation of hydrodynamic loads on vertical cylinders. A problem when using this formulation for calculation of hydrodynamic loading on offshore wind turbines is that it does not include nonlinear loads when the loading is dominated by mass forces, and thus it is not sufficient to describe excitation from second order loading for mass dominated structures. This can easily be seen from the formulation of Morison's equation in Equation 3.26, as the inertia term only includes linear contributions.

$$dF = \rho\pi\frac{D^2}{4}C_M a_1 + \frac{\rho}{2}C_D D|u|u \tag{3.26}$$

In order to capture the second-order loads that may cause springing, a nonlinear hydrodynamic load model must be utilized. There are a number of such models available that must be evaluated in terms of validity range, accuracy and its ability to model the second order loads correctly for the case studied in this thesis.

Faltinsen-Newman-Vinje Load Model

One non-linear wave model that has been used widely for studying the concept of ringing is the Faltinsen-Newman-Vinje model (FNV). This model is presented in Faltinsen et al. (1995) for regular waves and extended to include irregular waves by Newman (1996). This model is applicable for load calculations on fixed slender cylinders when the wave amplitude ζ_A is of the same order of magnitude as the radius a of the cylinder, and that these two parameters are small compared to the wavelength. The second order loading causing springing can be calculated by use of the second order term of the FNV-model. More correctly this means that the second order loading is calculated by long wave theory without short wave diffraction. This is the correct way of referring to this method of calculation of second order loading, however for simplicity the calculation of the second order loads by this method will be referred to as calculation of the second order term of the FNV-model for the remaining par of this thesis.

The FNV-model is derived from the linear first order velocity potential, the quadratic first order potential and the nonlinear potential by using perturbation technique and the following assumptions:

- the wavelength, λ, is long compared to the radius of the cylinder, a, $ka < a$
- the wave height,A, and the radius of the cylinder, a, is of the same order of magnitude,$A/a = O(1)$

The diffraction problem is divided into two domains. In the outer domain, far away from the cylinder, conventional linear analysis is used. In the inner domain, significant nonlinearities are present. These nonlinearities are associated with the free-surface boundary condition and thus a perturbation expansion of the inhomogeneous free surface is imposed on a horizontal plane, which moves up and down with the incident wave at the center of the cylinder(Tromans et al., 2006).

The first term of the FNV-load model is exactly the same as the inertia term of Morison's equation. Hence, as the offshore wind turbine in question in this thesis is assumed to be mass dominated, the first order wave loading from the FNV-model should be the same as the loading calculated according to Morison's equation. For this reason the FNV-model gives better results for mass dominated structures.

The FNV load model has different formulations depending on the nature of the waves that are being modeled. For both regular and irregular waves the total FNV-force is expressed as a sum of the first and higher order components originating from the total diffraction potential and the nonlinear potential. However, as only the second order term is of importance for springing, only this term will be presented here. For further information and the derivation of the FNV-model, reference is made to Faltinsen et al. (1995) for regular waves and Newman (1996) for irregular waves.

The second order load term for a regular wave $\zeta^{(1)} = Acos(kx - \omega t)$ and water depth h,is formulated as follows:

$$F_{FNV}^{(2)} = \rho\pi a^2 g^2 A^2 k \left[\frac{5}{4} + \frac{1}{4}e^{-kh}\right] \sin 2\omega t \tag{3.27}$$

For irregular waves the second order term can be formulated as by Krokstad et al. (1998) based on Newman's extension of the FNV-model to irregular waves in Newman (1996):

$$F_{FNV}^{(2)} = 2\pi\rho a^2 u_t\Big|_{z=0} \zeta^{(1)} + \pi\rho a^2 \int_{-h}^{0} w u_z \mathrm{d}z \tag{3.28}$$

It is important to notice that the FNV-model assumes a constant cross section of the circular column being subjected to wave loading. As the substructure above the suction bucket and the tower in the scope of this thesis is slightly conical, this means that the calculated second order loading will not be entirely accurate. By using the radius at the mudline, which has the largest cross section, conservatism is ensured. In addition, Krokstad and Standsberg (1995) showed that the second order force was overpredicted significantly when compared to experimental results. However the results had a better correspondence for the smallest steepness values and shortest waves, as shown in Figure 3.6. According to Krokstad et al. (1998), this overprediction of second

order loads with the FNV-model indicated that the second order load had dependency on the steepness of the waves. As the waves including the most nonlinearities are in fact the steepest waves, this overprediction should be kept in mind when evaluating the results of second order loading obtained by use of the second order term of the FNV-model.

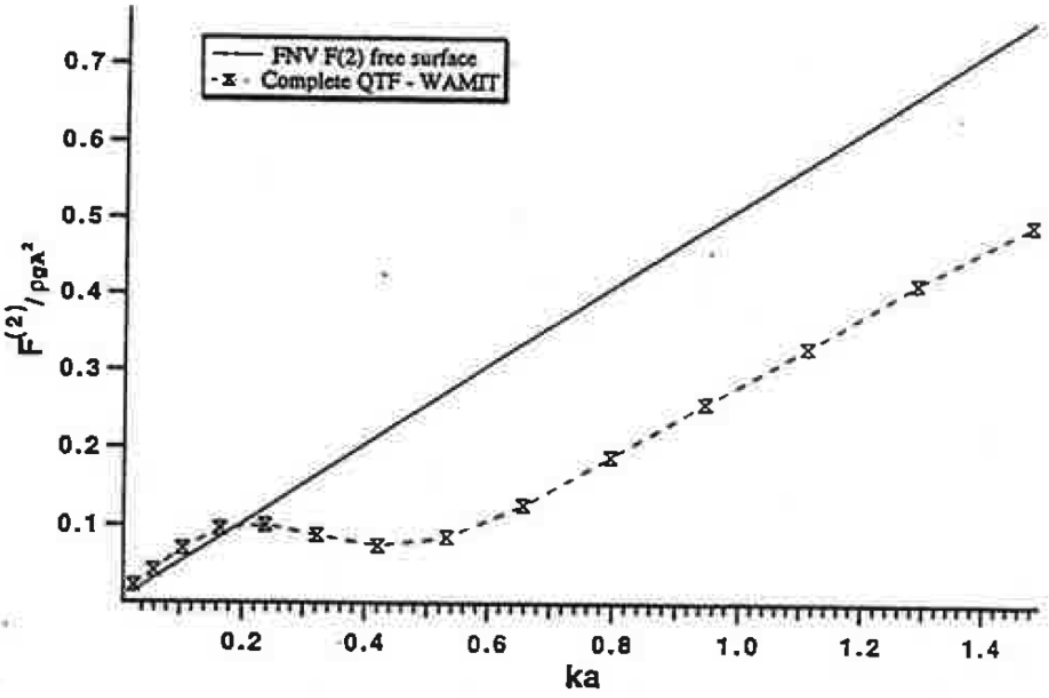

Figure 3.6: Comparison of quadratic transfer function for loads computed with the FNV second ordet term and full diffraction WAMIT as a function of normalised wavelength ka (Krokstad and Standsberg, 1995).

Chapter 4

Review of Load Cases

For fatigue design of offshore wind turbines, a range of load cases needs to be analysed to obtain the fatigue life and to ensure conservatism. These loads cases have different conditions for wind, waves and current and should include all operational states, such as power production, start-up and parked conditions. In DNV (2010a) seven load cases have been recommended for analysis of the Fatigue Limit State (FLS). These load cases are listed in Table 4.1. The load cases define the conditions that should be used to determine the loads relevant for fatigue analysis of an offshore wind turbine. In the table NTM is the abbreviation for Normal Turbulence Model, NWP is an abbreviation for Normal Wind Profile and NSS is and abbreviation for Normal Sea State.

4.1 Normal Operation in Codirectional Wind and Waves

DNV (2010a) suggests that for expected characteristic load effect distribution, in this case the distribution of stress ranges, contains load effects from two or more simultaneously acting processes, the stress ranges from each of these separate processes can be combined. As the stress ranges of the combined loading will be somewhat larger that for the separate loading processes, DNV (2010a) recommends an idealised procedure for combination of stress ranges so that conservatism is preserved. This procedure is based on a combination of stress ranges so that the largest stress range of all simultaneous load processes are added together, then the second largest, and so on.

Although it is evident that the maximum loading will occur when wind and waves are aligned, it is important to note that the response of the structure is also dependent on the dynamics of the system. This means that the maximum response to the loading does not neccessarily occur when the maximum loading occurs, since loading at the frequencies within the bandwidth of the transfer functions will lead to dynamic amplification and larger responses. Thus the response is also very dependent on the damping as this

The stress range combination method recommended by DNV (2010a) implies that the stress in calculated separately for each load process. Another option is to calculate the stress ranges from integrated analysis so that the stress ranges from the combines loading is obtained directly from the analyses. Given that the modelling of the load processes is correct, and that a

sufficient number of analyses for the given environmental states are performed to eliminate any statistical uncertainties, this procedure will give a more accurate calculation of the fatigue damage. However, it is important to note that this method will not necessarily ensure conservatism in the same way as the method recommended by DNV (2010a).

4.2 Normal Operation in Misaligned Wind and Waves

In addition the temporal variation of the loads, the directional variation must also be taken into account when evaluating a set of load cases. Both wind and waves vary in magnitude and direction, and the relative misalignment between the loads from these processes may influence the fatigue life. The load cases listed in Table 4.1, have all codirectional loading from wind and waves. However, DNV (2010a) recommends that misaligned load cases are included when considered relevant for the specific site. This may in some cases be regarded as conservative as the maximum loading on the structure will occur when the loads are codirectional. However, it is important to note that the stress ranges that are used in the fatigue analysis is a response of the loading, and is hence not necessarily connected to the loading in a linear relation. The dynamics of the system also influence the stress ranges, and hence also damping and natural frequencies.

For an offshore wind turbine subjected to wind and wave loading the largest contribution to the overall damping comes from aerodynamic damping. This damping effect only acts in the fore-aft direction. This means that for misaligned wind and waves, where the wind is acting perpendicular to the rotor disc and the waves are acting from an angle of 90° to the wind direction, there will be no aerodynamic damping for the side-side direction, which is the direction the waves are acting from. As the overall damping is much lower for the wave excitation, the effect of wave excitation will be larger than for the case with the same level of damping as the aligned loading. This means that the fatigue damage in this will be larger as well due to larger stress ranges.

4.3 Parked or Idling Wind Turbine

In a parked or idling operational condition the offshore wind turbines will have the lowest damping ratio. The reason for this is that the blades are pitched to make the thrust force as small as possible, which will make the aerodynamic damping small. Due to this absence of aerodynamic damping, these operational conditions will be most prone to fatigue damage since the overall damping is smaller than for a wind turbine in operation. This also means that

from a theoretical point of view, the effect of second order loading will be more significant for these conditions than for normal operational conditions.

Table 4.1: Recommended load cases for FLS (DNV, 2010a).

Design situation	Load case	Wind condition	Wave condition	Wind/Wave directionality	Current	Water level	Other conditions
Power production	1.2	NTM	NSS	Codirectional in one direction	Can be ignored in many cases*	Range between upper and lower 1-year WL	-
Power production plus occurrence or fault	2.4	NTM	NSS	Codirectional in one direction	Can be ignored in many cases*	Range between upper and lower 1-year WL	Control or protection system fault including loss of electrical network
Start up	3.1	NWP	NSS	Codirectional in one direction	Can be ignored in many cases*	Range between upper and lower 1-year WL	-
Normal shutdown	4.1	NWP	NSS	Codirectional in one direction	Can be ignored in many cases *	Range between upper and lower 1-year WL	-
Parked	6.4	NTM	NSS	Codirectional in multiple directions	Can be ignored in many cases*	Range between upper and lower 1-year WL	-
Parked and fault conditions	7.2	NTM	NSS	Codirectional in multiple directions	Can be ignored in many cases*	Range between upper and lower 1-year WL	-
Transport, assembly, maintenance and repair	8.3	NTM	NSS	Codirectional in multiple directions	Can be ignored in many cases	Range between upper and lower 1-year WL	-

Chapter 5

Metocean Conditions

The NORA10 metocean data from the given location at Doggerbank have been analysed in order to determine the probability of the different environmental states and to give a basis for determining which load cases to investigate for effects of misalignment and second order loading. The wind data are given for a height of 100 m, while the wave data are the data corresponding to wind driven sea.

Table A.17 gives the probability of occurrence for each sea state bin based on the hindcast data in the NORA10 database from September 1, 1957 to December 31, 2010. As can be seen from the table the most probable significant wave heights are in the range between 0 and 2.0 m, while the most probable peak periods are between 3 and 7 s.

Scatter diagrams are computed for each wind speed for the analyses of the effect of second order loading, without including the misalignment between wind and waves. The wind speed has been sorted into bins of 2 m/s, significant wave height into bins of 0.5 m and the peak periods into bins of 1 s. These bin sizes correspond to the bin sizes that are normally used to produce scatter diagrams (Schløer, 2013). Scatter diagrams are also computed for the relative angle between the wind direction and the wave direction. The bin sizes for the relative angle are set to 15°. These scatter diagrams are found in Appendix A.1 and A.2.

Table 5.1: Scatter diagram for H_S and T_p, occurences given in percentage of total number of occurrences. The values for H_S and T_p denotes the highest value for each bin.

Hs\Tp	1	2	3	4	5	6	7	8	9	10	11	12	13	14	15	16	17	SUM
0.5	9.858	-	11.229	9.036	0.273	0.048	0.010	-	-	-	0.001	-	-	-	-	-	-	30.455
1.0	-	-	0.203	6.992	10.810	2.933	0.043	0.007	0.005	0.002	-	-	-	-	-	-	-	20.994
1.5	-	-	-	0.042	3.268	9.000	2.814	0.029	0.008	0.003	0.001	0.001	-	-	-	-	-	15.166
2.0	-	-	-	-	0.101	3.818	6.138	0.705	0.076	0.010	0.001	0.001	0.001	-	-	-	-	10.851
2.5	-	-	-	-	-	0.355	5.494	1.437	0.520	0.117	0.006	0.003	0.001	0.001	-	-	-	7.934
3.0	-	-	-	-	-	0.007	2.442	1.960	0.752	0.321	0.071	0.001	0.001	-	-	-	-	5.555
3.5	-	-	-	-	-	0.001	0.370	1.683	1.019	0.397	0.185	0.029	0.002	-	-	-	-	3.687
4.0	-	-	-	-	-	-	0.017	0.591	0.955	0.464	0.216	0.071	0.007	-	-	-	-	2.321
4.5	-	-	-	-	-	-	0.001	0.073	0.548	0.461	0.216	0.110	0.025	0.001	-	-	-	1.435
5.0	-	-	-	-	-	-	-	0.003	0.132	0.293	0.216	0.103	0.037	0.002	-	-	-	0.786
5.5	-	-	-	-	-	-	-	-	0.017	0.137	0.116	0.087	0.049	0.008	-	-	-	0.414
6.0	-	-	-	-	-	-	-	-	-	0.033	0.064	0.040	0.049	0.013	0.002	-	-	0.203
6.5	-	-	-	-	-	-	-	-	-	0.004	0.023	0.024	0.024	0.012	0.003	-	-	0.091
7.0	-	-	-	-	-	-	-	-	-	0.001	0.012	0.012	0.016	0.012	0.001	-	-	0.055
7.5	-	-	-	-	-	-	-	-	-	-	0.006	0.004	0.007	0.008	0.006	-	-	0.032
8.0	-	-	-	-	-	-	-	-	-	-	-	0.003	0.002	0.006	0.004	-	-	0.014
8.5	-	-	-	-	-	-	-	-	-	-	-	0.002	-	0.001	0.001	-	-	0.004
9.0	-	-	-	-	-	-	-	-	-	-	-	-	-	-	0.001	-	0.001	0.002
9.5	-	-	-	-	-	-	-	-	-	-	-	-	-	-	-	-	-	0.000
10.0	-	-	-	-	-	-	-	-	-	-	-	-	-	-	-	-	0.001	0.001
SUM	9.858	0.000	11.432	16.069	14.453	16.162	17.329	6.488	4.032	2.246	1.135	0.490	0.221	0.065	0.019	0.000	0.002	100.000

5.1 Directionality of Wind and Waves

A wind rose and wave rose have been computed from the metocaen data to give an indication of the degree of misalignment between the wind at a height of 100 m and waves. The roses are plotted in correspondence with the compass directions, so that 0° is North, 90° is East, 180° is South and 270° is West. By comparing the wind rose in Figure 5.1 and the wave rose in Figure 5.2, it is seen that the dominating direction of both the wind and the waves coincide well. The wind is more evenly distributed in its direction than the waves, which have most of the waves coming from the south-west at an angle of 225°. The most frequently occurring wind directions are within the range between 217.5° and 247.5°. However, the difference in occurrence between the different directional bins is smaller for wind than for waves.

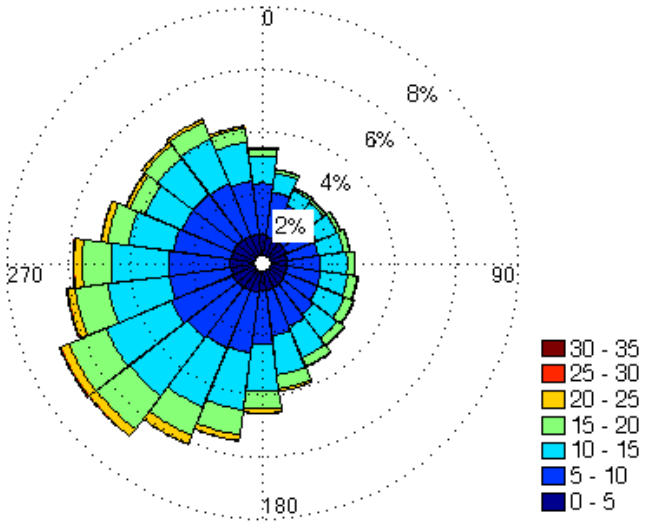

Figure 5.1: Wind rose for wind speed at 100 m height at Doggerbank, based on NORA10 data.

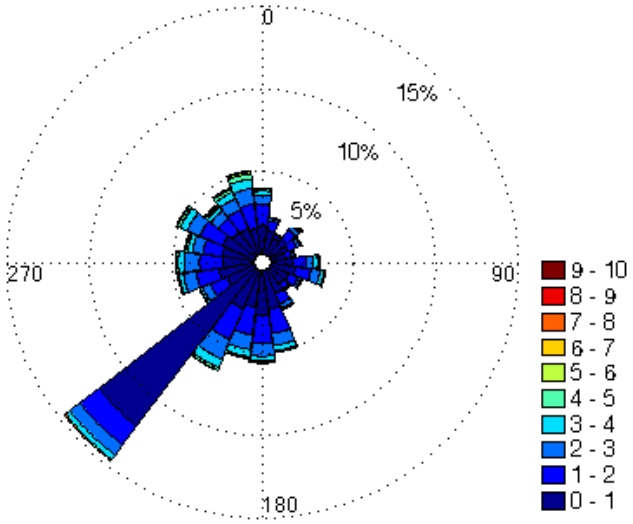

Figure 5.2: Wave rose for wind driven sea at Doggerbank, based on NORA10 data.

5.2 Misalignment between Wind and Waves

As the wind and wave roses does not give any information about the angle between the wind and waves for every 3 hour period, the relative angle is computed for each environmental state given in the NORA10 data. The absolute values of the misalignment angle have been computed, and the distribution of the misalignment in percentage of total occurrences over 180° is given in Figure 5.3. The angles are sorted into bins of 5° to show how the distribution changes with increasing angles.

As is seen from the distribution plot, the misalignment angles with the largest probability of occurrence are in the range between 0° and 20°. Approximately 90% of the misalignment angles are in the range between 0° and 30°. From the distibution one can clearly see that the degree of misalignment for this site at Doggerbank is not very large, and there are few occurrences in the data where the angle of misalignment is larger than 30°.

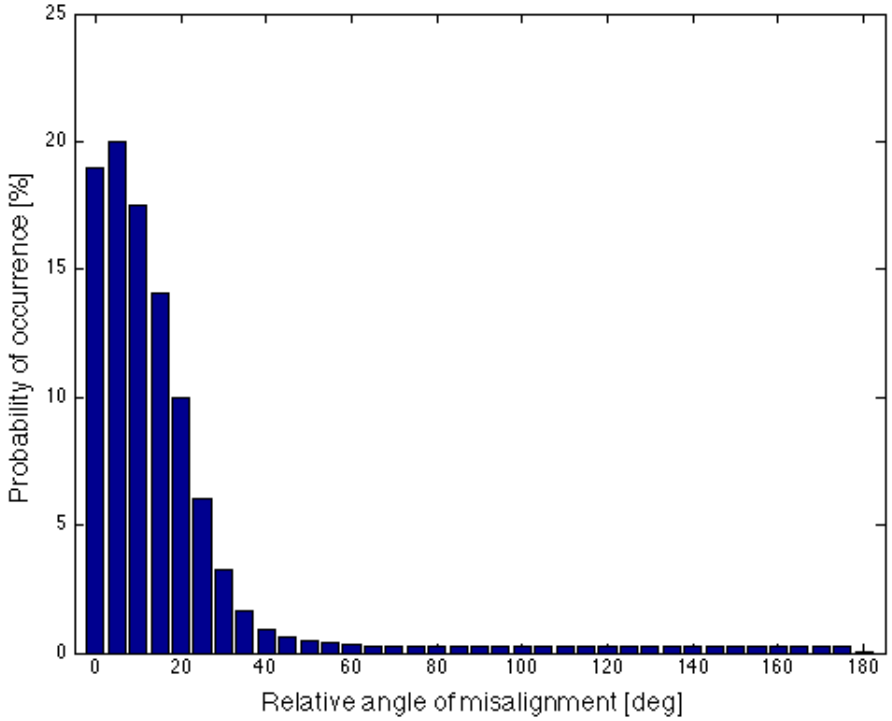

Figure 5.3: Distribution of misalignment angles, given as percentage of total number of enviromental states, based on NORA10 data.

Scatter diagrams for the sea states at different relative angles between the wind and waves are also computed for misalignment angles between 0° and 90°, to form the basis for selection of environmental states for the investigation of the effect on misalgned wind and waves. The relative angle is divided into bins with a size of 15° and one scatter diagram is computed for each bin. These bins are denoted by the mean value for each bin. The probabilities of each misalignment bin are listed in Table 5.2 below. The scatter diagrams are presented in Appendix A A.2.

Table 5.2: Probability of each misalignment bin.

Relative angle [°]	0	15	30	45	60	75	90
Probability of occurrence [%]	33.841	47.696	14.512	2.478	1.094	0.859	0.881

5.3 Wind Speed

The wind speed at a height of 100 meters is also processed in order to determine the probabilities of each wind speed. The histogram in Figure 5.4 below gives the probability of occurrence for each wind speed bin.

Figure 5.4: Histogram of the probability of occurrence for wind speeds, given for intervals of 2 m/s.

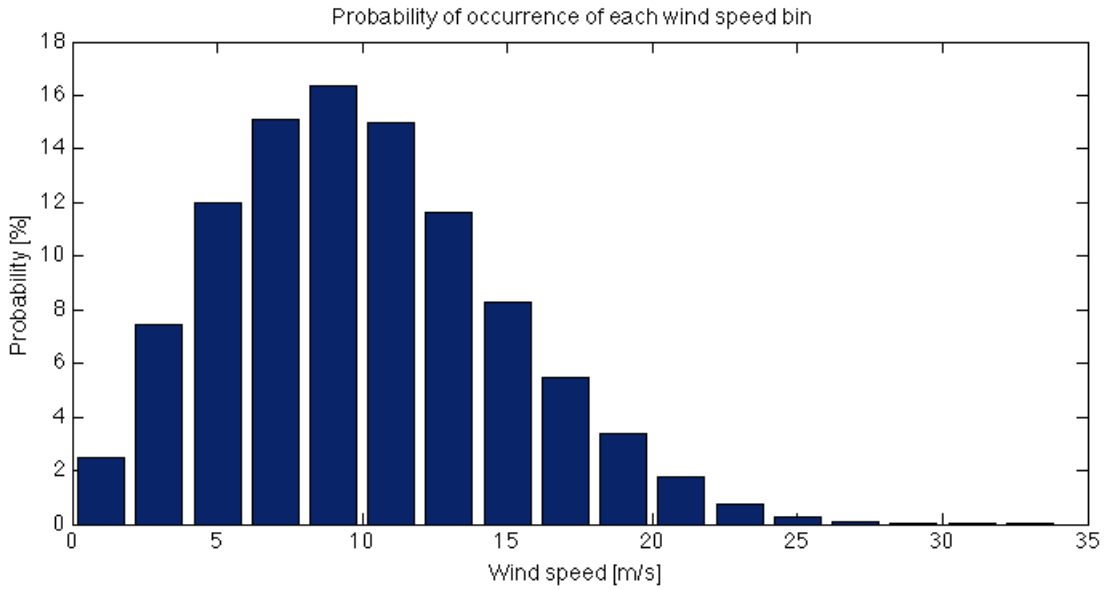

As seen from the histogram the bin with wind speeds between 8 m/s and 10 m/s has the largest probability of occurrence.

A scatter diagram has also been computed for the wind speeds and misalignment angles to be able to determine which wind speeds to use in the load cases for the investigation of the effect of misaligned wind and waves on the fatigue damage. This is given in Table 5.3. The wind speed bins are denoted by the highest value in the interval while the angles are given by the mean value of each bin.

Table 5.3: Scatter diagram for wind speed at 100 meters and misalignment angle. Probabilities given in percentage of total number of occurrences.

Wind Speed / Angle	0	15	30	45	60	75	90	TOT
2	0.105	0.223	0.204	0.208	0.255	0.211	0.218	1.424
4	1.070	0.999	0.664	0.603	0.563	0.539	0.557	4.994
6	5.177	4.902	1.393	0.334	0.116	0.105	0.103	12.131
8	6.516	6.773	1.896	0.468	0.056	0.003	0.003	15.714
10	6.297	8.272	2.127	0.318	0.066	0.001	0.000	17.081
12	5.017	8.155	2.217	0.187	0.021	0.001	0.000	15.597
14	3.477	6.516	2.010	0.131	0.008	0.000	0.000	12.142
16	2.214	4.821	1.490	0.118	0.004	0.000	0.000	8.646
18	1.274	3.268	1.123	0.053	0.001	0.000	0.000	5.718
20	0.730	2.030	0.709	0.029	0.002	0.000	0.000	3.501
22	0.373	1.078	0.383	0.013	0.003	0.000	0.000	1.850
24	0.161	0.424	0.187	0.009	0.000	0.000	0.000	0.781
26	0.047	0.166	0.080	0.003	0.000	0.000	0.000	0.295
28	0.015	0.050	0.024	0.003	0.000	0.000	0.000	0.092
30	0.005	0.014	0.005	0.001	0.000	0.000	0.000	0.025
32	0.003	0.003	0.001	0.000	0.000	0.000	0.000	0.007
34	0.001	0.002	0.000	0.000	0.000	0.000	0.000	0.003
TOT	32.481	47.696	14.512	2.478	1.094	0.859	0.881	100

5.3.1 Choice of Environmental States to be Used in Investigations

As it is very time consuming to perform analyses for all environmental states that are relevant for the location of the offshore wind turbine at Doggerbank, a number of environmental states are chosen for the analyses. The choice of environmental states is based on the hindcast data presented in the above subchapters.

The choice of load cases for the investigation of the effect of misalignment between wind and waves is based on the computed scatter diagrams and probability of each direction bin. The sea states with a peak period between 2 and 4 seconds and a significant wave height between 0 and 0.5 meters are the most probable sea states for all the directional bins. These sea states are disregarded as they will not have a great impact on the response of the structure for one individual sea state. Among the more probable sea states with a higher significant wave height and higher period is the sea state with a peak period between 5.0 and 6.0 seconds and a wave height between 1.0 and 1.5 meters. As this sea state bin is among the bins with the highest probability of occurrence for several of the directions, this bin will be used for the sea states investigating the effect of misalignment on the fatigue life of the offshore wind turbine. In order to not have a period that is too close to the natural period of the substructure, a peak period of 6.0 seconds is chosen. The highest significant wave height within the bin is also chosen as this will give a larger effect of the wave loading.

As the probability of occurrence for the three largest angles is very small, the probability of each environmental state within these direction bins will be low compared to smaller angles of misalignment. For this reason the bins with 60° and 75° misalignment are not included in the load cases. One load case with a misalignment of 90° is however included as this will be the

situation with the least damping in the side-side direction, as the waves are acting perpendicular to the wind. This load case does not exist in the wave data from NORA10, but is included to investigate how the fatigue damage is affected if this misalignment should occur.

The wind speed for the misaligned load cases is selected as the wind speed for which this sea state is the most probable. From the computed scatter diagrams for each wind speed bin at a height of 100 meters, the probability of the sea state is found to be highest for a wind speed between 8 and 10 m/s when the wind speed is the same for all load cases. A wind speed of 8.3 m/s is hence chosen.

The probability of the environmental states and the environmental parameters are given in Table 5.4 below.

Table 5.4: Probability of each misalignment bin.

Load case	2.1	2.2	2.3	2.4	2.5
Significant wave height, H_S [m]	1.5	1.5	1.5	1.5	1.5
Peak period, T_p [s]	6.0	6.0	6.0	6.0	6.0
Mean wind speed at hub, U_{hub} [m/s]	8.3	8.3	8.3	8.3	8.3
Relative angle [°]	0	15	30	45	90
Probability of occurrence, sea state [%]	3.126	4.699	1.126	0.054	-
Probability of occurrence, environmental state [%]	0.534	0.803	0.192	0.092	-

For investigation of springing effects on the fatigue life, it is desirable to have sea states that will demonstrate the which range of frequencies that are relevant for springing and sea states that will demonstrate the effect of steepness on the magnitude of the second order loading. In addition it is desirable to trigger resonance of the first mode when investigating springing effects. It is also interesting to investigate whether the level of damping will alter the effect of the second order loading. These criteria have resulted in a total of 12 environmental states that are divided into groups listed in Table 5.5. The sea state parameters have been chosen based on their expected ability to demonstrate desired effects, while the wind speed is chosen in order to give the highest probability for the environmental state.

Table 5.5: Probability of each misalignment bin.

Load case	3.1	3.2	3.3a	3.3b	3.3c	3.3d	3.4a	3.4b	3.4c	3.5a	3.5b	3.5c
Sign. wave height [m]	1.0	1.5	2.5	2.5	2.5	2.5	2.5	2.5	2.5	3.0	3.5	4.0
Peak period [s]	4.5	5.5	6.0	7.0	8.0	9.0	6.0	7.0	8.0	8.0	8.0	8.0
Mean wind speed [m/s]	8.3	11.1	13.9	13.9	13.9	13.9	0	0	0	16.7	19.5	19.5
Probability of occ. [%]	3.7	1.63	0.02	1.78	0.92	0.35	-	-	-	0.61	0.78	0.21

Chapter 6

Approach of Investigations and Modelling

The methods and models used for the investigations of the effect of misalignment, second order load effects and damping on the fatigue damage of the offshore wind turbine is described in the following subchapters. The approach of investigation of the main objectives are outlined first, together with the load cases used for the investigation. Further information about the models used in the dynamic analysis follows in the next subchapter. The offshore wind tubine defined in Chapter 2, Scope and Limitations, is used for all the analyses.

6.1 Approach

6.1.1 Damping Estimation

The aerodynamic damping of the offshore wind turbine is predicted by performing logarithmic decay tests in Fedem Windpower according to the procedure outlined in Kühn (2001) and Burton et al. (2011). No wave loading is applied in any of these logarithmic decay simulations. The first test determines the overall damping of the structure without wind, meaning the overall damping of the wind turbine excluding aerodynamic damping. A constant load is applied to the hub of the turbine, and then removed over a single time step, initiating vibrations in the tower. The displacement of the tower is recorded and the logarithmic decrement is calculated from the time series of the vibrations.

The same test will be performed for turbulent wind with wind speeds at 2 m/s intervals at the reference height of 10 m, corresponding to intervals of 2.8 m/s at hub height. The turbulent wind is applied in addition to the constant step pulse load at the hub, to investigate how the overall damping changes with wind speed when the aerodynamic damping is included. The same simulation is performed without the constant step pulse load and the results are subtracted from the original simulation to obtain the deterministic part of the free vibrations. The duration of the simulations is set to 500 seconds and the constant loading is removed after 100 seconds in order to avoid any transient effects in the start phase of the simulation. An overview of the logarithmic decay tests that are performed is given in Table 6.2.

Finally, the damping ratio corresponding to the aerodynamic damping is determined by

subtracting the damping ratio of the simulation without aerodynamic loading from the total damping ratio at each wind speed.

Table 6.1: Logarithmic decay load cases for investigation of damping.

Load case	1.0	1.1	1.2	1.3	1.4	1.5	1.6	1.7	1.8	1.9
Wind speed, U_{10} [m/s]	0	2	4	6	8	10	12	14	16	18
Wind speed U_{hub}[m/s]	0	2.7	5.5	8.3	11.1	13.9	16.7	19.5	22.3	25.1
Constant load [kN]	10	80	80	80	80	80	80	80	80	80

6.1.2 Investigation of Effects of Misalignment

The investigation of the effects of misalignment on the fatigue damage is conducted by performing dynamic analysis of the offshore wind turbine for a set of load cases with selected environmental states with different angles of misalignment between wind and waves. The results of these analyses are them compared to the corresponding set of load cases with no misalignment. The direction of the incoming wind is the same for all analyses, whereas the direction of the incoming waves is changed by altering the definition of the coordinate system of the waves in Fedem Windpower, so that it corresponds to the desired angle of misalignment. All analyses are performed with wind loading, as the lack of aerodynamic damping in the side-side direction of the offshore wind turbine is expected to give increase in fatigue damage for the load cases with misalignment.

An investigation into the effect of second order loading on the load cases for misaligned wind and waves is also performed. As the aerodynamic damping contribution to the damping of waves is smaller for the misaligned load cases, the effect of springing might be even larger for these load cases. Hence, the same analyses are also performed using the first and second order terms of the FNV-method to calculate the wave loading.

Table 6.2: Load cases for investigation of misalignment.

Load case	2.1	2.2	2.3	2.4	2.5
Wind speed hub height, U_{hub} [m/s]	8.3	8.3	8.3	8.3	8.3
Direction [°]	0	15	30	45	90
Peak period, T_P [s]	6.0	6.0	6.0	6.0	6.0
Significant wave height, H_s [m]	1.5	1.5	1.5	1.5	1.5

6.1.3 Investigation of the Effect of Springing

The investigation of the impact of second order loading is investigated for 12 load cases. All load cases are simulated in Fedem Windpower using both Morison's equation and the first two terms of the FNV-method for calculation of the wave loads. Simulations of load case 3.1 and 3.2 are performed in order to investigate the response of the offshore wind turbine for environmental states where the second order loading is expected to have no effect on the response of the offshore wind turbine. The environmental state of these two load cases are, as mentioned in the previous chapter, among the most probable environmental states.

Load case 3.3a to 3.3d investigates the effect of second order loading with changing periods. The significant wave height, H_S and the wind speed at hub height, U_{hub} are kept constant, while the peak period of the wave spectrum is changed for each simulation.

Three load cases, 3.4a - 3.4c, corresponding to a load situation where the turbine is parked are also performed. As the wave loading will dominate over the wind loading in these load cases, since the turbine blades are pitched to give the minimum thrust force on the turbine, the wind speed is set to 0 m/s. These load cases are performed in order to investigate the effect of the second order loading when there is negligible aerodynamic damping, and are expected to represent the worst case scenario in terms of responses to second order loading.

The last three load cases, laod case 3.5a to 3.5c are analysed in order to investigate whether increased steepness of the waves will have any effect on the response to the second order loading. The significant wave height is increased by 0.5 meters for each load case, while the wind speed is set as the wind speed giving the highest probability of occurrence for the environmental state.

The dynamic analyses are performed using the software Fedem Windpower, a software customized for offshore wind turbines.

6.2 Finite Element Model of Wind Turbine and Substructure

6.2.1 Rotor and Nacelle Assembly

The rotor and nacelle assembly used for the model in Fedem Windpower is a sample 5 MW turbine supplied by Fedem together with the software. The model is based on the NREL 5MW turbine, and the main characteristics of the turbine are listed in Table 2.1.

Table 6.3: Load cases for investigation of springing.

Load Case	Significant wave height H_S [m]	Peak period T_P [s]	Mean wind speed hub height U_{hub} [m/s]
3.1	1.0	4.5	8.3
3.2	1.5	5.5	11.1
3.3a	2.5	6.1	15.3
3.3b	2.5	7.0	15.3
3.3c	2.5	8.0	15.3
3.3d	2.5	9.0	15.3
3.4a	2.5	6.0	0.0
3.4b	2.5	7.0	0.0
3.4c	2.5	8.0	0.0
3.5a	3.0	8.0	16.7
3.5b	3.5	8.0	18.1
3.5c	4.0	8.0	19.5

6.2.2 Tower

The tower is modelled by beam elements with a diameter of 5 m and two lengths. The elements from the interface between the tower and the substructure and 10 m upwards to z = 30 m, are modelled by elements with a length of 2 m. The upper part of the tower, from z = 30 m to z = 95.1 m are modelled with beam elements with a length of 13.2 m. The choice of fewer elements in the upper part of the tower is based on the lesser need for accurate load calculation in this part of the structure, as the focus of the thesis is the loading on the substructure and foundation.

6.2.3 Substructure

The substructure is also modelled by means of beam elements, however with for this part of the model the diameter decreases from 8 m at the mudline, to 6 m at the interface between the tower and substructure at z = 20 m. 130 beam elements with a length of 0.5 m each. This part of the structure is grouted from the mudline up to z = 15 m. The inner diameter of the substructure shaft with grouting included is 5.84 m, which is the same as the inner diameter for the rest of the remaining part of the substructure. In order to take the increased stiffness due to the grouting into account, an equivalent wall thickness and material properties have been applied to each beam element to obtain the stiffness and mass corresponding to the physical substructure that is modelled.

A damping ratio of 0.75% has been applied to all the elements in the model as of a stiffness proportional damping. Only stiffness proportional damping has been used, as the mass proportional damping is most efficient at lower frequencies. The stiffness proportional damping is assumed to be sufficient for the damping of the natural frequency of the first mode of the support structure. The damping ratio has been chosen lower than the specified damping in the OC3 project. The conservative choice of a lower structural damping is made as the effect of second order loading is assumed to be more pronounced when a lower damping level is chosen.

6.2.4 Suction Bucket Foundation

The suction bucket model is modelled by a finite element model that is integrated in the soil model. By using this modelling approach, the material properties of the suction bucket and the soil can be kept separate while the soil-structure interaction is maintained in the model. The dimensions of the bucket have been chosen based on an internal study performed for Statkraft (Fedem Technology AS, 2012). This study concluded on a diameter of 20 m and a skirt length of 14 m for the bucket foundation for an offshore wind turbine at 45 m water depth.

The factor for stiffness proportional damping for the foundation and the surrounding soil is set to a value of 0.0045. This is a very conservative value for the damping, as this corresponds to a damping ratio of 0.3%. The choice of the low damping is made on the same basis as the structural damping in the rest of the support structure.

6.3 Environmental Conditions

6.3.1 Wave Model and Wave Loading

For the analyses of the fatigue damage accumulated for the offshore wind turbine, a linear wave model is used and irregular waves are created from the JONSWAP spectrum. This choice is regarded to have limited implications on main objectives of this thesis, as the objective is to investigate the effects of springing/sum-frequency effects and misalignment of the fatigue life of the structure. The choice of linear wave theory is also based on the limitations of Fedem Windpower, as there is a limited choice of wave theories that are included in the software.

By default, irregular linear waves are subjected to Wheeler strethcing in Fedem. When using linear wave theory, the wave kinematics are only calculated to the mean sea level, thus in order to obtain wave kinematics all the way to the free surface, stretching techniques must be used.

By use of Wheeler stretching the wave kinematics at the mean sea level is transferred to the free surface. This is done by computing the velocity of each frequency component in the time record for the waves, and strecthing the vertical component for each step according to Equation 6.1 (DNV, 2010b).

$$z = \frac{z_s + \eta}{1 + \frac{\eta}{d}} \tag{6.1}$$

for

$$-d < z < 0; -d < z_s < \eta$$

6.3.2 Wind Model and Wind Loading

Turbulent wind is modeled by means of the Kaimal spectrum for different mean wind speeds. Time series of turbulent wind are created by use of TurbSim, a stochastic inflow turbulence tool developed by NREL (Jonkman, 2009). Tursim generates turbulent wind according the IEC61400-1 to -3 and a set of predefined parameters that are set in the input file. The power law given in Equation 3.9 is used to model the wind profile. The turbulence intesity used in all generated wind files is set to a value of 0.16.

The aerodynamic loads are obtained by use of AeroDyn which is implemented in Fedem Windpower. The aerodynamic loading on the blades is calculated by means of the Blade Element Method, which is the most common method for calculation of aerodynamic loads.

6.3.3 Soil Model

As suction buckets are outside the validity range of the p-y curves, commonly used for soil modelling in the industry, these curves cannot be used for the analyses. In stead the soil is modelled as a three dimensional finite element model. The model is based on the soil stiffness in the Doggerbank zone and represents a two layered soil, where the upper part consists of sand and the lower part of soft clay as seen in Figure 6.1. The soil properties for each layer are listed in Table 6.4 as given in Fedem Technology AS (2012).

As already mentioned, the bucket is modelled in the same finite element model as the soil. An advantage of using a finite element volume model is that the bucket can be included in the same model, and that the stiffness of the soil and the material can be modelled separately. The alternative to this approach is to represent the properties of both the soil and the suction bucket foundation by use of a rotational spring with six DOFs at the mudline. The preanalysis required

to determine the stiffness of this spring is very extensive, and a finite element volume model is thus preferred.

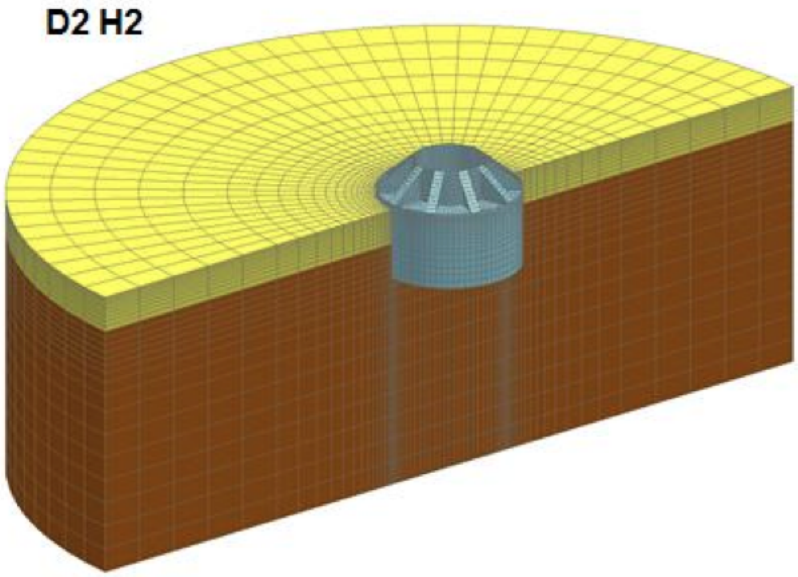

Figure 6.1: Two-layered soil model including bucket.

Table 6.4: Soil properties used in soil model.

Elevation below mudline [m]	Soil type [-]	Effective weight [kN/m^3]	Undrained shear strength [kPa]	Internal friction Φ [°C]	Cohesion C [kPa]	CPT cone resistance [MPa]		E_{dyn} [kN/m^2]	E_{stat} [kN/m^2]
						Top	Bottom		
0 - 3	Medium dense sand	10.0	-	37	0	0.0	7.5	69000	34500
3 - 40	Clay till	10.0	250	-	-	5.0	5.0	188000	37600

6.4 Post-processing

6.4.1 Spectral Analysis

In order to investigate the response of the offshore wind turbine in the frequency domain, spectra for the wave elevation, first and second order loading, mudline moment and mudline shear force are produced. The spectra show the distribution of the loading and response for all frequencies. This means that resonance occurrences due to both first and second order loading can be identified. The spectra are plotted in Matlab, using the predeveloped function SPEGEN_T. This code transforms the time series to spectra by employing FFT, a filter and a user defined number of windows. In the generation of the wave and response spectra 6 windows are used. This number is lower than what is recommended by Chakrabati (1987), however a larger number of windows will smoothen the spectrum even more, so that important peaks in the spectrum might be lost in the spectral representation.

6.4.2 Calculation of Fatigue Damage

The fatigue damage will be predicted at the mudline, as this is the location where the moment will be the largest, since this point is the furthest from the from the point of attack of the various loading. The time series of the loading are post-processed using a Matlab script that calculates the fatigue damage. The rainflow counting function from Wafo (**?**) is used for rainflow cycle counting. The script has been verified by calculating the fatigue damage from a time series of regular waves with an amplitude og 2 meter and period of 10 seconds, and comparing the resulting fatigue damage with hand calculations. Both the script and the hand calculations gave the same result with a damage of 0.0015.

The damage is calculated according to S-N-curve D for corrosion protected structures in sea water as defined in DNV (2012). A utilization factor of 3 is applied as required in DNV (2010a), and a stress concentration of 1.0. The weld detail at the interface between the lid of the bucket and the rest of the substructure should have a stress concentration factor that is larger than 1.0. However a detailed hot spot analysis of the weld details is required to determine this factor. This is considered outside the scope of the thesis and a stress concentration factor of 1.0 is applied since the sensitivity of the fatigue life to the loading will still be demonstrated. For the same reason the flanges supporting the substructure at the interface with the bucket are disregarded in the fatigue analysis.

In order to calculate the stress at the mudline in the Matlab script, the inner diameter at the mudline is needed. As the cross section of the substructure elements and the material properties

of each element are adjusted to model grouting at the inside, the inner diameter in the finite element model does not correspond with the inner diameter needed to compute the stress in the cross section. Hence, an equivalent inner diameter must be derived. By using the stiffness of the cross section at the mudline as the dimensioning parameter, an equivalent wall thickness for the mudline cross section is obtained. The equivalent inner diameter obtained from this calculation of 7.879 meters and this diameter is applied in the fatigue calculations.

For load cases with misalignment the fatigue damage must be calculated using both mudline moment about the y-axis and the about the x-axis, corresponding to the fore-aft moment and side-side moment. As one cannot predict the exact point along the cross section where the maximum damage will occur for the misaligned load cases, the fatigue damage is calculated for 8 evenly distributed points along the half the cross section at the mudline as illustrated in Figure 6.2. The stress at the opposite point of the cross section will have the same value only the opposite sign. Hence, the fatigue damage is only calculated for half the cross section. The point where the maximum damage occurs will be used for evaluation of the fatigue damage.

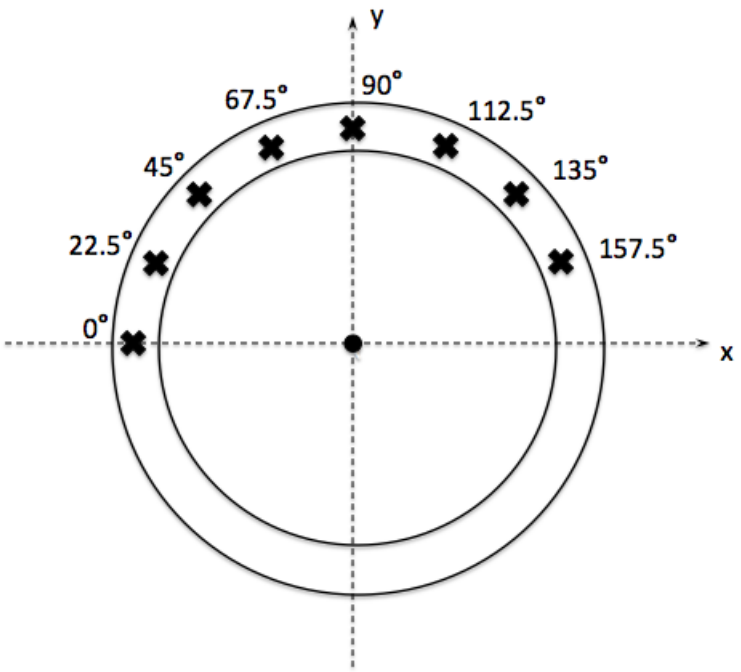

Figure 6.2: Illustration of points along the mudline cross section where the fatigue damage will be assessed. The angles are given relative to the x-axis, which is the same as the direction of the wind for the misaligned load cases.

Chapter 7

Results

Simulations have been performed to investigate the damping effects and the effect of misalignment and springing, on the fatigue damage on the current offshore wind turbine. The mudline moment about the y-axis will in the following chapter be referred to as the fore-aft moment, and the moment about the x- axis will be referred to as the side-side moment. This terminology is used in order for the reader to more easily understand the connection between the moments and the direction of the excitation loads. The results are presented in the following subchapters. Observations in the results are commented for each load case and trends summarised at the end of every subchapter.

7.1 Damping

7.1.1 Structural Damping Contribution

The damping of the offshore wind turbine without accounting for the aerodynamic damping is determined for load case 1.0 by means of a logarithmic decay test with no wind or waves applied. As seen from the time series of the displacement of the tower top in the fore-aft direction in Figure 7.1, it takes 400 seconds until the vibrations are fully damped. This indicates that the damping in the structure is low.

The logarithmic decrement and the corresponding damping ratio is determined by calculation of the logarithmic decrement with x_0 as the amplitude of the first oscillation after the removal of the step pulse load at 100 seconds and x_n given by the amplitude of the last full oscillation of the time series. The values used in the calculation and the results are given in Table 7.1. The resulting damping ratio is in correspondence with the damping factor applied for the stiffness proportional damping, as defined in 6.2.2 Tower and 6.2.3 Substructure.

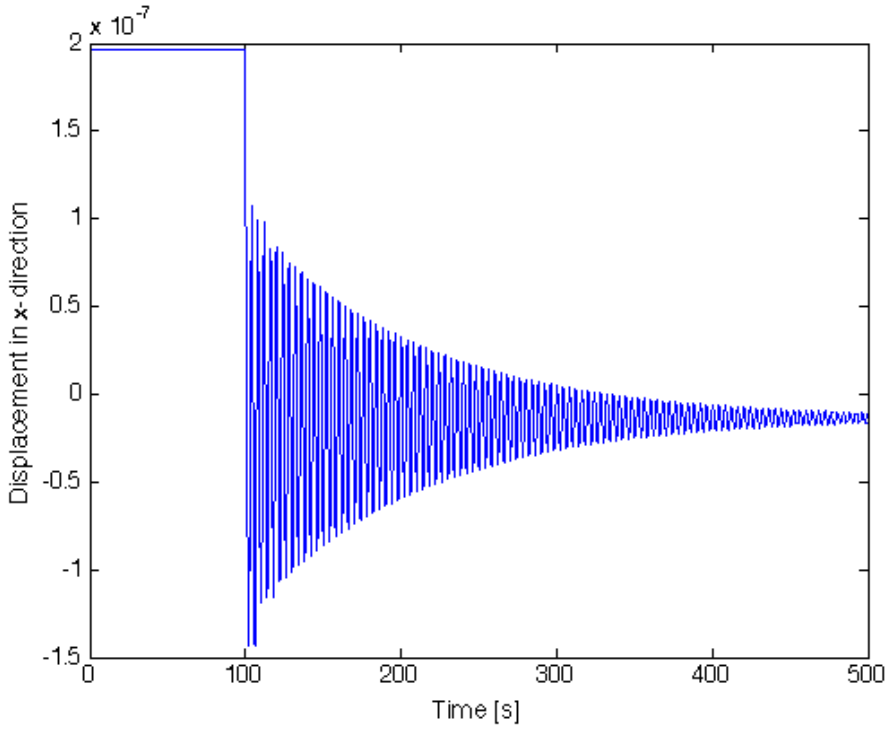

Figure 7.1: Time series of the free vibrations of the tower top of the offshore wind turbine after application of a step pulse loading of 80 kN.

Table 7.1: Parameters used in calculation of logarithmic decrement and results for load case 1.0.

Load Case	Amplitude first oscillation [m]	Amplitude last oscillation [m]	Number of oscillations [-]	Logarithmic decrement [-]	Damping ratio [%]
1.0	$1.074 \cdot 10^{-7}$	$3.088 \cdot 10^{-8}$	25	0.0499	0.749

Additional Simulation for Increased Soil Damping

As the damping assigned to the finite element model of the suction bucket foundation is very low, a decay test is performed to investigate the sensitivity of the total loading to an increase of the combined damping of the soil and suction bucket. The soil damping is increased 8.6, from 0.35% to 3.0%. As seen from Figure 7.2, it takes far less time before the vibrations are damped out when the soil damping is increased.

As seen from the results listed in Table 7.2, the damping ratio is increased from 0.749% to 1.75%. Thus the total damping in increased by a factor of 2.36 when the soil damping is increased by a factor of 8.6. Hence there is a significant difference in the total damping ratio between the conservative value used for the main simulations and the more realistic value of 3.0%.

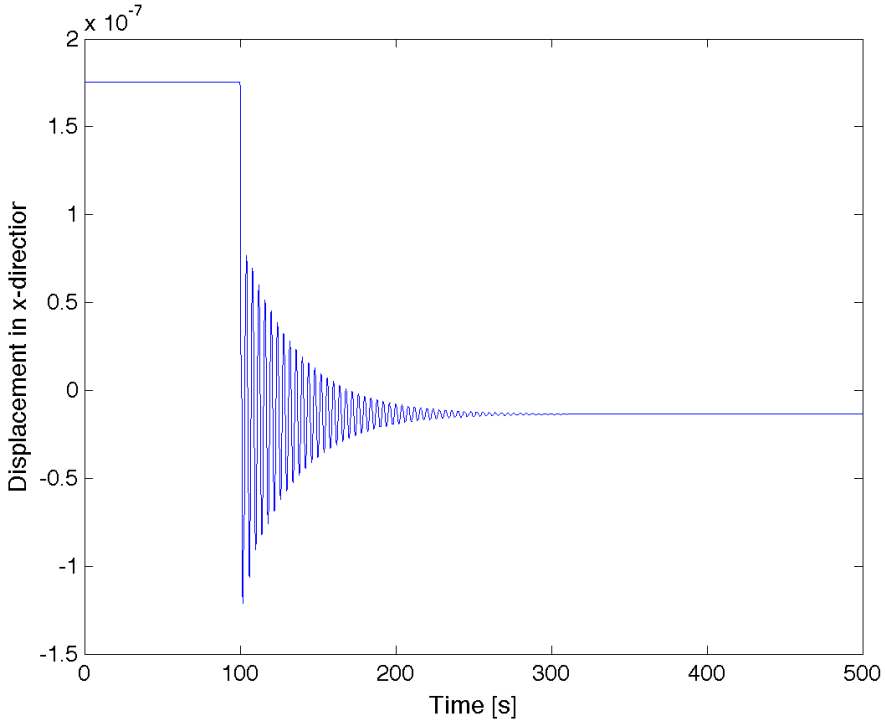

Figure 7.2: Time series of the free vibrations for increased damping of soil and suction bucket.

Table 7.2: Parameters and results for calculation of damping for additional sensitivity analysis.

Load Case	Amplitude first oscillation [m]	Amplitude last oscillation [m]	Number of oscillations [-]	Logarithmic decrement [-]	Damping ratio [%]
1.0	$9.029 \cdot 10^{-8}$	$5.770 \cdot 10^{-9}$	25	0.110	1.75

7.1.2 Aerodynamic and Total Damping from Logarithmic Decay Test

The total damping of the offshore wind turbine, including the aerodynamic damping is predicted for the range of wind speeds given in Table 6.2, by performing two logarithmic decay tests for each wind speed. In the first simulation a turbulent wind field and a step pulse loading of 80 kN is applied to the wind turbine. The second simulation applies the same wind field but no step pulse loading. The total damping is derived from the deterministic part of the response to the step pulse loading in terms of displacement of the tower top. The green curve in Figure 7.3 presents the deterministic part of the time history of the free vibrations in the tower top for at a wind speed of 11.1 m/s. The time series for the remaining wind speeds are found in Appendix B. As seen from the green curve in Figure 7.3 there is still some disturbance left in the time series after the removal of the stochastic part of the response. This makes is more difficult to calculate the logarithmic decay as the oscillations are not as evenly distributed as for the decay of free vibrations with no wind excitation. Hence, a Butterworth filter is applied to filter out the noise that is still left in the signal. The filtered signal is presented by the red curve in Figure 7.3.

As seen in Figure 7.4, load case 1.5 for a wind speed of 13.9 m/s is has particularly much noise in the deterministic part of the displacement at the tower top, making it difficult to determine the damping from the curve. Even after filtering the time series of the displacement, it is not a clear decay in the signal. However as there is a small trend in the first peaks, the total damping is calculated based on the logarithmic decrement of the three first peaks after the step pulse load is released.

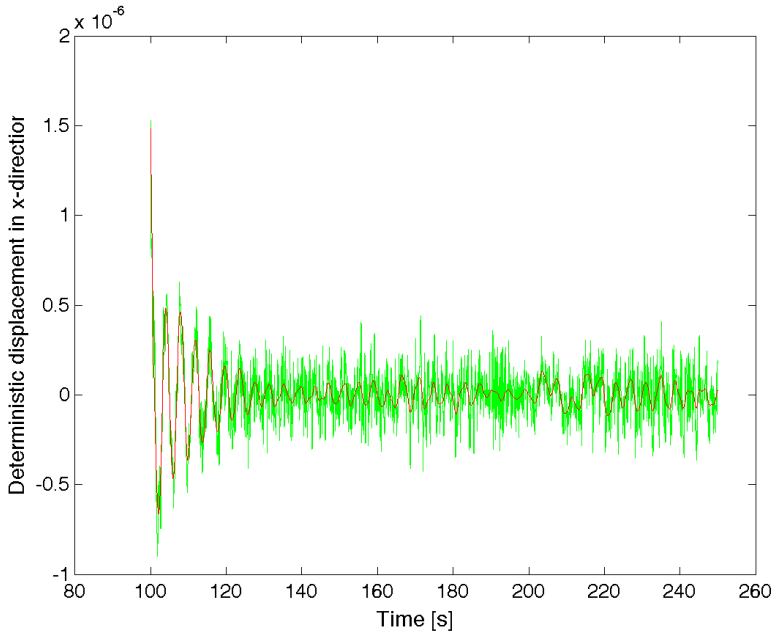

Figure 7.3: Time series of the unfiltered (green curve) and filtered (red curve) deterministic part of free vibrations of the tower top in the x-direction for a mean wind speed at the hub of 11.1 m/s.

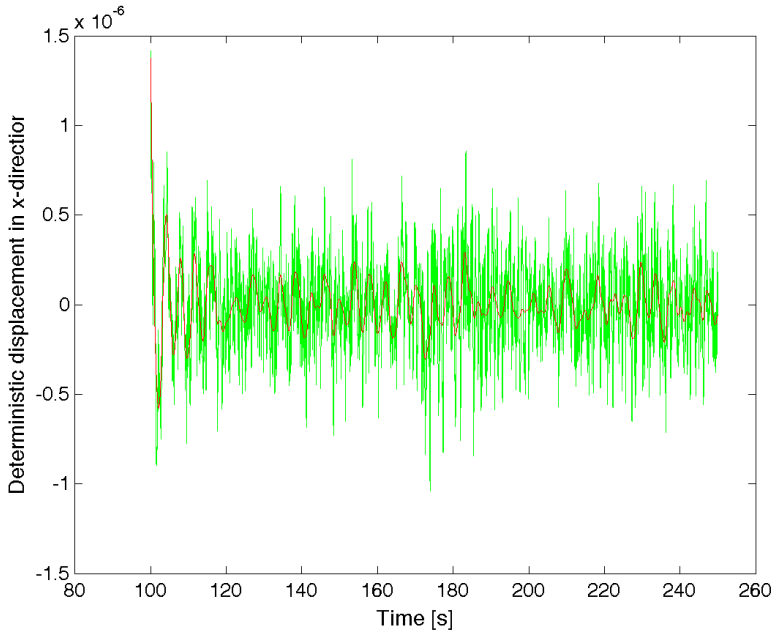

Figure 7.4: Time series of the unfiltered (green curve) and filtered (red curve) deterministic part of free vibrations of the tower top in the x-direction for a mean wind speed at the hub of 13.9 m/s.

The logarithmic decrement and the damping ratio corresponding to the total damping of the offshore wind turbine are calculated for each wind speed and the parameters used in the calculations and the results are listed in Table 7.3. The aerodynamic damping is also given in Table 7.3, and is calculated by assuming simple superposition of the damping contributions is valid.

As the disturbance in the filtered deterministic displacement of the tower top varies for each load case, the number of peaks used in the computation of the total damping is not the same for each load case. The number of peaks has been taken as the last succeding peak for which the amplitude of the vibration at the tower top decreases. This does however not apply to load case 1.5 as there is not a clear gradual decrease in the amplitude for this load case. As there is a certain trend in the decrease of the amplitude until the third peak, this is chosen as x_n. For all wind speeds above rated speed, there is more noise in the filtered displacement, which is the reason for a lower number of osclillations included in the computation of the logarithmic decrement.

The damping ratio is also plotted against the wind speed, and presented in Figure 7.5. This plot shows how the total damping changes with wind speed. The damping increases up to rated wind speed and decreases slightly for a wind speed of 13.9 m/s before it increases towards the maximum value of 9.66%, obtained at 19.5 m/s. For the two logarithmic decay tests with wind speeds above this value, the total damping is decreased by 3.5%.

Table 7.3: Parameters used in calculation of logarithmic decrement and results for load case 1.1 to 1.9.

Load Case	Mean wind speed [m/s]	Amplitude first oscillation [m]	Amplitude last oscillation [m]	Number of oscillations [-]	Logarithmic decrement [%]	Damping ratio [%]	Aerodynamic damping ratio [%]
1.1	2.7	$7.904 \cdot 10^{-7}$	$5.277 \cdot 10^{-7}$	9	4.49	0.71	-0.03
1.2	5.5	$7.705 \cdot 10^{-7}$	$4.208 \cdot 10^{-7}$	9	6.72	1.07	0.32
1.3	8.3	$7.133 \cdot 10^{-7}$	$1.438 \cdot 10^{-7}$	9	17.79	2.83	2.08
1.4	11.1	$4.819 \cdot 10^{-7}$	$0.573 \cdot 10^{-7}$	7	30.42	4.84	4.09
1.5	13.9	$5.037 \cdot 10^{-7}$	$2.192 \cdot 10^{-7}$	3	27.73	4.41	3.66
1.6	16.7	$6.494 \cdot 10^{-7}$	$0.298 \cdot 10^{-7}$	6	51.36	8.15	7.40
1.7	19.5	$5.557 \cdot 10^{-7}$	$0.143 \cdot 10^{-7}$	6	61.00	9.66	8.91
1.8	22.3	$6.261 \cdot 10^{-7}$	$0.612 \cdot 10^{-7}$	6	38.76	6.16	5.41
1.9	25.1	$6.940 \cdot 10^{-7}$	$0.672 \cdot 10^{-7}$	7	38.91	6.18	5.43

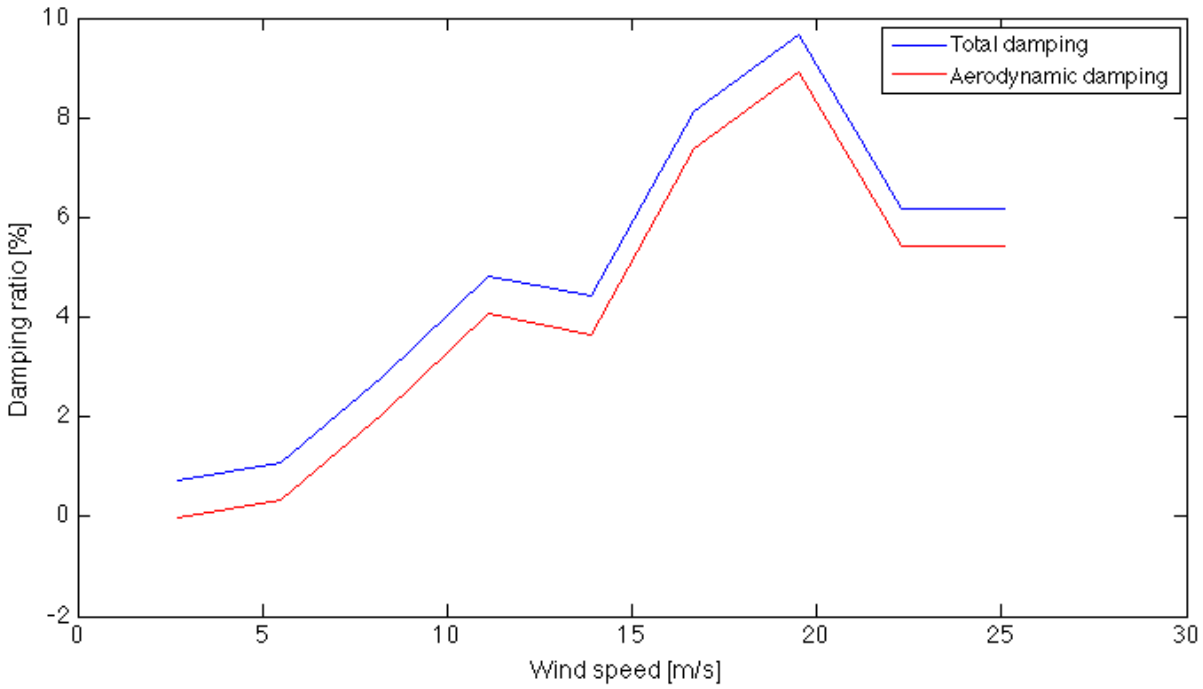

Figure 7.5: Variation of total damping ratio with wind speed.

7.1.3 Summary

The damping of the wind turbine is determined from simulations by applying a step pulse loading at the hub of the offshore wind turbine. The damping ratio of the offshore wind tubine structure itself, excluding aerodynamic damping is determined as 0.75% which is the same as the damping applied to the sower and substructure in the model. As the damping in finite element model is very low an additional simulation is performed to investigate how the total damping is altered when soil damping is increased. The results show that the total damping of the offshore wind turbine is increased from 0.75% to 1.75% when the soil damping is set to a more realistic level with a damping ratio of 3.0%.

The aerodynamic damping contributes significantly to the total damping of the offshore wind turbine. The total damping increases with increasing wind speed to a maximum of 9.66% at 19.5m/s. After reaching its maximum, the damping drops 3.5% for the next two load cases.

7.2 Misaligned wind and waves

Simulations for misaligned wind and waves are performed for all load cases listed in 6.1.2 Investigation of Effects of Misalignment. The wave loads are determined using both Morison's equation and the second order FNV-method. The response spectra for the mudline moment in the fore-aft and side-side directions are presented for each load case. The wave spectrum for each load case simulation is also included in the resonse spectra plots, so that the frequency range where the waves can excite the structure linearly is indicated in the spectra. The statistics of the mudline moment time series are also summarised in Table 7.4 at the end of this subchapter.

7.2.1 Results from Analyses with Morison's Equation and the FNV-method

Load Case 2.1 - 0° misalignment

The response spectra for the fore-aft and side-side mudline bending moment is given in Figure 7.6 for the mudline moments computed with Morison's equation and in 7.7 for mudline moments computed with the second order FNV-method. As seen from the spectrum there is a significant peak for the fore-aft mudline bending moment at a frequency of approximately 0.25 Hz for both figures. This peak corresponds to the value of the natural frequency of the first mode of the support structure and indicates an excitation of this mode from linear wave loading. The spectral density of the side-side mudline moment is much smaller than the spectral density of the side-side mudline bending moment and is barely seen in the plot of the spectra, as its value is low compared to the fore-aft mudline moment for this load case. A small peak is also seen at very low frequencies, corresponding to the frequencies of the low frequent wind excitation.

Figure 7.7 shows that the peak of the fore-aft moment at the natural frequency of the first mode is increased compared to the same plot for wave loads calculated according to Morison's inertia term which is presented in Figure 7.6. The spectral density is higher for all frequencies, not just those around the natural frequency that is excited at resonance.

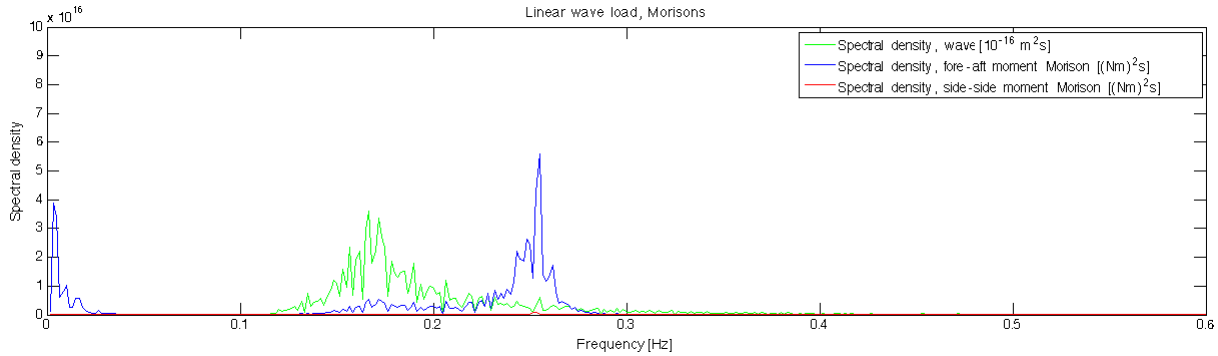

Figure 7.6: Spectral density of waves and the fore-aft and side-side mudline bending moment computed with Morison's equation and misalignment equal to 0°.

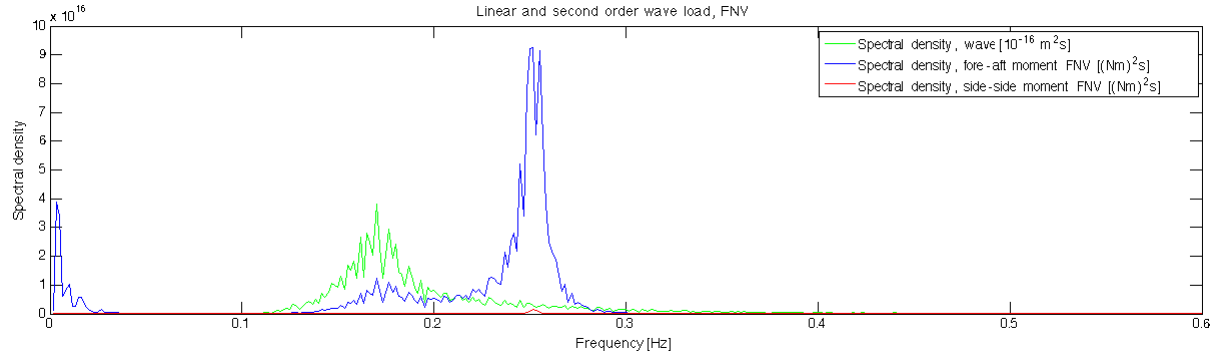

Figure 7.7: Spectral density of waves and the fore-aft and side-side mudline bending moment computed with the second order FNV-method misalignment equal to 0°.

Load Case 2.2 - 15° misalignment

From the response spectra for the 15° misalignment angle in Figure 7.8 it is observed that the peak of the fore-aft mudline moment for frequencies close to the natural frequency of the first mode is slightly decreased and that the side-side mudline moment is increased compared to load case 2.1. This indicate that the offshore wind turbine is being excited at resonance in both directions.

For load case 2.2 performed with the second order FNV-method the spectral density as given in Figure 7.9 of the fore-aft and side-side mudline moment is increased compared to the same simulation using Morison's equation. The spectral density of the peaks for the moment in both directions is increased to approximately the double value when second order loading is included in the computations. However, the spectral density from the FNV-method is generally higher than the spectral density of from analyses with Morison's equation.

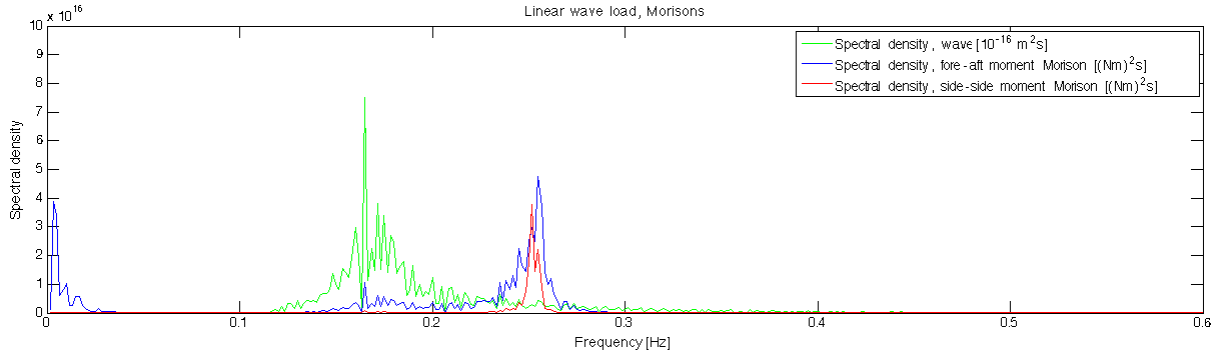

Figure 7.8: Spectral density of waves and the fore-aft and side-side mudline bending moment computed with Morison's equation and misalignment equal to 15°.

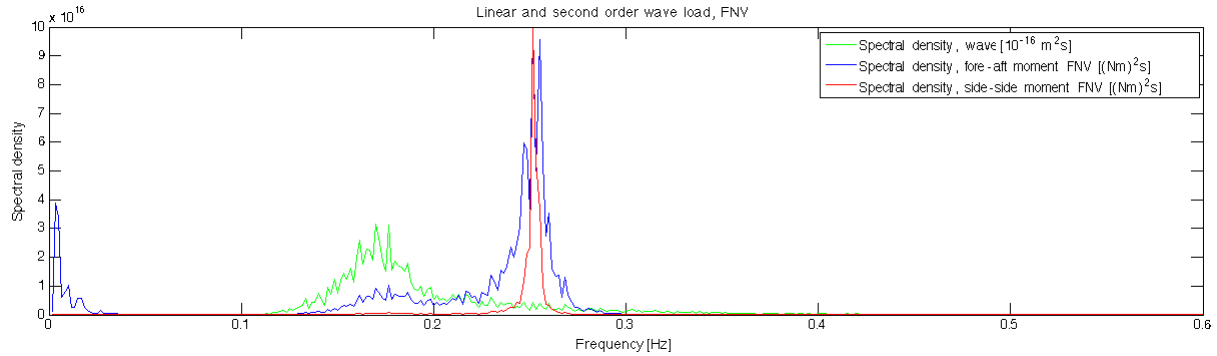

Figure 7.9: Spectral density of waves and the fore-aft and side-side mudline bending moment computed with second order FNV and misalignment equal to 15°.

Load Case 2.3 - 30° misalignment

For load case 2.3, with an angle of misalignment of 30°, the spectral density of the side-side bending moment is nearly tripled in magnitude compared to the previous load case for the moments computed with Morison's equation. Due to this large increase in magnitude, two plots are presented for each calculation method. The upper plot in each figure has a limit on the y-axis of 10^{17}, while the limit is $1.3 \cdot 10^{18}$ for the lower plot. The same increase is seen in the results from the FNV-simulations.

The spectral density of the fore-aft bending moment is approximately the same as for the previous load case for the results from the simulation with Morison's equation. The fore-aft bending moment for the simulations with the FNV-method for computation of wave loads however, is reduced at the peak compared to load case 2.2. However, the spectral density of the mudline moment computed with the FNV-method is still higher than the results from the simulation with Morison's equation.

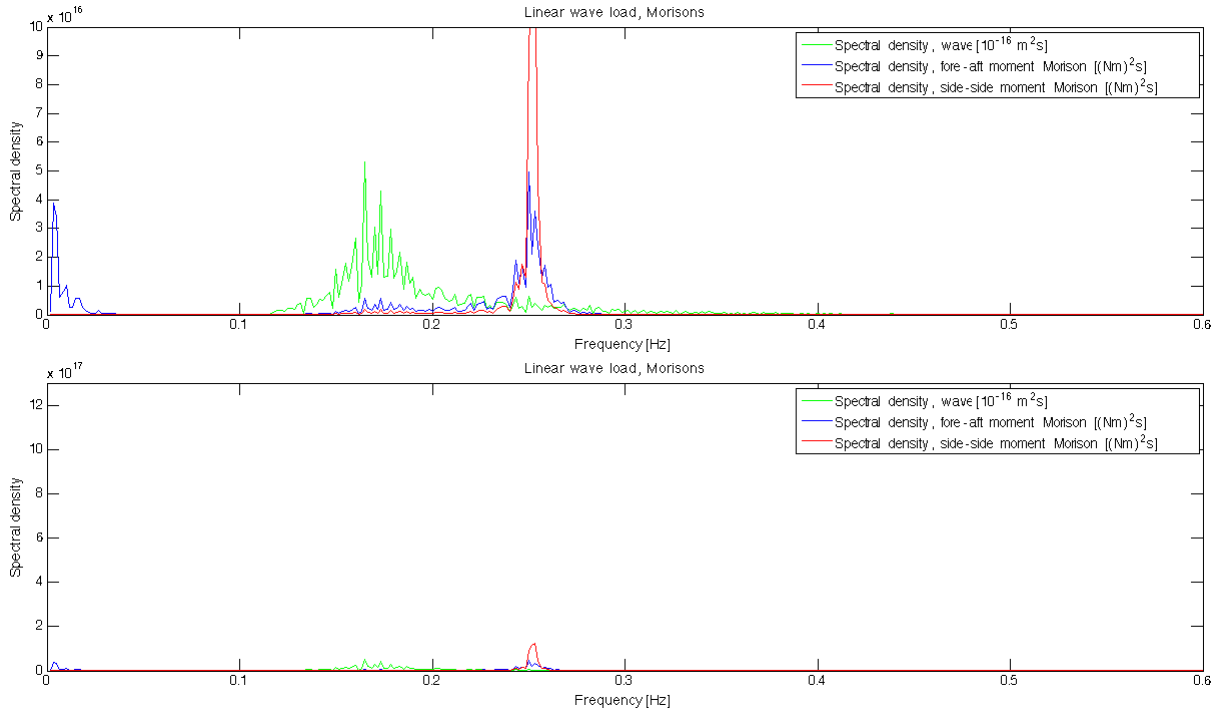

Figure 7.10: Spectral density of waves and the fore-aft and side-side mudline bending moment computed with Morison's equation and misalignment equal to 30°.

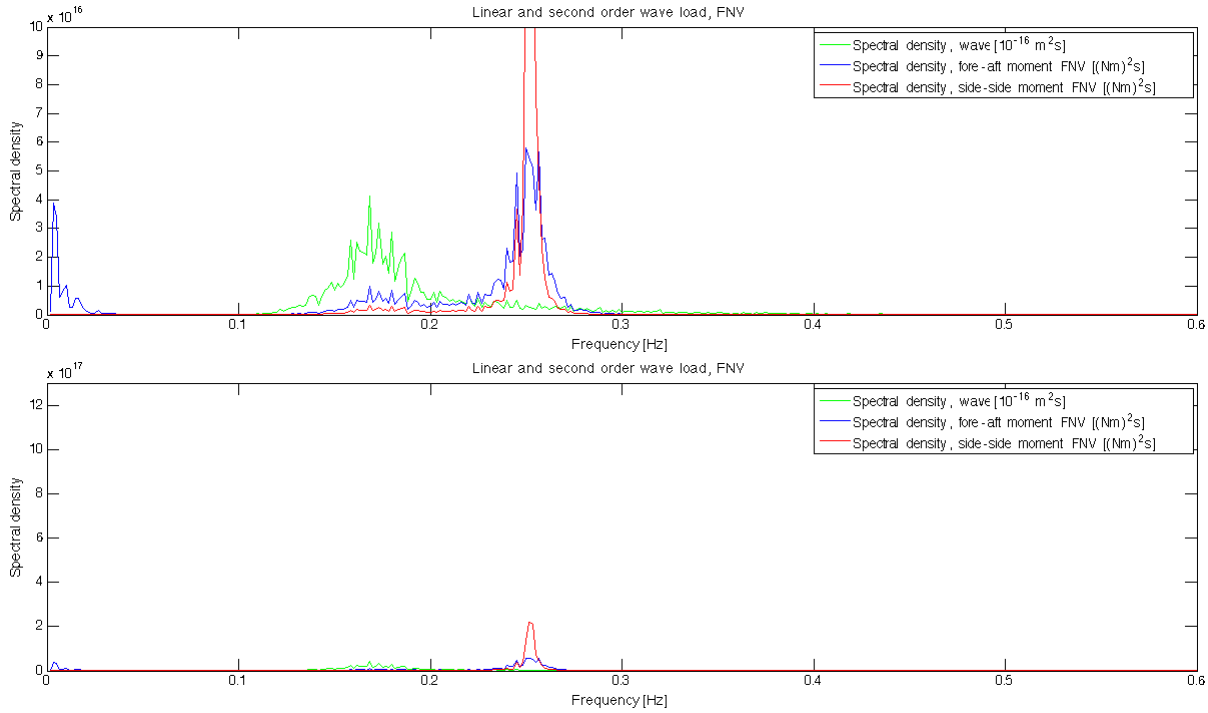

Figure 7.11: Spectral density of waves and the fore-aft and side-side mudline bending moment computed with second order FNV and misalignment equal to 30°.

Load Case 2.4 - 45° misalignment

In the spectral plot for load case 2.4 in Figure 7.12, the response is dominated by the side-side moment at the natural frequency of the first mode. It is clear from the figure that resonance in the side-side direction is more severe for this load case than for the previous ones. It should also be noted that the spectral density of the fore-aft moment is only slightly decreased when the angle is increased to 45°.

For load case 2.4 two spectral plot are included. The reason for this is that the peak of the spectral density of the side-side moment at the mudline is too large to fit within the limits of the y-axis needed to present the plots in a sufficient scale. The y-axis of the second plot which presents the whole spectra is the same as for load case 2.5 with Morison's equation, which also is presented by use of two plots of different scales.

From Figure 7.13 one can clearly see that the side-side moment dominates the respose at the natural frequency. The spectral density of the fore-aft moment is somewhat decreased from the load case 2.3, and the peak value is about a ten times smaller than the spectral density of the side-side moment.

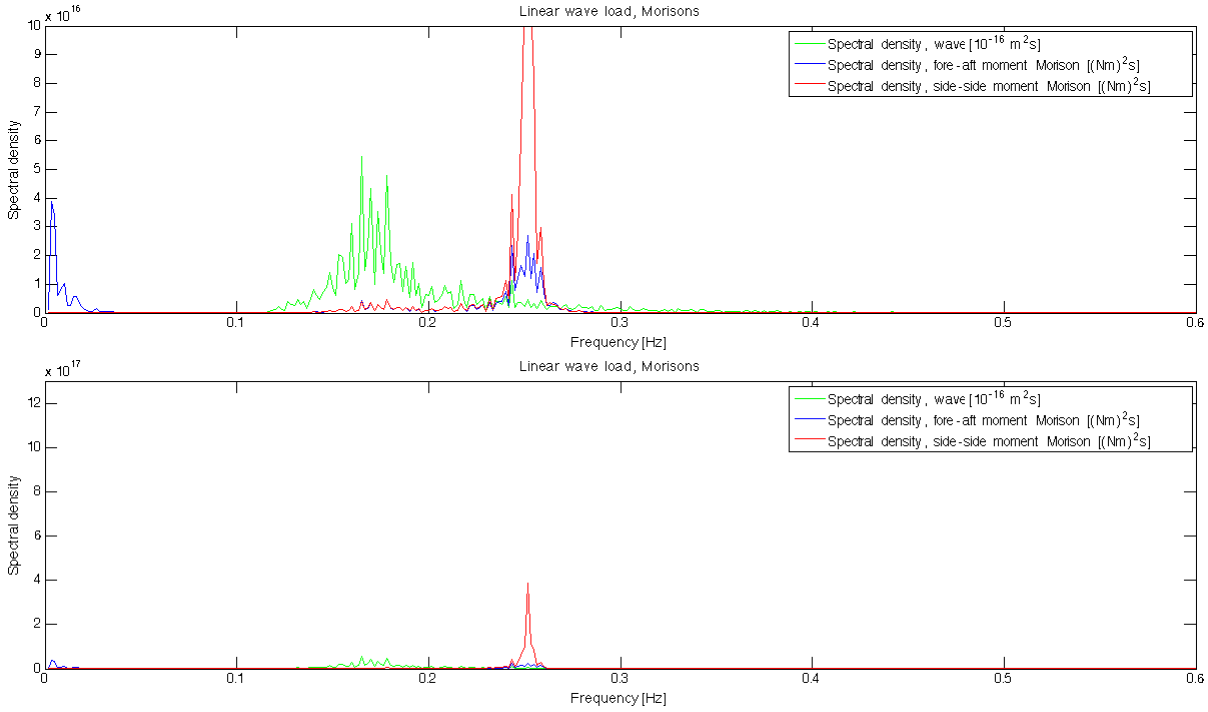

Figure 7.12: Spectral density of waves and the fore-aft and side-side mudline bending moment computed with Morison's equation and misalignment equal to 45°.

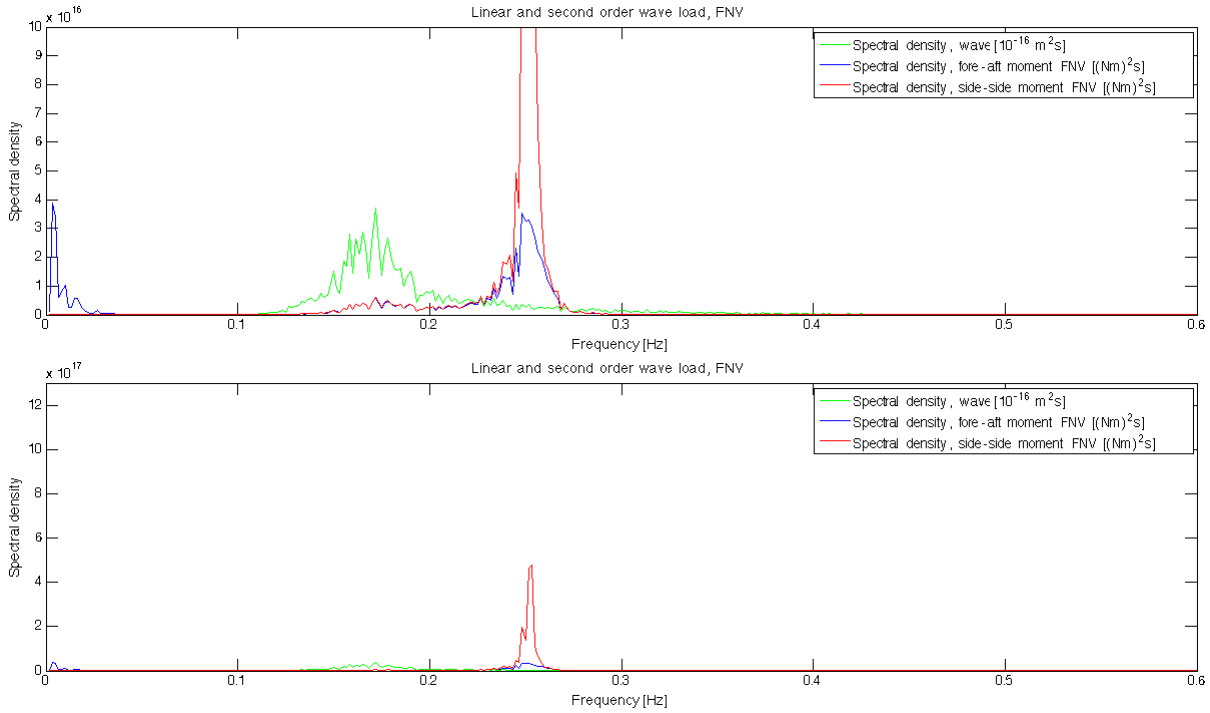

Figure 7.13: Spectral density of waves and the fore-aft and side-side mudline bending moment computed with second order FNV and misalignment equal to 45°.

Load Case 2.5 - 90° misalignment

For the 90° load case, the side-side bending moment is dominating the response both for the moments computed with Morison's equation and with second order FNV. There is no excitation of the first mode natural frequency in the fore-aft direction. An interesting observation in the spectra is that the side-side mudline moment spectrum is slightly wider and has a somewhat lower peak than in the previous load case.

The spectra for load case 2.5 are also presented in terms of two differently scaled plots, for the same reason as described above. By comparing the spectrum for the side-side moment in Figure 7.14 for load calculation with Morison's equation to the spectrum of the same moment in Figure 7.15, it is evident that the computation of the combined linear and second order loading with the FNV method has a large effect on response in the side-side direction for load case 2.5 with a 90° misalignment. The maximum value of the spectral density for the side-side moment is increased by a factor of 3.4 when the second order loading is included.

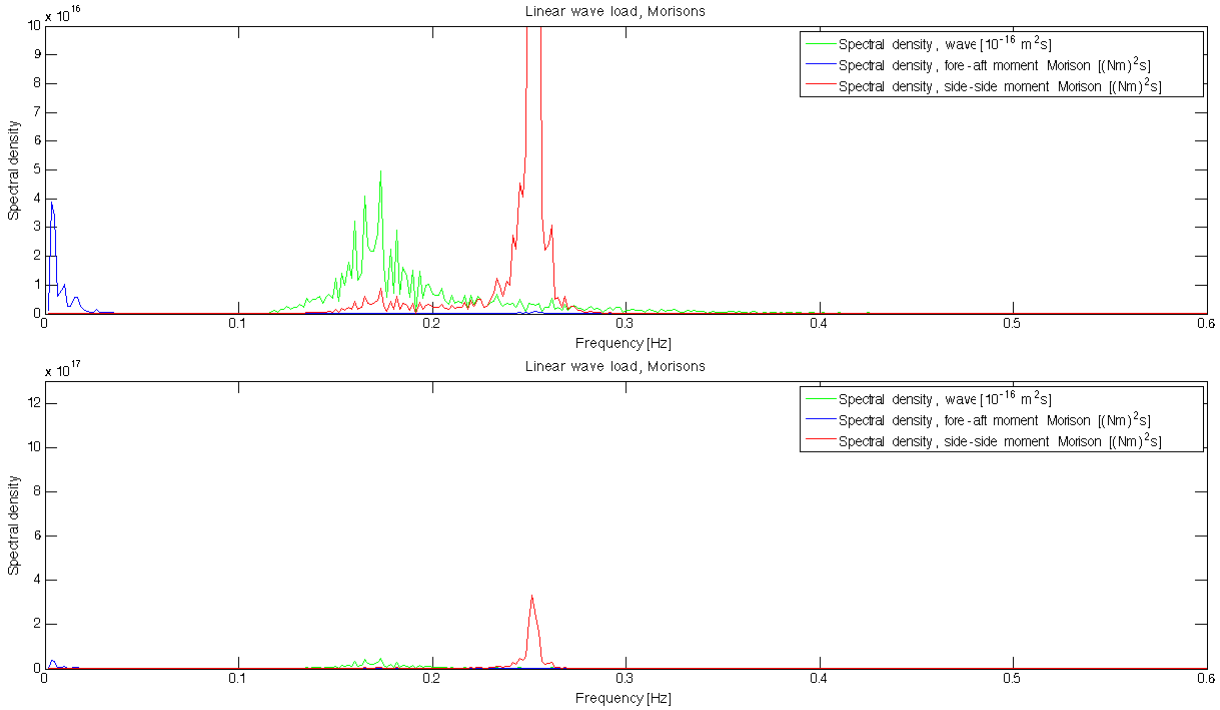

Figure 7.14: Spectral density of waves and the fore-aft and side-side mudline bending moment computed with Morison's equation and misalignment equal to 90°.

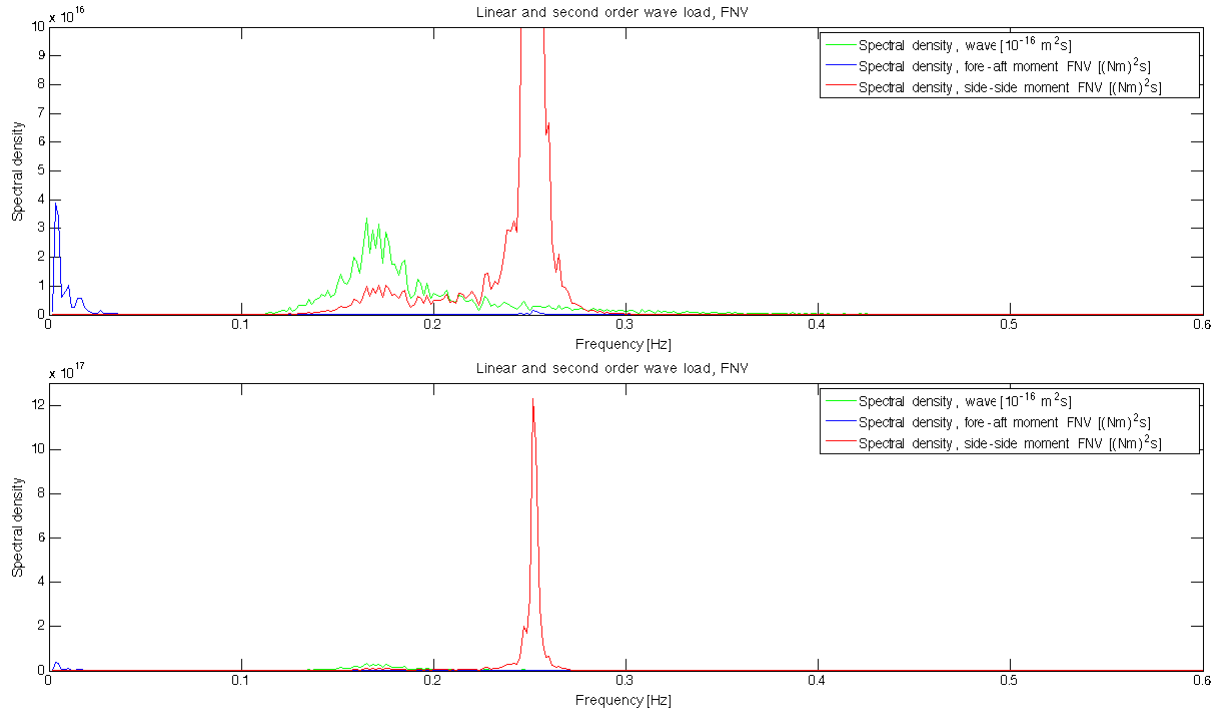

Figure 7.15: Spectral density of waves and the fore-aft and side-side mudline bending moment computed with second order FNV and misalignment equal to 90°.

7.2.2 Time Series Statistics

The standard deviation, mean, maximum and minimum values of the time series of the moment in both directions is determined for each load case and listed in Table 7.4. As the fatigue is dependent on the standard deviation of the load process this statistical parameter is the most important. In order to determine the effect of the second order loading on the response, the ratio between the standard deviation of the analyses performed with the second order FNV-method and the analyses using Morison's equation are calculated and listed in Table 7.5.

As seen from the ratios in Table 7.5 the ratio decreases for the fore-aft moment as the angle increases. For load case 2.5 where the angle of misalignment is 90°, the ratio is equal to 1.00. For the side-side moment the ratio of the standard deviations increase with the angle of misalignment.

Table 7.4: Standard deviation, mean, minimum and maximum value of fore-aft mudline moment for all load cases with Morison's equation and second order loading from FNV-method.

		Fore-Aft Mudline Moment			
	Load Case	Standard Deviation [MNm]	Mean [MNm]	Minimum [MNm]	Maximum [MNm]
Morison	2.1	34.61	60.39	-59.63	188.8
	2.2	33.81	60.40	-81.56	164.9
	2.3	31.47	60.40	-57.60	167.6
	2.4	28.12	60.41	-31.07	162.6
	2.5	17.88	60.40	14.20	119.5
FNV	2.1	47.84	60.41	-114.8	246.0
	2.2	45.72	60.39	-102.1	233.7
	2.3	40.88	60.39	-93.59	209.0
	2.4	35.14	60.42	-76.95	177.1
	2.5	17.94	60.40	14.51	118.8
		Side-Side Mudline Moment			
	Load Case	Standard Deviation [MNm]	Mean [MNm]	Minimum [MNm]	Maximum [MNm]
Morison	2.1	2.808	2.587	-6.446	14.68
	2.2	15.50	2.582	-48.52	52.03
	2.3	29.12	2.580	-103.6	103.7
	2.4	40.41	2.567	-125.8	144.5
	2.5	51.14	2.593	-178.2	172.8
FNV	2.1	3.431	2.586	-8.954	15.65
	2.2	22.45	2.587	-63.35	70.46
	2.3	39.95	2.577	-142.6	147.6
	2.4	57.12	2.563	-199.2	195.5
	2.5	80.84	2.555	-318.5	327.3

Table 7.5: Ratio of standard deviation from analyses with Morison's equation and second order loading from FNV-method.

Load Case	Ratio of standard deviation from Morison analyses and FNV analyses	
	Fore-Aft Moment	Side-Side Moment
2.1	1.38	1.22
2.2	1.35	1.45
2.3	1.30	1.37
2.4	1.25	1.41
2.5	1.00	1.58

7.2.3 Observed Trends and Summary

It can clearly be observed from the spectra presented and the time series data, that the fore-aft mudline bending moment decreases and that the side-side mudline moment increases with increasing angle of misalignment between wind and waves. The rate of increase in the response in the side-side direction is larger than the rate of decrease for the fore-aft mudine moment when the angle of misalignment is increased. This trend is observed for both wave load models used.

In addition, the spectral density of the mudline moment in both directions is increased for all load cases when second order loading is included in the wave load calculations. The least effect is seen for load case 2.5 in the fore-aft direction. The small effect of second order loading on the fore-aft moment in this load case is natural as the waves are acting perpendicular to the direction of the moment. As the waves are exciting the structure in the side-side direction it is natural that the effect of second order loading is insignificant for the fore-aft moment. The largest effect of the second order loading is seen for the load case with a misalignment angle of 90° for the side-side moment. The ratio between the standard deviations of the results from each load model is also larger for the side-side moment when the waves are acting perpendicularly on the wind direction, than it is for the fore-aft moment when the waves are acting parallell to the wind direction.

7.2.4 Fatigue Damage

The calculated maximum fatigue damage along the cross section of the support structure at the mudline for each load case for misaligned wind and waves are presented in Table 7.6 below. The same table also presents the probability of occurrence of each load case and the fatigue life of the structure when only subjected to the environmental conditions in the specific load case. A utilisation factor of 3 has been used for the computation of the fatigue life, as is required in DNV (2010a).

The maximum damage for each load case with the two load models is presented in Figure 7.16. As seen from both the results listed in Table 7.6 and Figure 7.16, the fatigue damage of the simulations using the FNV-method to compute the second order wave load, is approximately 3-4 times larger for all load cases. For load case 2.5, which has the largest fatigue damage, the relative difference between the two load models is the largest. The damage from the simulation with second order loading is 4.3 times higher than the corresponding damage from the simulation with Morison's equation. Hence the second order loading will have the largest effect on the fatigue life when the angle between the

Table 7.6: Fatigue results for Load Case 2.1-2.5 for simulations with Morisons equation and the FNV-method to the second order.

Load Case	Fatigue damage $[\cdot 10^{-3}]$		Fatigue life for environmental state [Years]		
	Morison	FNV	Morison	FNV	Ratio of fatigue life
2.1	0.3428	1.2377	0.1110	0.0307	3.61
2.2	0.3774	1.2492	0.1008	0.0305	3.31
2.3	0.6207	1.7097	0.0613	0.0223	2.75
2.4	1.0918	3.2439	0.0349	0.0117	2.97
2.5	1.7455	7.5169	0.0218	0.0051	4.31

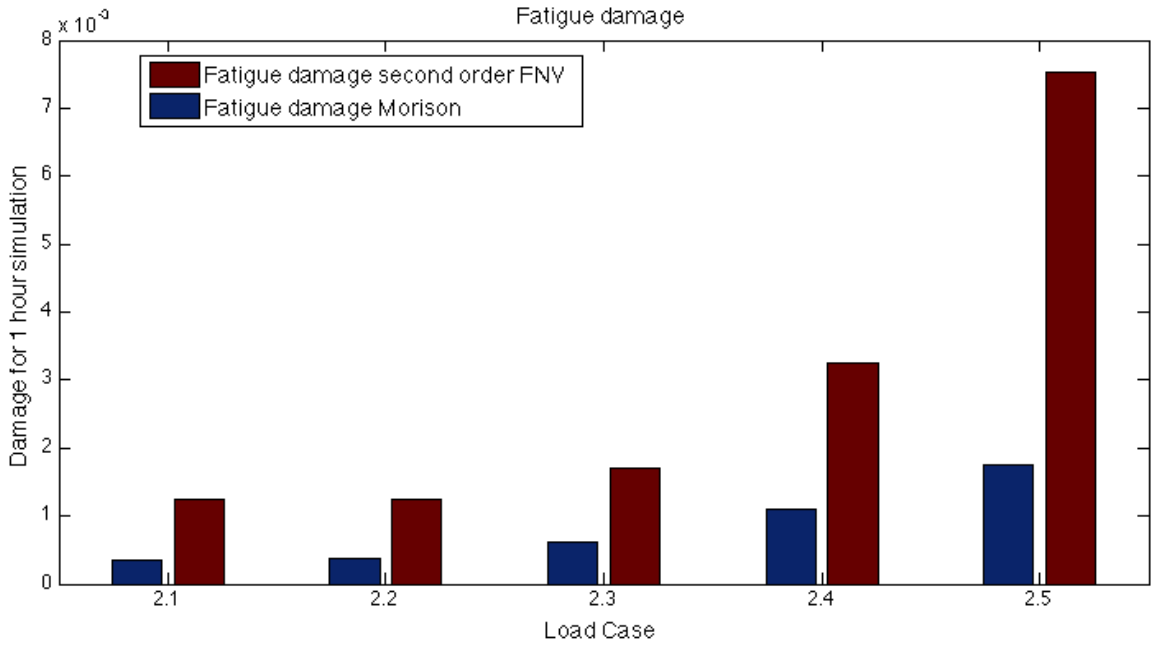

Figure 7.16: Fatigue damage for each load case computed using linear wave loading and combined linear and second order wave loading.

7.3 Investigation of Sum-Frequency Effects

In the following subchapter, results from the investigation of the effect of springing on the fatigue life of the offshore wind turbine are presented. Time domain simulations are performed for the load cases listed in Table 6.3. One simulation of each load case is performed with only linear wave load, computed from the inertia term of Morison's equation. The same simulations are performed again with linear and second order loading computed according to the FNV-model truncated at the second order. The results are compared in terms of spectral plots, time series statistics and the fatigue damage accumulated for each load case.

Load case 3.1, H_S = 1.0 m, T_P = 4.5 s, U_{hub} = 8.3 m/s

Load case 3.1 has been simulated using the most probable environmental parameters in the NORA10 data, and is investigated in order to have a reference load case to compare the results of the environmental states with larger nonlinearities to. As seen from Figure 7.17, the offshore wind turbine is excited at resonance, which can be observed from the peak of the spectral density of the fore-aft moment at a frequency of 0.25 Hz. This is expected as the natural period of the waves is close to the natural period of the first mode of the support structure. Figure 7.17 also shows that the spectral density of the fore-aft moment computed with second order loading accoding to the FNV-method is larger than the same moment for linear wave loading.

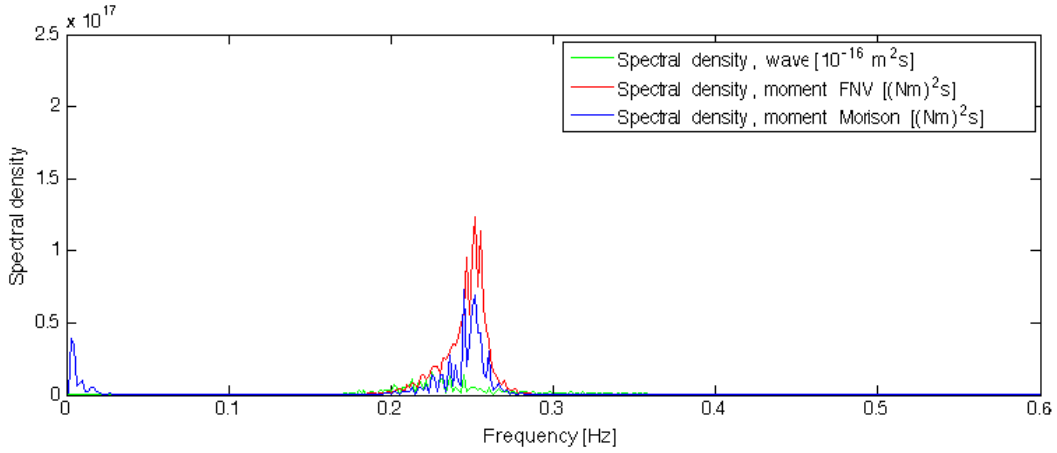

Figure 7.17: Spectral density of waves and fore-aft mudline moment for load case 3.1.

Load case 3.2, H_S = 1.5 m, T_P = 5.5 s, U_{hub} = 11.1 m/s

Load case 3.2 has also been simulated to have a reference load case that is expected to be dominated by linear loading. As load case 3.1 has a peak period close to the natural frequency of the first mode of the support structure, this load case has a higher peak period in order to have a load case that is expected to excite the first mode less than load case 3.1.

As seen from Figure 7.18 the response spectra for the mudline moment is lower for load case 3.2 than for load case 3.1. In addition the shape of the response spectra follows the shape of the wave spectrum up to a frequency of approximately 0.22 Hz, before they increase towards a peak located at 0.26 Hz. This peak indicate the dynamic amplification of the wave loading within the bandwidth of the transfer function of the mudline moment at the first mode natural frequency. As obseved for load case 3.1, the spectral density of the fore-aft mudline moment is consistently larger for the moment computed with the second order FNV-method than for the moment computed with Morison's equation for load case 3.2 as well. However, the difference in the spectral densities for the two load models is less for load case 3.2 than for load case 3.1.

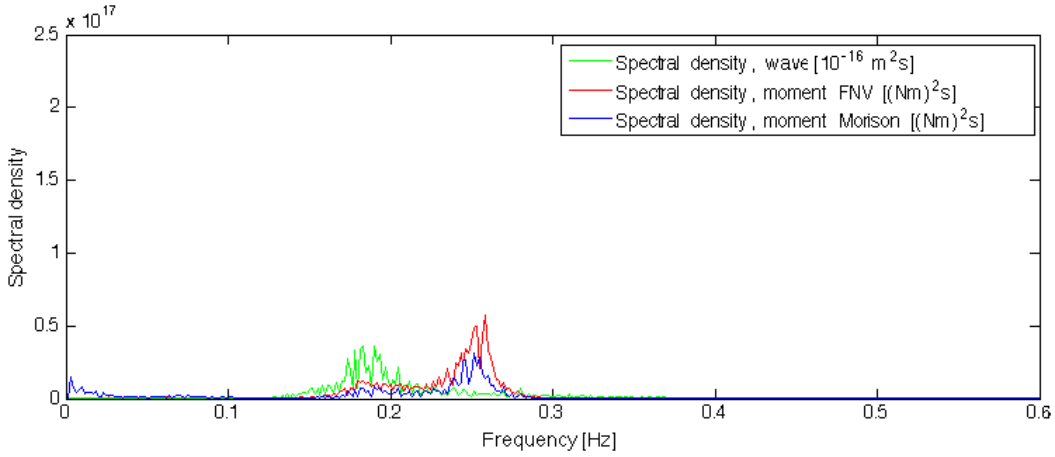

Figure 7.18: Spectral density of waves and fore-aft mudline moment for load case 3.2.

Load case 3.3a, H_S = 2.5 m, T_P = 6.1 s, U_{hub} = 13.9 m/s

Load case 3.3a to 3.3d investigates the effect of second order loading for a set of environmental states where only the peak frequency of the wave spectrum is altered for each load case. The aim is to investigate which frequencies that will have a contribution from the second order loading in the excitation of the first mode natural frequency.

As seen from the spectral density of the mudline moment computed using Morison's equation in Figure 7.19, resonance still occurs for the first mode. This indicates that there is still sufficient energy in the waves at this frequency to excite the natural frequency. For this load case, as for the two previous load cases, it is observed that the spectral density of the moment computed with the FNV-method is consistently higher than the spectral density of the moment computed with Morison's equation for all frequencies. One can also see that the difference between the spectral densities of the moments has increased compared to the two previous load cases.

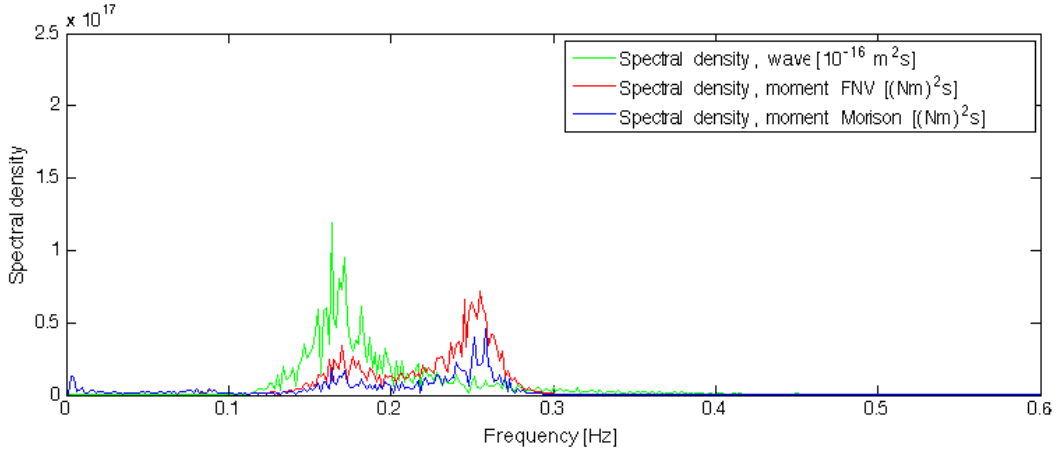

Figure 7.19: Spectral density of waves and fore-aft mudline moment for load case 3.3a.

Load case 3.3b, H_S = 2.5 m, T_P = 7.0 s, U_{hub} = 13.9 m/s

For load case 3.3b the spectral density of the moments are decreased compared to load case 3.3a. This applies to both the frequency range corresponding to the quasi-static response and the resonance response. Spectral density of the moment including second order loading is hilgher over the whole range of frequencies for the wave excitation, as is also observed for all the previously discussed load cases for investigation of springing. The reponse at the natural frequency is lower for both load models, indicating that there is less resonance for this load case.

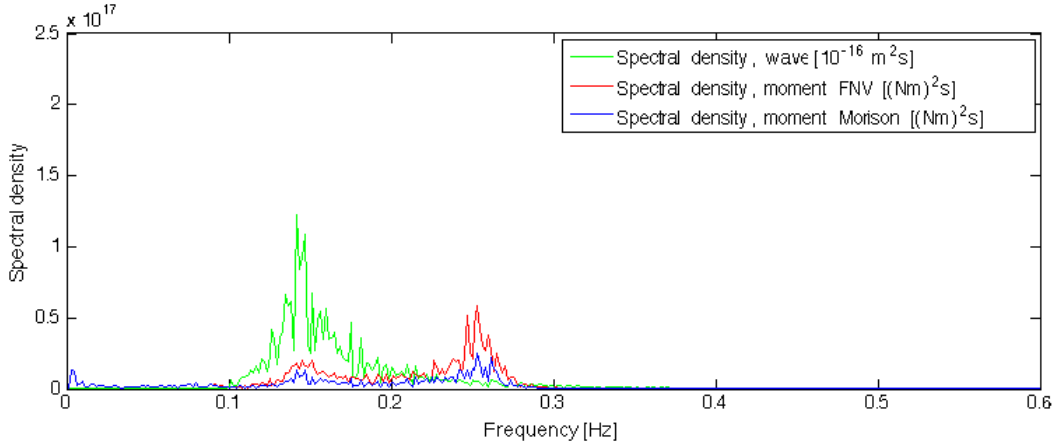

Figure 7.20: Spectral density of waves and fore-aft mudline moment for load case 3.3b.

Load case 3.3c, H_S = 2.5 m, T_P = 8.0 s, U_{hub} = 13.9 m/s

Load case 3.3c stands out from the previous load cases as one can clearly see the effect of second order loading contributing to resonance of the first mode. The spectral density of the moment due to linear wave loading has a small peak for the quasi-static response and the resonace response. For the quasi-static part of the response, the spectral density of the moment due to combined linear and second order loading is approximately the same as for the response due to linear wave loading. For the resonance response however the peak is much larger for the spectrum for combined linear and second order wave loading, showing a significant effect of the second order loading.

In addition to the large peak in the spectrum for combined linear and second order, two other peaks are observed in the spectrum at 0.2 Hz and 0.4 Hz. These peaks are quite high compared to the rest of the response apart from the resonance of the support structure, and only occurs for the mudline moment spectrum for the combined linear and second order loading computed with the FNV-method.

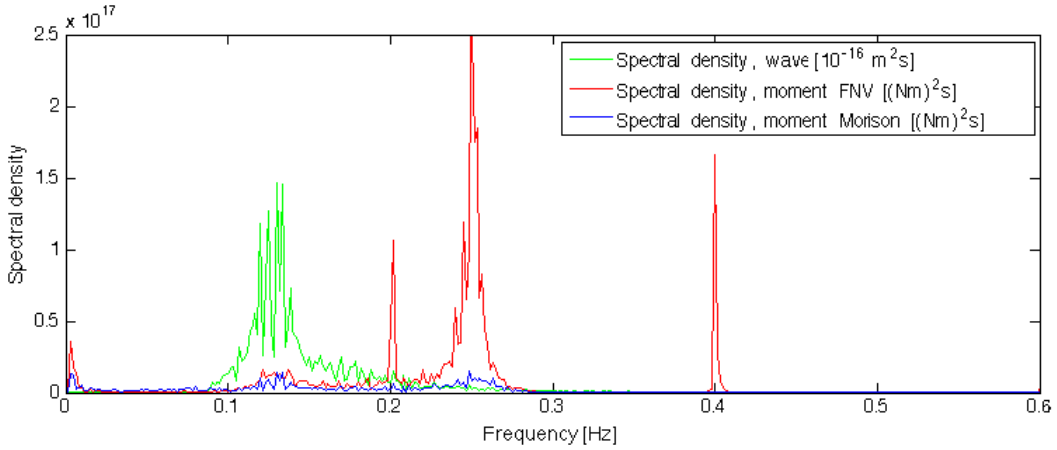

Figure 7.21: Spectral density of waves and fore-aft mudline moment for load case 3.3c.

Load case 3.3d, H_S = 2.5 m, T_P = 9.0 s, U_{hub} = 13.9 m/s

Load case 3.3d has similar response spectra as load case 3.3c, however the peak at the natural frequency is lower than the peak in load case 3.3c indicating less excitation of the first mode natural frequency of the support structure. Thus, the effect of second order loading in this load case is less than for load case 3.3c. The same characteristic peaks at 0.2 Hz and 0.4 Hz is also observed for the response spectrum for the combined linear and second order loading in this simulation. The peaks are however not observed in the response spectrum for linear wave loading for this load case either.

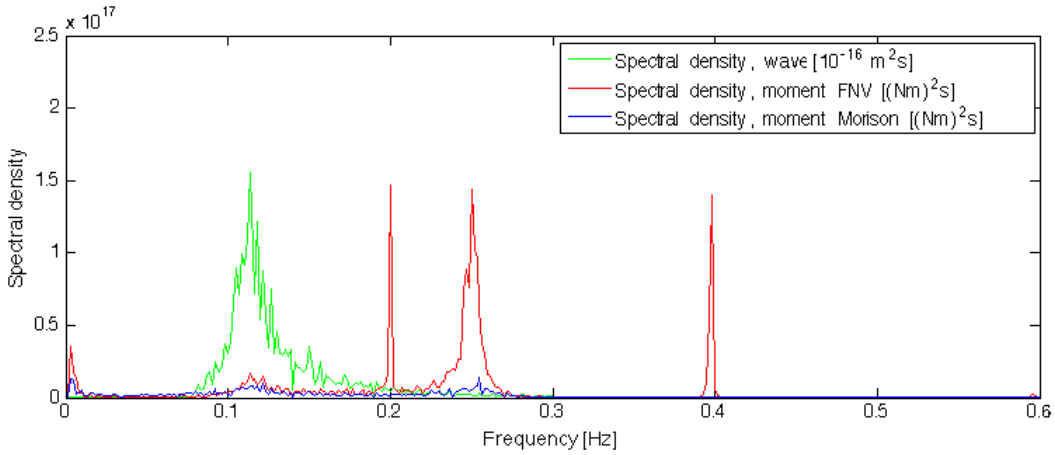

Figure 7.22: Spectral density of waves and fore-aft mudline moment for load case 3.3d.

Load case 3.4a, H_S = 2.5 m, T_P = 6.0 s, U_{hub} = 0 m/s

Three load cases without wind loading are performed to investigate the effect of springing in the absence of aerodynamic damping. The load cases represent what can be seen as the worst case scenario in terms of structural response as the damping is very low. Simulations of load case 3.4a show that the response is significantly increased in the absence of aerodynamic damping. The spectral density of the mudline moment at the natural frequency is very large compared to the previous load cases and the spectral plot is thus presented by two plots with different values for the y-axes. The plots clearly show significant excitation of the offshore wind turbine at its forst mode natural frequency. Again it is observed that the spectral density of the moment computed with the second order FNV-method is consistently larger than the spectral density of the mudline moment from the simulation with Morison's equation, also in the region of quasi-static response.

Compared to load case 3.3a, which is defined with the same wave parameters and a wind speed of 13.9 m/s one can see that the aerodynamic damping has a large impact on the response when the offshore wind turbine is excited in resonance.

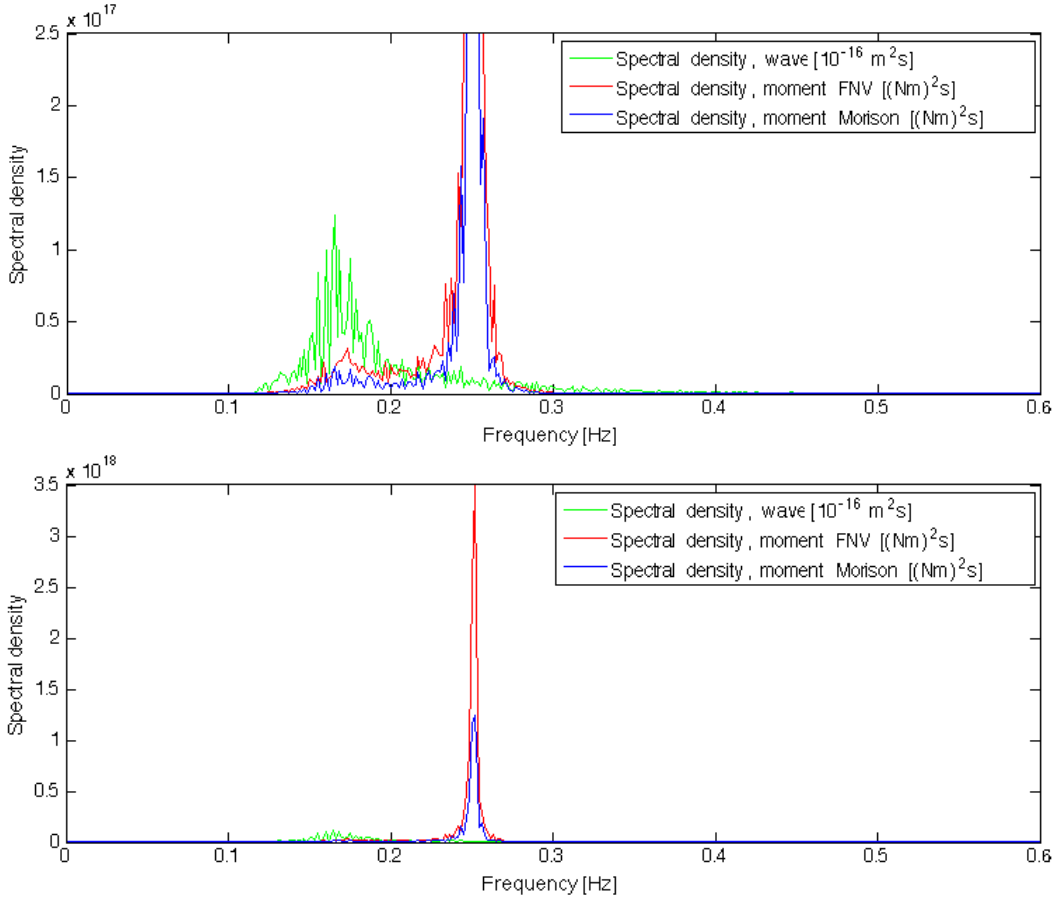

Figure 7.23: Spectral density of waves and fore-aft mudline moment for load case 3.4a.

Load case 3.4b, H_S = 2.5 m, T_P = 7.0 s, U_{hub} = 0 m/s

The peaks of the response spectra from load case 3.4b are also too large to be presented by only one plot, and is hence presented in two plots in Figure 7.24. As seen in this figure, the spectral peak at the first mode natural frequency is lower for this load case than for the previous load case. As the peak period of the wave spectrum is larger for this load case the wave spectrum is shifted to the left to a lower peak frequency. Thus the amount of linear wave energy that excites the offshore wind turbine at the natural frequency is less than for load case 3.4a. The same trend in the magnitude of the spectral density for the moment due to combined linear and second order loading as observed for all the previous load cases is also seen in the spectral plot for load case 3.4b.

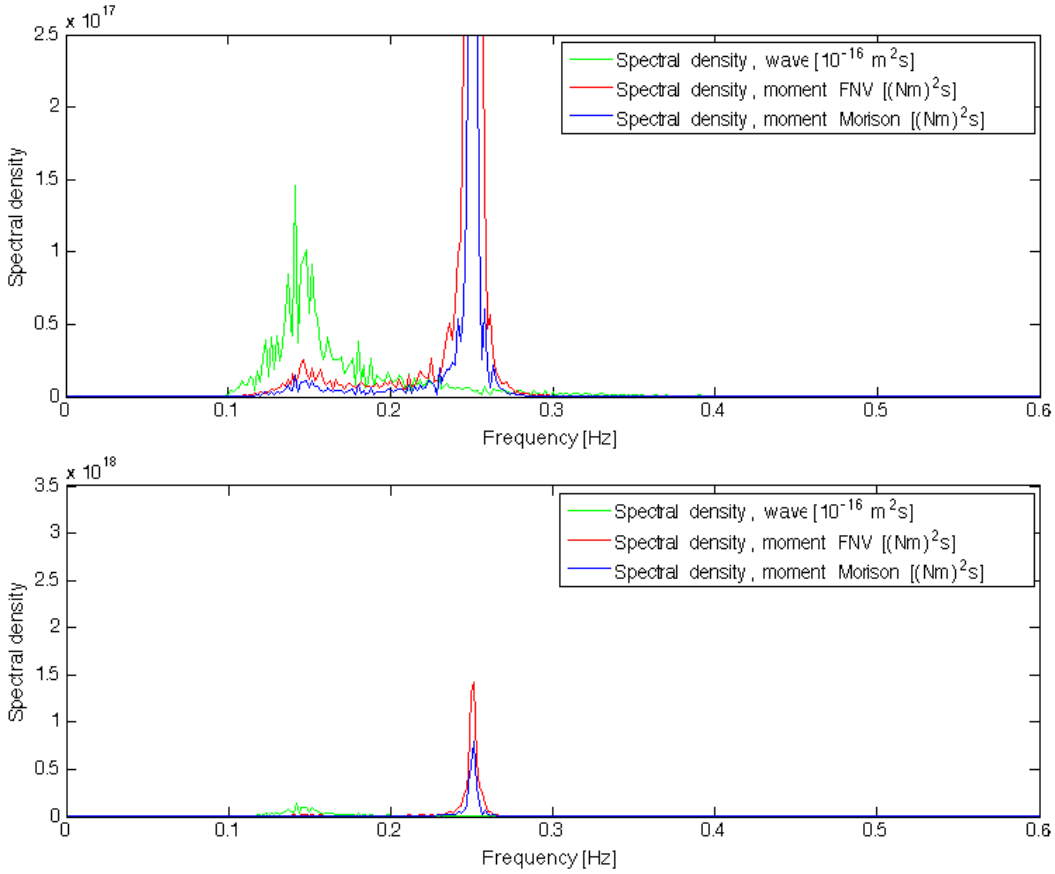

Figure 7.24: Spectral density of waves and fore-aft mudline moment for load case 3.4b.

Load case 3.4c, H_S = 2.5 m, T_P = 8.0 s, U_{hub} = 0 m/s

As seen from the plot of the spectral density in Figure 7.25 peak at 0.25 Hz for the moment computed with Morison's equation is lower for loads case 3.4c than for 3.4a and 3.4b. The peak is however larger than the peak for load case, where a turbulent wind with a mean speed of 13.9 m/s is applied. The spectral peak for the moment computed using FNV is on the other hand larger for load case 3.4c than for 3.4b. This is an indication that the second order loading is more significant for the response in this load case than the two other ones performed without wind loading.

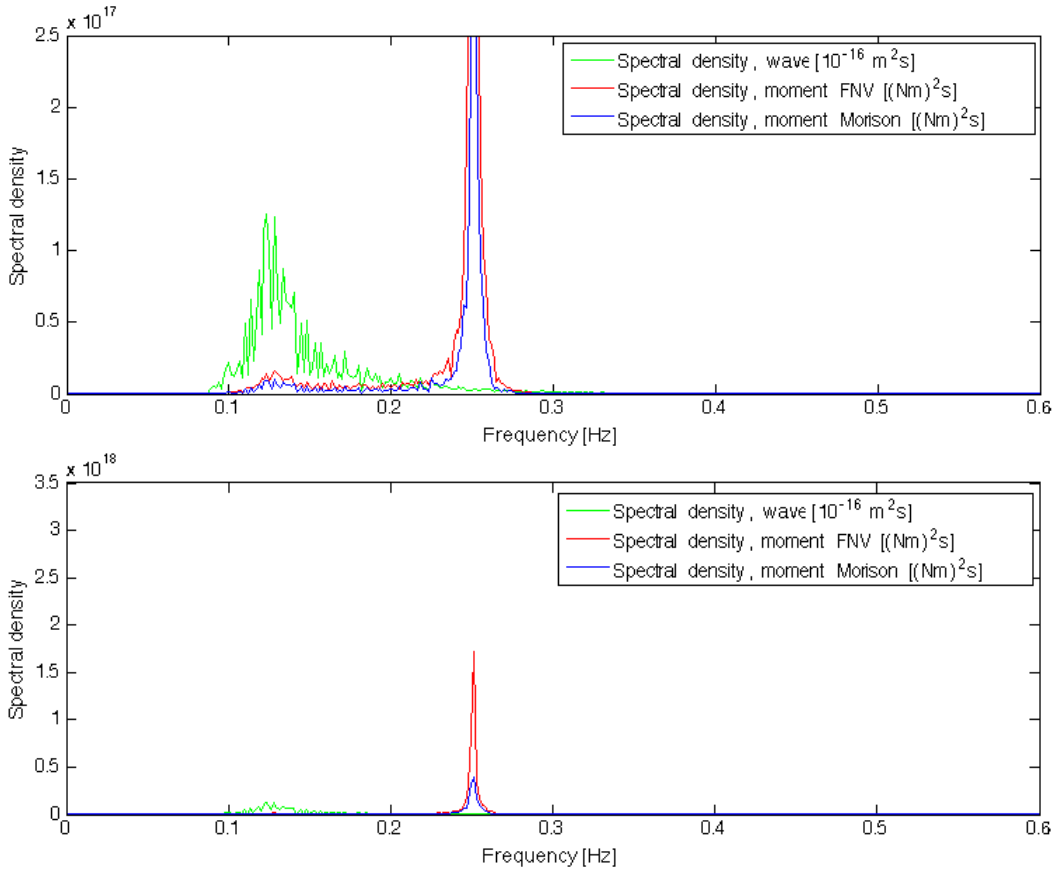

Figure 7.25: Spectral density of waves and fore-aft mudline moment for load case 3.4c.

Load case 3.5a, H_S = 3.0 m, T_P = 8.0 s, U_{hub} = 16.7 m/s

Load case 3.5a to 3.5c are based on the sea states with increasing wave height for a peak period of 8.0 seconds, to investigate the effect of increased steepness of the waves on the response and fatigue life of the offshore wind turbine.

As seen from Figure 7.26 the response to the wave loading is less when the offshore wind turbine is subjected to wind loading than when there is no wind loading. Another note to make is that the response spectra have a lower magnitude at the natural frequency for the mudline moment computed according to the FNV-model in this load case than in load case 3.3c. Load case 3.3c has the same peak period of the waves, however H_S and U_{hub} is lower for load case 3.3c than for load case 3.5a. The quasi-static and resonance response is only a little larger for the mudline moment due to the linear wave loading in load case 3.5a than in 3.3c. The response spectrum for the combined linear and second order wave load has for this load case, as for all previous load cases, a higher spectral density for all frequencies that are excited by wave loading.

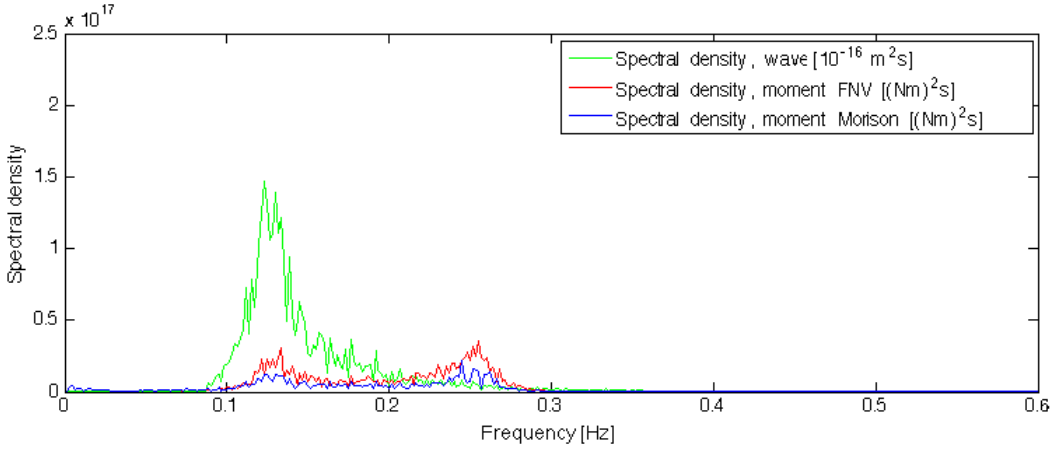

Figure 7.26: Spectral density of waves and fore-aft mudline moment for load case 3.5a.

Load case 3.5b, H_S = 3.5 m, T_P = 8.0 s, U_{hub} = 19.5 m/s

Load case 3.5b has a significant wave height that is 0.5 meters higher than load case 3.5a and a wind speed at the hub that is 2.8 m/s higher than in load case 3.5a. The response spectra for this load case are very similar to the spectra in the previous load case. The difference is that the peak for the quasi-static response is a little higher, due to the increase in significant wave height, and that the peak at the first mode natural frequency is also increased somewhat compared to load case 3.5a.

The mudline bending moment computed from the FNV-method still produce a higher spectral density for all frequencies in the plot, while the general shape of the spectrum is similar to the shape of the spectrum for the mudline moment computed with Morison's equation.

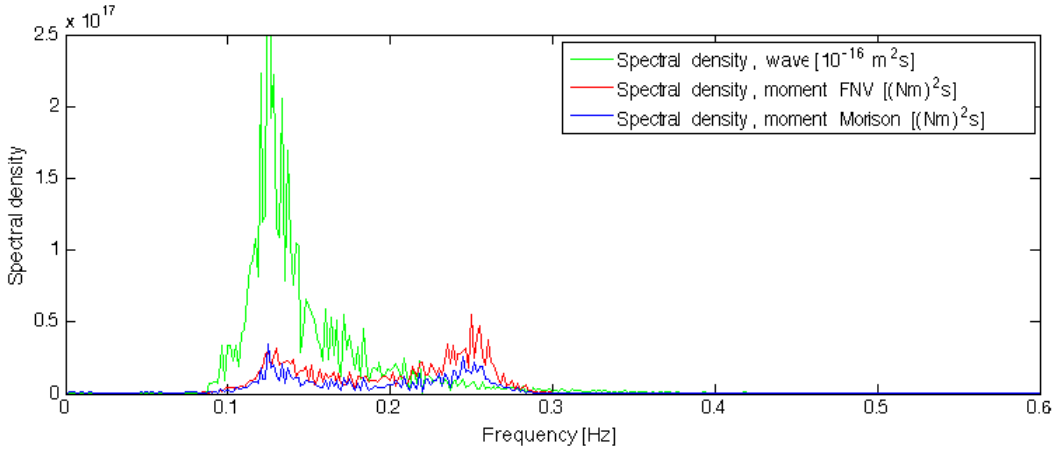

Figure 7.27: Spectral density of waves and fore-aft mudline moment for load case 3.5b.

Load case 3.5c, H_S = 4.0 m, T_P = 8.0 s, U_{hub} = 19.5 m/s

As seen from Figure 7.28, the spectral density peaks are increased further in load case 3.5c. A significantly larger peak is located just above the natural frequency of the first mode for both response spectra for the fore-aft mudline moment. The shape of the response spectrum is also here very similar for both calculation methods for the wave loading. However, the spectrum for the mudline moment computed by the second order FNV is higher than the spectrum based on calculations with Morison's equation for all frequencies. This trend has been seen in all the response spectra for the investigation of the effect of springing on the fatigue life, and will be discussed further in Chapter 8.

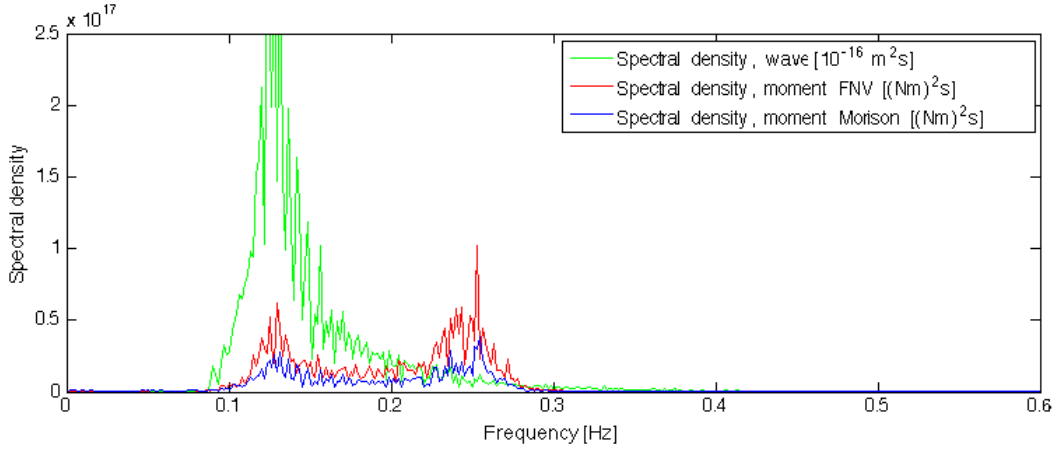

Figure 7.28: Spectral density of waves and fore-aft mudline moment for load case 3.5c.

Time Series Statistics and Trends

The standard deviation and mean values of the fore-aft mudline bending moment are listed in Table 7.7. The largest standard deviation is found for load case 3.4a, which has a significant wave height of 2.5 meters, a peak period of 6.0 seconds and no wind loading. This is also the load case with the largest observed peak in the spectral density at the natural frequency for both calculation methods.

Excluding load case 3.3c and 3.3d, one can see from the time series statistics that the standard devitaion follows the same trends for both calculation methods. The difference between the two methods of computation of the wave loading, is that the moments where the wave loads are computed with the FNV-method are consistently higher than the moments where Morison's equation is used. From Table 7.7 it is seen that the standard deviation for load case 3.1 is higher than the standard deviation of load case 3.2. These are two of the most probable environmental states in the NORA10 data, and both contribute to resonance at the first mode natural frequency as seen in the spectra for these load cases in the previous section. This result shows clearly that the effect of resonance is larger for load case 3.1, which is natural as the peak frequency of the wave spectrum for this load case is closer to the natural frequency of the first mode than for load case 3.2.

One can also clearly see the effect of aerodynamic damping by comparing the standard deviations for load case 3.3a to 3.3c, with the equivalent load cases with no wind loading in load case 3.4a to 3.4c. The standard deviations are significantly larger for the load cases without wind loading, as there is no aerodynamic damping. It is also observed that the standard deviation of the moments computed with Morison's equation decrease as the peak period of the wave spectrum inceases, and the peak of the wave spectrum is moved further away from the natural frequency of the support structure's first mode.

An important observation is made for the mean and standard deviation for load case 3.3c and 3.3d. For these two load cases the mean value of the mudline moment is significantly reduced for the moments computed with second order FNV compared to the moments computed with Morison's equation. The mean value of the load cases for the simulations where second order FNV is used, less than half the mean value of the moment for the simulations using Morison's equation. For all other load cases in the investigation of springing, the mean values for the FNV-computations and the Morison's computations are close to being exactly the same.

In addition, the trend of decreasing standard deviations as the peak of the wave spectrum is moved further from the natural frequency as observed for the moments computed with Morison's equation, is not appliccable for the second order FNV computations. Load case 3.3c has a standard deviation that is 17 MNm larger than load case 3.3b, and the standard deviation of load case 3.3d is 10 MNm larger than load case. Hence there is no such trend for the

FNV-simulations for load cases 3.3a to 3.3d.

The ratios between the standard deviation of the simulations with Morison's equation and the simuations with the second order FNV-method are also found in order to compare the effect of second order loading for the different load cases. As the load cases have different environmental parameters the direct comparison between the standard deviations from different load cases will not give a correct representation of the degree of second order loading.

As seen from Table 7.8 the highest ratio between the standard deviations is obtained for load case 3.3c and 3.3d, with a value of 2.07 and 1.98 respectively. For load case 3.4a to 3.4c, the highest ratio is obtained for load case 3.4c with a value of 1.61. The remaining load cases all have ratios in the range between 1.33 and 1.40.

Table 7.7: Standard deviation, mean, minimum and maximum value of fore-aft mudline moment for all load cases with Morison's equation and second order loading from FNV-method.

	Load Case	Mudline Moment Morison		Mudline Moment FNV	
		Standard Deviation [MNm]	Mean [MNm]	Standard Deviation [MNm]	Mean [MNm]
Morison	3.1	37.081	60.416	50.797	60.398
	3.2	33.326	82.028	44.340	82.033
	3.3a	42.018	68.500	58.345	68.488
	3.3b	36.374	68.482	49.798	68.504
	3.3c	32.305	68.495	66.946	30.695
	3.3d	30.122	68.489	59.583	30.719
	3.4a	91.576	-1.6060	136.50	-1.6038
	3.4b	71.649	-1.6444	107.24	-1.6342
	3.4c	55.164	-1.6222	88.728	-1.6332
	3.5a	35.455	55.114	48.144	55.113
	3.5b	41.255	47.768	55.459	47.789
	3.5c	45.729	47.794	64.168	43.204

Table 7.8: Ratio of standard deviation from analyses with Morison's equation and second order loading from FNV-method.

Load Case	Ratio of standard deviation Fore-Aft moment [-]
3.1	1.37
3.2	1.33
3.3a	1.39
3.3b	1.37
3.3c	2.07
3.3d	1.98
3.4a	1.49
3.4b	1.50
3.4c	1.61
3.5a	1.36
3.5b	1.34
3.5c	1.40

7.3.1 Fatigue Damage Results

From the fatigue damage results presented in Table 7.9, one can see that the fatigue damage is closely related to the standard deviation. This is seen from the fact that the fatigue damage follow the same trends as the standard deviation described previously in Time Series Statistics. The largest fatigue damage is obtained for load case 3.4a. This is the load case with the smallest peak period of the load cases without wind, and hence the load case of the three load cases without wind with the most linear wave loading in the range of the first mode natural frequency.

The largest ratio between the results from simulations with Morison's equation and simulations with the second order FNV-method is however seen for load case 3.3c and 3.3d. The large difference in the ratios for the fatigue life and the ratios for the standard deviation, show how large stresses will contribute to decreasing the fatigue life of the offshore wind turbine.

Table 7.9: Fatigue results for H_S=2.5 m, T_P=6.08 s and U_{hub} for simulations with Morisons equation and the FNV-method to the second order.

Load Case	Fatigue damage 1 hr simulation $[\cdot 10^{-3}]$		Fatigue life for environmental state [Years]		
	Morison	FNV	Morison	FNV	Ratio of fatigue life
3.1	0.0682	0.2918	0.5577	0.1304	4.28
3.2	0.0420	0.1739	0.9051	0.2189	4.14
3.3a	0.1302	0.4655	0.2922	0.0817	3.57
3.3b	0.0596	0.2485	0.6385	0.1531	4.17
3.3c	0.0306	0.8230	1.2446	0.0462	26.92
3.3d	0.0198	0.5506	1.9239	0.0691	27.84
3.4a	2.0879	7.6733	0.0182	0.0050	3.68
3.4b	0.9913	3.8595	0.0384	0.0099	3.89
3.4c	0.3981	2.0597	0.0956	0.0185	5.17
3.5a	0.0558	0.2168	0.6815	0.1756	3.88
3.5b	0.1159	0.3641	0.3284	0.1045	3.14
3.5c	0.1779	0.6048	0.2138	0.0629	3.40

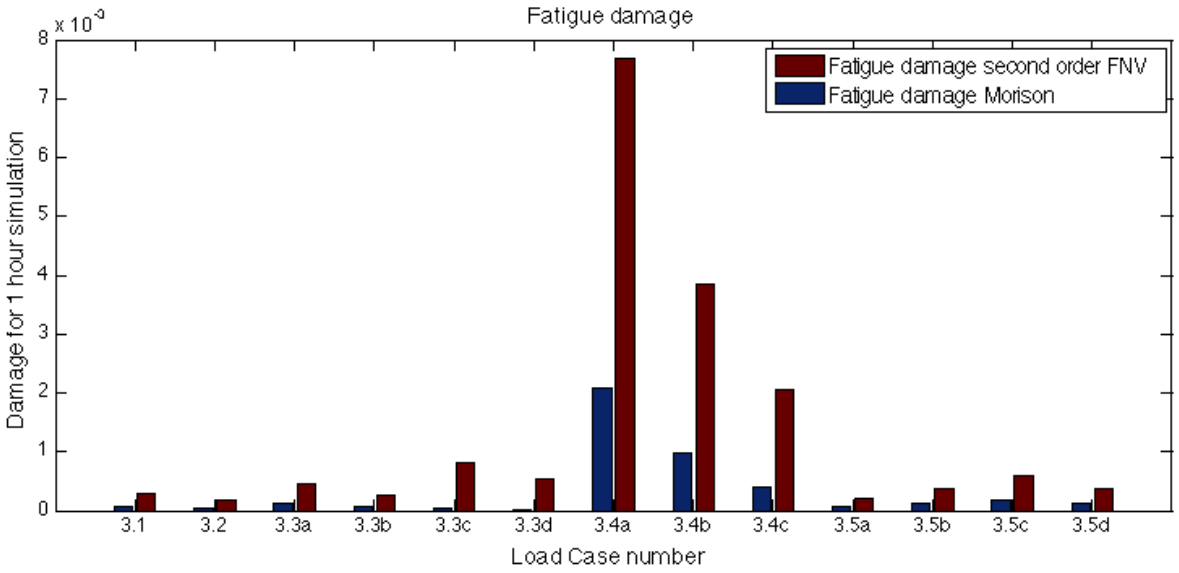

Figure 7.29: Fatigue damage for each load case from a 1 hour simulation.

7.3.2 Normalised Wavelength

The normalised wavelength for the sea states used in the investigation of springing effects on the fatigue life has been calculated in order to investigate whether there is reason to believe that the second order loading computed with the FNV-method overpredicts the loading. As no experimental data or results from full diffraction analyses for this wind turbine are available, the values will be compared to the results obtained by Krokstad and Standsberg (1995). The normalised wavelength is calculated for a diameter of 8.0 meters, as this is the diameter used in the FNV-simulations.

Table 7.10: Values of normalised wave length, ka, for all load cases.

Load Case	Cross section mudline		
	Wave number k [rad/m]	Radius a [m]	Normalised Wavelength ka [rad]
3.1	0.199	4.00	0.796
3.2	0.133	4.00	0.533
3.3a	0.109	4.00	0.436
3.3b	0.082	4.00	0.329
3.3c	0.063	4.00	0.252
3.3d	0.050	4.00	0.199
3.4a	0.112	4.00	0.448
3.4b	0.082	4.00	0.329
3.4c	0.063	4.00	0.252
3.5a	0.063	4.00	0.252
3.5b	0.063	4.00	0.252
3.5c	0.063	4.00	0.252

As seen from Table 7.10 the values of the normalised wavelengths ranges from 0.796 to 0.199. The load cases with a peak period of 8.0 seconds have a normalised wave length of 0.252. Comparing this value to the plot by Krokstad and Standsberg (1995) in Figure 3.6, it is seen that the agreement between the full diffraction WAMIT results and the second order FNV-term is good. This is an indication that the overprediction will not be caused by diffraction effects for these load cases. For the load cases with a lower period, the difference between the full diffraction WAMIT and the second order wave load from the FNV-model will be larger, as seen from Figure 3.6

Chapter 8

Discussion

8.1 Damping of the Offshore Wind Turbine

Damping Contributions from Soil and Structure

The damping from the logarithmic decay test is for the offshore wind turbine excluding the aerodynamic damping has a value of 0.75%. This in correspondence with the stiffness proportional damping applied to the individual elements of the support structure. The damping of the soil does not have any impact on the overall damping in this case, implying that the damping in this part of the model is either too low to be of significance for the overall damping, or that the displacements in the soil are not large enough for the soil damping to have any significance for the total damping.

To investigate whether the it is the soil damping that is too low, or the displacements in the soil that are insignificant, an additional simulation with an increased soil damping is performed. The results from the additional simulation show that the damping contribution from the finite element soil model is of significance for the total damping of the offshore wind turbine. The increase of the damping from the finite element model from a damping ratio of 0.35% to 3.0% resulted in an increase of the total damping ratio from 0.75% to 1.75%. This means that the displacements of the foundation in the soil are of significant magnitude, so that the soil damping has an effect on the total damping. This also shows that the applied soil damping in the model used for the investigation of the effect of misalignment and second order loading is low and a correctly estimated soil damping will for this specific wind turbine will have an effect on the response of the structure.

Aerodynamic Damping

The aerodynamic damping has a significant contribution to the overall damping when the turbine is operational. According to theory, the aerodynamic damping is dependent on the change in thrust force on the turbine. This means that the magnitude of the aerodynamic damping should follow the thrust curve for the 5MW NREL wind turbine. Hence, it is expected

that the aerodynamic damping should increase until the wind speed reaches rated speed, and then decrease for wind speeds above rated speed. As observed in the results, this is not the case for the aerodynamic damping obtained from the analysis of the logarithmic decay in the tower top displacements. In stead of gradually decreasing after reaching rated speed, the aerodynamic damping keeps increasing until reaching a maximum at 19.5 m/s, which is 8.1 m/s above rated speed. An increase in the aerodynamic damping ratio after a small drop just after rated speed was also obtained in the simulations performed by Cerda and van der Tempel (2005) for some of the variable speed wind turbine designs analysed. However, the increase in the aerodynamic damping after the initial drop obtained from simulations was not as large as the increase obtained in this thesis.

There is some uncertainty in the results for the aerodynamic and overall damping as is not possible to filter out all of the stochastic response at the tower top. Hence, there is still some noise left in the vibrations, making it difficult to determine the decay for each cycle. Load case 1.5, with a wind speed of 13.9 m/s, has the most noise in the results. However, a general trend is that there is more noise in the filtered vibrations for the wind speeds above rated speed. As the blades are pitched for the wind speeds above rated speed, this may be the reason for the increased noise in the filtered results for these wind speeds.

The noise in the filtered vibration time series may is a source of uncertainty in the results and a reason to why the damping level obtained from the simulations above rated wind speed are higher than expected. If the amplitudes included in the computation of the logarithmic decays is a result of the noise in the signal rather than the actual response to the step pulse loading, this will affect the results.

Load case 1.9 has a mean speed above cut-off speed, however the damping is still in the range of the aerodynamically damped load cases. As the mean wind speed is just above rated speed and the turbine is subjected to turbulent wind, the damping level of 5.41% can be explained by the wind speed being below the cut-off speed for the turbine for the duration of the simulation.

8.2 Overconservatism in the Second Order FNV-Method

The formulation of the FNV-method up to the second order has been used to investigate the effect of springing on the fatigue life for both misaligned load cases and the investigation of the effect of second order loading. In order to discuss the results with regard to the overprediction in loads by applying this method of calculation for the second order loading, the discussion regarding the overconservatism in this method is discussed before the results themselves.

For all load cases, both for the investigation of the effect of misalignment and springing on the

fatigue life, a general trend in the results is that the spectral density of the fore-aft mudline bending moment is larger for the simulations where the wave loads are computed according to the FNV-method to the second order. This trend is observed for both the quasi-static part of the response and the resonance part of the response to the wave loading. For the load cases that are expected to be dominated by linear loading, such as load case 3.1 ans 3.2 the standard deviations are also higher for the simulations using the FNV-method for wave load computation. The reason for the higher spectral densities and standard deviations when the FNV-method is used, is partly due to the fact that the diameter of the substructure at the mudline is used to compute the wave loading. An underlying assumption for the FNV-method is that the structure subjected to wave loading has a constant cross section. This means that the wave loading, even when only considering the first order term of the FNV-model, will be larger than the wave load computed with Morison's equation since the diameter used in the computation is larger for all cross sections above the mudline. As the linear wave loading will be amplified at the natural frequency, this may also be the reason why a much larger peak in the response spectrum for the mudline moment for simulations with the second order FNV-method is observed for load case 3.1 and 3.2, even though the second order loading is expected to be negligible for these load cases.

Another important aspect of the use of a larger diameter for the computation of wave loads with the FNV-method is that the effect of an increased diameter on the magnitude of the loading is larger closer to the water surface. The reason for this is that the acceleration of the wave particles decrease with increasing depth, and thus the inertia force due to the waves decrease with depth in the same manner. Hence as the difference between the actual diameter of the cross section and the diameter used in the FNV-method is largest where the water particle acceleration is at its maximum value (in the z-direction), the effect of the constant diameter assumption on the magnitude of the mudline bending moment will be even larger. As the difference in the wave loading due to the different diameters used is largest for the cross sections that are furthest from the mudline, where the moment is computed, the effect on the magnitude of the moment will be even larger.

Load case 3.1 has a period that is very close to the natural period of the offshore wind turbine, and should hence not be exited by second order loading according to theory. The results show a ratio between the standard deviations for the mudline bending moment computed with the two different wave load models, of 1.37. With regard to this it would be fair to assume a rough estimate of approximately 30% overprediction of the mudline moment when computing the wave loading according to the FNV-method.

The considerations discussed above must be kept in mind when analysing the results and evaluating the effect of misalignment and second order loading on the offshore wind turbine.

8.3 Effect of Misaligned Wind and Waves on the Fatigue Life

The results from the analyses of the offshore wind turbine in misaligned wind and waves clearly show that the fatigue life of the offshore wind turbine decrease for the load cases with an angle of misalignment larger than 15°. This is mainly due to the increase in the side-side moment which has a much lower damping than the fore-aft moment.

The structure is excited at resonance for all load cases, which can be seen from the peaks in the response spectra located at the same frequency as the natural frequency of the first mode of the support structure. These are identified as resonance as they do not follow the shape of the wave spectrum, which is the case for the quasi-static response. This means that there is sufficient excitation from linear wave loading at the natural frequency for significant resonance vibrations to occur. For the analyses where the second order wave loading is included by computing the wave loads according to the FNV-method, the excitation at resonance is even larger, leading to a fatigue damage that is up to 4.3 times higher than the analyses with only linear wave loading. However, the ratio between the standard deviations of the mudline moment computed with the two different load models in the fore-aft direction is at its maximum for load case 2.1. The ratio is for this load case 1.38 which is close to the ratio of load case 3.1 which is discussed in the above section. Taking the overprediction of the linear loading when computed with FNV-method compared to Morison's equation, and assuming that the overprediction is approximately 30%, the effect of the second order loading is not very large in the fore-aft direction. This means that the second order loading will also have an effect on the response of the offshore wind turbine, even if the peak period of the applied wave spectrum is not a multiplum of 2 of the natural frequency. It should also be mentioned that the structural damping applied to the offshore wind turbine is only 0.75%. This value is 0.25% lower than the value specified in the OC3 project Jonkman et al. (2007). The low structural damping may be a reason for the large responses in resonance for the side-side mudline moment. As previously discussed in 3.6 Natural Frequencies and Dynamic Response, the dynamic transfer function of the offshore wind turbine is dependent on the damping of the structure. As the values of the structural damping and soil damping used in the analyses are low compared to the values given in the literature, the responses to the excitation are amplified more than for the equivalent structure with a higher damping level. This

As the all sea states used in the analyses have a peak period of 6.0 seconds, the effect of second order loading is not expected to have a large effect on the resulting response of the offshore wind turbine. For a sea state with a peak period of 6.0 seconds the maximum value of the second order loading will have a frequency of approximately 0.33 Hz according to the theory. As this is 0.08 Hz above the natural frequency of the first mode of the support structure, the effect on the response from this loading is assumed to be small. Comparing the results of the mudline moment in both directions computed with Morisons equation to the same moments computed with the second

order FNV-method it is however a significant effect of the second order loading.

The second order loading has a larger effect on the side-side mudline moment than the fore-aft mudline moment. This can be explained by the negligible of aerodynamic damping in the side-side direction. The ratio between the standard deviations of the mudline moment from the two computation methods increases as the angle increases for the side-side mudline moment. This effect is caused by the waves becoming more domuínating for the response in this direction as the angle is increased.

The opposite trend is seen for the fore-aft mudline moment. This shows that the wave loading is becoming less important for the response. For load case 2.5 the ratio is 1.00, which shows that the response in terms of the mudline moment is no longer affected to any significant degree by the wave loading. This statement can also be argued by the fact the there is no overprediction in the loading from the FNV-method for this laod case.

The calculated fatigue lifes for each of load cases are all very low, and in the range of only a few days. It is important to note in this regard that for a complete fatigue analysis for design purposes will include a wide range of different environmental states that are more likely to occur than the ones used in this investigation. Hence the probability of the environmental state must be taken into account as well when evaluating the fatigue damage. Load case 2.5 has a probability of occurrence of zero according to the NORA10 data. Hence, even though the fatigue damage is larger for the load case 2.5 than any of the other load cases, it will in reality have no effect on the total fatigue life of the offshore wind turbine. The most probable load cases, 2.1 and 2.2, do not have as high standard deviations as load case 2.5 and have a probability of 0.534% and 0.803% respectively. These load cases will have more significance for the total fatigue life in a full fatigue analysis.

From the ratios of the standard deviation between the mudline moment computed with Morison's equation and the moment computed with the FNV-method one can see that the effect of second order loading is larger for the side-side direction than the fore-aft direction. This shows that the effect of second order loading is larger when the damping is low. This effect is further amplified in the calculation of the fatigue damage and fatigue life, as can be seen in the large difference in the fatigue loads.

8.4 Effect of Second Order Loading on the Fatigue Life

Investigation of Response to Second Order Loading with Increasing Peak Periods

The results from the computations with Morison's equation show that the standard deviation of the mudline moment increases with the increase in the wave period. This is expected as the peak frequency of the wave spectrum is moved further away from the natural frequency of the first mode.

The results for load cases 3.3a to 3.3d show that there is significant response at the natural frequency, at 0.2 Hz and at 0.4 Hz. The last two responses do not coincide with any of the natural frequencies of the offshore wind turbine, and is hence difficult to explain. The fact that they are only observed for the FNV-computation and not for the other load cases with the same wind speed makes it even more difficult to explain. One suggestion is that the peaks may be due to pitching of the blades, which may also be supported by the observations for the computations of the aerodynamic damping in which it was difficult to filter out the noise in the tower top vibrations. Further investigation into the source of these peaks should be conducted to determine how much effect the peaks have on the total response.

The ratio between the standard deviations for these load cases is also much higher than expected. In addition the mean is decreased to half the value of the mean for the results from simulations with Morison's equation. This gives reason to believe that the standard deviation is affected by the additional contributions from the peaks will have a significant impact on the results.

Investigation of Response in Negligible Aerodynamic Damping

For load case 3.4a to 3.4c, which are performed without applying wind one can clearly see the effect of the aerodynamic damping in the resutls. The response to the wave loading is the largest for all load cases for these load cases, both in terms of the response spectra and the standard deviation of the as the total damping is only 0.75%. The largest responses are found for load case 3.4a which has a peak period of 6.0 seconds. This is the load case with the most linear wave loading close to the natural frequency of the first mode of the support structure, and shows that the linear loading is more important than the second order loading for the response when the damping is low.

The largest effect of the second order loading is however obtained for load case 3.4c, which has a peak period of 8.0 seconds. The trend seen in the ratio between the standard deviation of

the mudline moment for these three load cases is that the ratio increases with increasing peak period. This is in compliance with the expectations to the results and literature, as the maximum second order loading according to theory excited the structure at a frequency that is twice the peak frequency of the wave spectrum.

8.4.1 Investigation of Response with Increasing Steepness

For load case 3.5a to 3.5c the standard deviation increases with each step up in significant wave height. The ratio between the standard deviations does however not follow the same pattern. From load case 3.5a to load case 3.5b there is a small drop in the standard deviation. This may be due to the aerodynamic damping, assuming that the damping ratios predicted are correct. The maximum damping is obtained for the same wind speed as applied in load case 3.5b. Hence the larger damping may be a reason for the slightly lower ratio obtained for this load case.

8.4.2 Fatigue Damage and Fatigue life

The fatigue lifes computed from the analyses are all very low, even for load case 3.1 and 3.2, which are the most probable environmental states investigated. The largest fatigue damage is obtained for load case 3.4a, with a value of $7.6733 \cdot 10^{-3}$ for the results from the FNV-simulation. This amount of damage corresponds to a fatigue life of approximately two days. This shows how important the damping is for the fatigue life.

In interesting obsertion in the results is that load case 3.3c and 3.3d have the largest fatigue lifes for the simulations with Morison's equation. For the simulations with the second order FNV-method on the other hand, the fatigue life is amping the lowest. The effect of a doubled standard deviation, which is the difference between the standard deviation from Morison's equation and the standard deviation from the FNV-method for load case 3.3c, results is a ratio of 26.29 for the computed fatigue damage and fatigue life. In this regard it is important to note that the probability of occurrence for these sea states have an impact on the total effect of the chosen environmental states throughout the life of the offshore wind turbine.

The low fatigue lifes for the offshore wind turbine in general is may be connected to the probability of the sea states and the design of the offshore wind turbine it self. None of the load cases with no wind loading are given in the metocean data from NORA10 and hence they will not occur due to the environment as the wave height and peak period is too high for the environmental states to occur when the wind speed is within the lowest wind speed bin. The conditions of load case 3.3a - 3.3c may however occur during fault conditions or maintenance stops. If this sea state should occur, the turbine will fail after only a couple of days.

Chapter 9

Summary and Recommendations for Further Work

In this thesis an investigation of factors that may influence the fatigue life of an offshore wind turbine is perfomed. The damping of the offshore turbine, with and without aeroaynamic damping is estimated for the range of wind speeds for which the turbine is in operation. The effect of misaligned wind and waves and second order loading in terms of springing is also investigated in terms of their contribution to the fatigue damage in the offshore wind turbine.

A review of the load cases relevant for the fatigue limit state for offshore wind turbines is also performed. This review emphasizes the focus on response and not excitation when evaluating load cases. The load cases giving the largest response should be used for the computation of the fatigue damage as this is relevant in a fatigue perspective. Hence, environmental states that does not necessarily have the most severe conditions must be evaluated for fatigue as the response to these conditions may be large if resonance occurs.

The metocean data in the NORA10 data are also post-processed in order to have a basis for the selection of sea states to investigate for the effects of springing and misalignment between wind and waves in the fatigue life of the offshore wind turbine. The data showed that the misalignment at this specific cite at Doggerbank is relatively small, as approximately 90% of the data sets for the environmental states over 57 years have a misalignment angle of 30° or less. The probability of occurrence for a misalignment angle of 90° is as low as 0.881, and the waves and peak periods that occur for this misalignment angle is on the range between 0 and 0.5 meters and 0 and 1.0 seconds. Hence the waves that will contribute to fatigue at this angle of misalignment will be small and short and are assumed to have a low impact on the fatigue life in a full fatigue analysis.

The set of load cases chosen for the investigation of misalignment is based on the most probable environmental conditions that have a peak period which is not too close to the natural period. This resulted in a set of five load cases with a significant wave height of 1.5 meters, a peak period of 6.0 seconds and a wind speed at hub height of 8.3 m/s. The angles of misalignment chosen are 0°, 15°, 30°, 45° and 90°. The load case with 90° misalignment is included despite the fact that it does not occur in the NORA10 data, in order to investigate the worst case scenario for the misalignment where there will be negligible aerodynamic damping of the wave excitation.

The load cases for the investigation of springing is also based on the same set of metocean data. A total of 12 load cases are chosen, where two of these correspond to environmental states that will be governed by the linear wave loading and that have a relatively high probability of occurrence. Four of the load cases are chosen to investigate the effect of springing and second order loading when the peak period of the wave spectrum is increased. Three load cases are chosen for the investigation of the effect of second oreder loading when there is negligible aerodynamic damping. The load cases has no wind excitation applied and correspond to a situation in which the turbine is stopped. The same significant wave height and peak periods as for the three first load cases for the investigation of how the peak period of the wave spectrum affects the degree of second order loading on the offhore wind turbine. The last three load cases are chosen for to investigate whether the steepness of the waves will have an effect on the second order loading.

The investigations of the damping ratio of the offshore wind turbine in the absence of wind loading showed that an increased soil damping would have and effect on the total damping of the structure. This means that there is sufficient displacement of the foundation in the soil for the soil damping to have an effect on the total damping. An increase of the soil damping ratio from 0.35% to 3.0% gives an increase in the total damping ratio of 1%. Thus for this specific offshore wind turbine a correct estimation of the damping contributions from the soil and the foundation is important to obtain a correct level of damping to be used in simulations, as this will have an effect on the response of the structure.

The total damping is determined by means of analyses of the free vibrations of the tower top of the offshore wind turbine. The results are not as expected as the maximum damping is obtained for a wind speed of 19.5 m/s and not at rated speed as would be expected according to theory. The explanation of the higher damping ratio may be that the controller of the wind turbine has an effect on the damping and that the pitching of the blades in the simulations will give a higher thrust force on the turbine. Another explanation might be that the noise observed in the filtered displacements at the tower top affects the amplitudes that the logarithmic decrement is calculated from, so that a higher damping level than expected is obtained from the results. This noise occurs for all wind speeds above rated speed and is assumed to be caused by the pitching of the blades.

For the investigation of the fatigue in misaligned wind and waves the highest fatigue damage is obtained for load case 2.5 with a 90° angle of misalignment. This is the case for both the simulations performed with Morison's equation for the computation of wave loads and for the simulations with the second order FNV-method. The results from the simulations with the FNV-method are generally higher for all frequencies where wave excitation occur, not only in the range of second order loading. This shows that the wave loading is overpredicted with the second order FNV-method as applied in this thesis. However, since the ratio between the standard deviation of the mudline moment in the side-side direction increases with increasing

angle one can conclude that the second order loading will be more pronounced for load cases where the damping of the wind tubine is small. This means that the effect of second order loading on the fatigue life of the offshore wind turbine will be larger for larger angles of misalignment.

The investigation of the effect of second order loading on the fatigue life shows that the second order loading will be most signifcant for the load cases with a peak period that is the double of the natural period. Also for this investigation the mudline moments computed with the FNV-method are overpredicted, which can be seen clearly from load case 3.1 which should only be affected by linear wave loading. The ratio between the mudline moments computed with the different load model is for this load case 1.37 which shows a significant overprediction for the simulation with the FNV-method. This overprediction of the mudline moments is further amplified in the computed fatigue damage resulting in even larger ratios between the fatigue damage and fatigue life computed with the different load models.

Despite of the overprediction with the FNV-method it is possible to see an effect of the second order loading for some of the load cases. Load case 3.3c and 3.3d have the highest effects of the second order loading when only comparing the standard deviations. However, two peaks in the response spectrum is observed at 0.2 and 0.4 Hz for the simulations with the FNV-method for these load cases. These peaks do not correspond with any of the natural frequencies of the offshore wind turbine, and are difficult to explain from a physical point of view. The peaks may be caused by the pitching of the blades, however a further investigation into this must be conducted in order to draw any conclusions. Nevertheless, they do contribute to an increase of the standard deviation of these two load cases for the simulations with the FNV-method, and may explain why the ratio of the standard deviations for these two load cases are higher than for the load cases with no aerodynamic damping. Load case 3.4 c, has the highest effect of second order loading disregarding the teo load cases mentioned above. Taking the overprediction of the FNV-method into account, the remaining load cases with a period of 8.0 seconds, load case 3.5a to 3.5c, does not have the same high effect of the second order loading and have ratios close to the ratio obtained for load case 3.1 which is assumed to only be governed by linear wave loading. These load cases also have a a higher overall damping than any of the other load cases, assuming that the predicted damping ratios in Chapter 7.1 are correct. This means that one can conclude that the damping of these load cases has an effect on the contribution of the second order loading in the total response of the offshore wind turbine, and hence also on the fatigue damage due to second order loading.

9.1 Recommendations for Further Work

Several improvements can be carried out to further investigate the objectives in this thesis. As the second order FNV-method, as applied in this thesis, will give overconservative results a first improvement is to apply an equivalent diameter in for the computation of first and second order wave loads with the FNV-method. The equivalent diameter should be determined so that the first order term of the FNV-method corresponds to the inertia term of Morison's equation. By doing this, the change in the diameter of the substructure of the offshore wind turbine is taken into account in the FNV-computations, and a better comparison of the two calculation methods can be performed.

In addition, the damping is seen to have an effect on the response to second order loading. The damping used for the soil and the structure in this thesis is very conservative. A further investigation into the effect of damping on the response of the structure to second order loading can give valuable information about the relation between the damping and response to second order wave loads

Moreover a comparison of the second order loading calculated with the FNV-method with experimental results and more accurate simulations can be interesting to investigate the implications in terms of accuracy of the second order loading when computing the loads according to the FNV-method. Alternative load models for the computation of second order loading can also be compared to the FNV-method for comparison in terms of the the accuracy. This might be of use as the accuracy in the prediction of fatigue loads can have a great impact on reliability of the design and costs.

The peaks observed for load case 3.3c and 3.3d should be further investigated to determine whether they are a result of physics or numerics. The fact that the peaks only occur for the simulations using the FNV-method and that they do not occur for all load cases with the same wind speed, although the same wind field is used for all simulations, suggest that these response peaks may be related to the wave loading or to the numerics of the software. However, the only explanation for the peaks that can be given in this thesis is that they might be realted to the pitching of the blades. The peaks may also be a response to the control system in terms of pitching, thus the aerodynamic loading and control system should also be evaluated in a further investigation. As the standard deviation obtained for these load cases are significantly larger, it is essential from a fatigue perspective that the origin of these responses is identified as they will significantly increase the fatigue damage.

References

Agarwal, P. and Manuel, L. (2011). Incorporating irregular nonlinear waves in coupled simulation and reliability studies of offshore wind turbines. *Applied Ocean Research*, 33(3):215 – 227.

Almar-Næss, A. (1985). *Fatigue Handbook*. Tapir.

Berge, S. (2006). Fatigue and fracture design (II): Fatigue design of welded structures.

Burton, T., Jenkins, N., Sharpe, D., and Bossanyi, E. (2011). *Wind Energy Handbook*. John Wiley & Sons Ltd.

Cerda, D. J. and van der Tempel, J. (2005). Aerodynamic Damping in the Design of Support Structures for Offshore Wind Turbines.

Chakrabati, S. K. (1987). *Hydrodynamics of Offshore Structures*. Computational Mechanics Publications.

Devrient, C., Jordaens, P. J., Sitter, G. D., and Guillaume, P. (2013). Damping Estimation of an Offshore Wind Turbine on a Monopile Foundation. *IET Renewable Power Generation*, 7(4):401–412.

DNV (2010a). *Offshore Standard DNV-OS-J101: Design of Offshore Wind Turbine Structures*. DNV.

DNV (2010b). *Recommended Practice DNV-RP-C205: Environental Conditions and Environmental Loads*. DNV.

DNV (2012). *Recommended Practice DNV-RP-C203: Fatigue Design of Offshore Steel Structures*. DNV.

Faltinsen, O. M. (1990). *Sea Loads on Ships and Offshore Structures*. Cambridge University Press.

Faltinsen, O. M., Newman, J., and Vinje, T. (1995). Nonlinear wave loads on a slender vertical cylinder. *Journal of Fluid Mechanics*, 289:pp. 179–198.

Fedem Technology AS (2012). Internal report: Integrated Numerical Analysis and Technology Qualification for Offshore Wind Turbines; Foundation Screening. Unpublished work, Fedem Technology AS.

Houlsby, G., Ibsen, L., and Byrne, B. (2005). *Suction Caissons for Wind Turbines*, pages 75–93. Marcel Dekker Incorporated.

Johannessen, K., Meling, T. S., and Haver, S. (2001). Joint Distribution for Wind and Waves in the Northern North Sea. In *Proceedings of the Eleventh (2001) International Offshore and Polar Engineering Conference*, pages 19–28, Stavanger, Norway.

Jonkman, B. J. (2009). *TurbSim user's guide: Version 1.50*. National Renewable Energy Laboratory Colorado.

Jonkman, J., Butterfield, S., Musial, W., and Scott, G. (2009). Definition of a 5-MW Reference Wind Turbine for Offshore System Development.

Jonkman, J., Passon, P., Kühn, M., Butterfield, S., Camp, T., and Larsen, T. J. (2007). OC3 - Benchmark Exercise of Aero-Elastic Offshore Wind Torbine Codes. In *Proceedings of the 2007 Science of Making Torque from Wind Conference. Journal of Physics: Conference Series 75.*, volume 75(1), page 12 pp. IOP Publishing Ltd.

Krokstad, J. R. and Standsberg, C. T. (1995). Ringing load models verified against experiments. In *OMAE 1995, 14th International Conference on Offshore Mechanics and Arctic Engineering*, Copenhagen.

Krokstad, J. R., Standsberg, C. T., Nestegård, A., and Marthinsen, T. (1998). A new nonslender ringing load approach verified against experiments. *Journal of Offshore Mechanics and Arctic Engineering*, 120:pp. 20–29.

Kühn, M. (2001). *Dynamics and Design Optimization of Offshore Wind Energy Conversion Systems*. PhD thesis, DUWIND Delft University Wind Energy Research Institute.

Langen, I. and Sigbjörnsson, R. (1979). *Dynamisk analyse av konstruksjoner*. Tapir.

Marino, E. (2010). *An Integrated Nonlinear Wind-Waves Model for Offshore Wind Turbines*. PhD thesis, University of Florence - TU-Braunschweig.

Marino, E., Lugni, C., and Borri, C. (2013). The role of the nonlinear wave kinematics on the global responses of an {OWT} in parked and operating conditions. *Journal of Wind Engineering and Industrial Aerodynamics*, 123, Part B:363 – 376.

Michel, W. H. (1968). Sea Spectra Simplified. *Marine Technology*, 5(1):17–30.

Newland, D. E. (1993). *An introduction to Random vibrations, spectral and wavelet analysis*. Longman Scientific and Technical, third edition edition.

Newman, J. N. (1996). Nonlinear scattering of long waves by a vertical cylinder. In Grue, J., Gjevik, B., and Weber, J. E., editors, *Waves and Nonlinear Processes in Hydrodynamics*, pages pp. 91–102. Springer Netherlands.

Reistad, M., Breivik, Ø., Haakenstad, H., Aarnes, O. J., Furevik, B. R., and Bidlot, J.-R. (2011). A high resolution hindcast of wind and waves for the North Sea, the Norwegian Sea and the Barents Sea. *Journal of Geophysical Research: Oceans (1978–2012)*, 116(C5).

Schløer, S. (2013). *Fatigue and extreme wave loads on bottom fixed offshore wind turbines; Effects from fully nonlinear wave forcing on the structural dynamics*. PhD thesis, DTU Wind Energy.

Seidel, M., von Mutius, M., Rix, P., and Seutel, D. (2005). Integrated analysis of wind and wave loading for complex support structures of Offshore Wind Turbines. In *Conference Proceedings Offshore Wind 2005. Copenhagen*.

Sieros, G., Chaviaropoulos, P., Sørensen, J. D., Bulder, B. H., and Jamieson, P. (2012). Upscaling wind turbines: theoretical and practicle aspects and their impact on the cost of energy. *Wind Energy*, 15:3–17.

Tarp-Johansen, N. J., Christensen, E. D., Mørch, C., and ans Sten Frandsen, B. K. (2009). Comparing Sources of Damping of Cross-Wind Motion. In *Conference Proceedings EOW 2009*, Stockholm.

Tromans, P., Swan, C., and Masterton, S. (2006). Nonlinear potential flow forcing: The ringing of concrete gravity based structures. Technical report, Health and Safety Executive.

Van der Tempel, J. (2006). *Design of Support Structures for Offshore Wind Turbines*. PhD thesis, TU Delft.

Appendix A

Scatter Diagrams

A.1 Scatter Diagrams for Wind Speed Bins of 2 m/s

The frequency diagrams for the NORA10 data for each wind speed bin are presented in the tables below. The values have been normalised so that they give the probability of occurrence of each sea state in percentage of total occurrences over the 57 years the data span. Hence, the total probability of each wind speed bin is given in the lower right corner cell of each scatter diagram.

Table A.1: Scatter diagram for H_S and T_p, occurences given in percentage of total number of occurrences for 0-2 m/s. The values for H_S and T_p denotes the highest value for each bin.

Hs\Tp	1	2	3	4	5	6	7	8	9	10	11	12	13	14	15	16	17	TOT
0.5	2.464	-	0.001	-	-	-	-	-	-	-	-	-	-	-	-	-	-	2.465
1.0	-	-	-	-	-	-	-	-	-	-	-	-	-	-	-	-	-	0
1.5	-	-	-	-	-	-	-	-	-	-	-	-	-	-	-	-	-	0
2.0	-	-	-	-	-	-	-	-	-	-	-	-	-	-	-	-	-	0
2.5	-	-	-	-	-	-	-	-	-	-	-	-	-	-	-	-	-	0
3.0	-	-	-	-	-	-	-	-	-	-	-	-	-	-	-	-	-	0
3.5	-	-	-	-	-	-	-	-	-	-	-	-	-	-	-	-	-	0
4.0	-	-	-	-	-	-	-	-	-	-	-	-	-	-	-	-	-	0
4.5	-	-	-	-	-	-	-	-	-	-	-	-	-	-	-	-	-	0
5.0	-	-	-	-	-	-	-	-	-	-	-	-	-	-	-	-	-	0
5.5	-	-	-	-	-	-	-	-	-	-	-	-	-	-	-	-	-	0
6.0	-	-	-	-	-	-	-	-	-	-	-	-	-	-	-	-	-	0
6.5	-	-	-	-	-	-	-	-	-	-	-	-	-	-	-	-	-	0
7.0	-	-	-	-	-	-	-	-	-	-	-	-	-	-	-	-	-	0
7.5	-	-	-	-	-	-	-	-	-	-	-	-	-	-	-	-	-	0
8.0	-	-	-	-	-	-	-	-	-	-	-	-	-	-	-	-	-	0
8.5	-	-	-	-	-	-	-	-	-	-	-	-	-	-	-	-	-	0
9.0	-	-	-	-	-	-	-	-	-	-	-	-	-	-	-	-	-	0
9.5	-	-	-	-	-	-	-	-	-	-	-	-	-	-	-	-	-	0
10.0	-	-	-	-	-	-	-	-	-	-	-	-	-	-	-	-	-	0
TOT	2.464	0	0.001	0	0	0	0	0	0	0	0	0	0	0	0	0	0	2.465

Table A.2: Scatter diagram for H_S and T_p, occurences given in percentage of total number of occurrences for 2-4 m/s. The values for H_S and T_p denotes the highest value for each bin.

Hs\Tp	1	2	3	4	5	6	7	8	9	10	11	12	13	14	15	16	17	TOT
0.5	6.301	-	1.124	0.002	-	-	-	-	-	-	-	-	-	-	-	-	-	7.427
1.0	-	-	0.001	-	-	-	-	-	-	-	-	-	-	-	-	-	-	0.001
1.5	-	-	-	-	-	-	-	-	-	-	-	-	-	-	-	-	-	0
2.0	-	-	-	-	-	-	-	-	-	-	-	-	-	-	-	-	-	0
2.5	-	-	-	-	-	-	-	-	-	-	-	-	-	-	-	-	-	0
3.0	-	-	-	-	-	-	-	-	-	-	-	-	-	-	-	-	-	0
3.5	-	-	-	-	-	-	-	-	-	-	-	-	-	-	-	-	-	0
4.0	-	-	-	-	-	-	-	-	-	-	-	-	-	-	-	-	-	0
4.5	-	-	-	-	-	-	-	-	-	-	-	-	-	-	-	-	-	0
5.0	-	-	-	-	-	-	-	-	-	-	-	-	-	-	-	-	-	0
5.5	-	-	-	-	-	-	-	-	-	-	-	-	-	-	-	-	-	0
6.0	-	-	-	-	-	-	-	-	-	-	-	-	-	-	-	-	-	0
6.5	-	-	-	-	-	-	-	-	-	-	-	-	-	-	-	-	-	0
7.0	-	-	-	-	-	-	-	-	-	-	-	-	-	-	-	-	-	0
7.5	-	-	-	-	-	-	-	-	-	-	-	-	-	-	-	-	-	0
8.0	-	-	-	-	-	-	-	-	-	-	-	-	-	-	-	-	-	0
8.5	-	-	-	-	-	-	-	-	-	-	-	-	-	-	-	-	-	0
9.0	-	-	-	-	-	-	-	-	-	-	-	-	-	-	-	-	-	0
9.5	-	-	-	-	-	-	-	-	-	-	-	-	-	-	-	-	-	0
10.0	-	-	-	-	-	-	-	-	-	-	-	-	-	-	-	-	-	0
TOT	6.301	0	1.125	0.002	0	0	0	0	0	0	0	0	0	0	0	0	0	7.428

Table A.3: Scatter diagram for H_S and T_p, occurences given in percentage of total number of occurrences for 4-6 m/s. The values for H_S and T_p denotes the highest value for each bin.

Hs\Tp	1	2	3	4	5	6	7	8	9	10	11	12	13	14	15	16	17	TOT
0.5	1.071	-	6.627	3.977	0.001	-	-	-	-	-	-	-	-	-	-	-	-	11.677
1.0	-	-	0.008	0.246	0.032	-	-	-	-	-	-	-	-	-	-	-	-	0.286
1.5	-	-	-	-	-	-	-	-	-	-	-	-	-	-	-	-	-	0
2.0	-	-	-	-	-	-	-	-	-	-	-	-	-	-	-	-	-	0
2.5	-	-	-	-	-	-	-	-	-	-	-	-	-	-	-	-	-	0
3.0	-	-	-	-	-	-	-	-	-	-	-	-	-	-	-	-	-	0
3.5	-	-	-	-	-	-	-	-	-	-	-	-	-	-	-	-	-	0
4.0	-	-	-	-	-	-	-	-	-	-	-	-	-	-	-	-	-	0
4.5	-	-	-	-	-	-	-	-	-	-	-	-	-	-	-	-	-	0
5.0	-	-	-	-	-	-	-	-	-	-	-	-	-	-	-	-	-	0
5.5	-	-	-	-	-	-	-	-	-	-	-	-	-	-	-	-	-	0
6.0	-	-	-	-	-	-	-	-	-	-	-	-	-	-	-	-	-	0
6.5	-	-	-	-	-	-	-	-	-	-	-	-	-	-	-	-	-	0
7.0	-	-	-	-	-	-	-	-	-	-	-	-	-	-	-	-	-	0
7.5	-	-	-	-	-	-	-	-	-	-	-	-	-	-	-	-	-	0
8.0	-	-	-	-	-	-	-	-	-	-	-	-	-	-	-	-	-	0
8.5	-	-	-	-	-	-	-	-	-	-	-	-	-	-	-	-	-	0
9.0	-	-	-	-	-	-	-	-	-	-	-	-	-	-	-	-	-	0
9.5	-	-	-	-	-	-	-	-	-	-	-	-	-	-	-	-	-	0
10.0	-	-	-	-	-	-	-	-	-	-	-	-	-	-	-	-	-	0
TOT	1.071	0	6.636	4.223	0.033	0	0	0	0	0	0	0	0	0	0	0	0	11.963

Table A.4: Scatter diagram for H_S and T_p, occurences given in percentage of total number of occurrences for 6-8 m/s. The values for H_S and T_p denotes the highest value for each bin.

Hs\Tp	1	2	3	4	5	6	7	8	9	10	11	12	13	14	15	16	17	TOT
0.5	0.022	-	2.571	4.141	0.178	0.003	-	-	-	-	-	-	-	-	-	-	-	7
1.0	-	-	0.065	3.067	4.488	0.531	-	-	-	-	-	-	-	-	-	-	-	8.151
1.5	-	-	-	-	0.005	0.015	-	-	-	-	-	-	-	-	-	-	-	0.020
2.0	-	-	-	-	-	-	-	-	-	-	-	-	-	-	-	-	-	0
2.5	-	-	-	-	-	-	-	-	-	-	-	-	-	-	-	-	-	0
3.0	-	-	-	-	-	-	-	-	-	-	-	-	-	-	-	-	-	0
3.5	-	-	-	-	-	-	-	-	-	-	-	-	-	-	-	-	-	0
4.0	-	-	-	-	-	-	-	-	-	-	-	-	-	-	-	-	-	0
4.5	-	-	-	-	-	-	-	-	-	-	-	-	-	-	-	-	-	0
5.0	-	-	-	-	-	-	-	-	-	-	-	-	-	-	-	-	-	0
5.5	-	-	-	-	-	-	-	-	-	-	-	-	-	-	-	-	-	0
6.0	-	-	-	-	-	-	-	-	-	-	-	-	-	-	-	-	-	0
6.5	-	-	-	-	-	-	-	-	-	-	-	-	-	-	-	-	-	0
7.0	-	-	-	-	-	-	-	-	-	-	-	-	-	-	-	-	-	0
7.5	-	-	-	-	-	-	-	-	-	-	-	-	-	-	-	-	-	0
8.0	-	-	-	-	-	-	-	-	-	-	-	-	-	-	-	-	-	0
8.5	-	-	-	-	-	-	-	-	-	-	-	-	-	-	-	-	-	0
9.0	-	-	-	-	-	-	-	-	-	-	-	-	-	-	-	-	-	0
9.5	-	-	-	-	-	-	-	-	-	-	-	-	-	-	-	-	-	0
10.0	-	-	-	-	-	-	-	-	-	-	-	-	-	-	-	-	-	0
TOT	0.022	0	2.637	7.208	4.671	0.548	0	0	0	0	0	0	0	0	0	0	0	15.086

Table A.5: Scatter diagram for H_S and T_p, occurences given in percentage of total number of occurrences for 8-10 m/s. The values for H_S and T_p denotes the highest value for each bin.

Hs\Tp	1	2	3	4	5	6	7	8	9	10	11	12	13	14	15	16	17	TOT
0.5	-	-	0.735	0.865	0.08	0.036	0.003	-	-	-	-	-	-	-	-	-	-	1.719
1.0	-	-	0.084	2.561	4.573	1.948	0.023	-	-	-	-	-	-	-	-	-	-	9.190
1.5	-	-	-	0.002	0.714	3.245	1.417	0.001	-	-	-	-	-	-	-	-	-	5.379
2.0	-	-	-	-	-	0.004	0.09	0.003	-	-	-	-	-	-	-	-	-	0
2.5	-	-	-	-	-	-	-	-	-	-	-	-	-	-	-	-	-	0
3.0	-	-	-	-	-	-	-	-	-	-	-	-	-	-	-	-	-	0
3.5	-	-	-	-	-	-	-	-	-	-	-	-	-	-	-	-	-	0
4.0	-	-	-	-	-	-	-	-	-	-	-	-	-	-	-	-	-	0
4.5	-	-	-	-	-	-	-	-	-	-	-	-	-	-	-	-	-	0
5.0	-	-	-	-	-	-	-	-	-	-	-	-	-	-	-	-	-	0
5.5	-	-	-	-	-	-	-	-	-	-	-	-	-	-	-	-	-	0
6.0	-	-	-	-	-	-	-	-	-	-	-	-	-	-	-	-	-	0
6.5	-	-	-	-	-	-	-	-	-	-	-	-	-	-	-	-	-	0
7.0	-	-	-	-	-	-	-	-	-	-	-	-	-	-	-	-	-	0
7.5	-	-	-	-	-	-	-	-	-	-	-	-	-	-	-	-	-	0
8.0	-	-	-	-	-	-	-	-	-	-	-	-	-	-	-	-	-	0
8.5	-	-	-	-	-	-	-	-	-	-	-	-	-	-	-	-	-	0
9.0	-	-	-	-	-	-	-	-	-	-	-	-	-	-	-	-	-	0
9.5	-	-	-	-	-	-	-	-	-	-	-	-	-	-	-	-	-	0
10.0	-	-	-	-	-	-	-	-	-	-	-	-	-	-	-	-	-	0
TOT	0	0	0.819	3.428	5.368	5.234	1.533	0	0	0	0	0	0	0	0	0	0	16.385

Table A.6: Scatter diagram for H_S and T_p, occurences given in percentage of total number of occurrences for 10-12 m/s. The values for H_S and T_p denotes the highest value for each bin.

Hs\Tp	1	2	3	4	5	6	7	8	9	10	11	12	13	14	15	16	17	TOT
0.5	-	-	0.144	0.049	0.013	0.007	0.006	-	-	-	-	-	-	-	-	-	-	0.219
1.0	-	-	0.031	0.936	1.541	0.425	0.017	0.005	0.001	0.001	-	-	-	-	-	-	-	2.958
1.5	-	-	-	0.01	1.629	4.114	1.234	0.024	0.005	0.001	-	-	-	-	-	-	-	7.017
2.0	-	-	-	-	0.004	0.717	2.834	0.606	0.06	0.003	-	-	-	-	-	-	-	4.225
2.5	-	-	-	-	-	-	0.12	0.266	0.15	0.005	-	-	-	-	-	-	-	0.540
3.0	-	-	-	-	-	-	-	-	0.002	0.001	-	-	-	-	-	-	-	0
3.5	-	-	-	-	-	-	-	-	-	-	-	-	-	-	-	-	-	0
4.0	-	-	-	-	-	-	-	-	-	-	-	-	-	-	-	-	-	0
4.5	-	-	-	-	-	-	-	-	-	-	-	-	-	-	-	-	-	0
5.0	-	-	-	-	-	-	-	-	-	-	-	-	-	-	-	-	-	0
5.5	-	-	-	-	-	-	-	-	-	-	-	-	-	-	-	-	-	0
6.0	-	-	-	-	-	-	-	-	-	-	-	-	-	-	-	-	-	0
6.5	-	-	-	-	-	-	-	-	-	-	-	-	-	-	-	-	-	0
7.0	-	-	-	-	-	-	-	-	-	-	-	-	-	-	-	-	-	0
7.5	-	-	-	-	-	-	-	-	-	-	-	-	-	-	-	-	-	0
8.0	-	-	-	-	-	-	-	-	-	-	-	-	-	-	-	-	-	0
8.5	-	-	-	-	-	-	-	-	-	-	-	-	-	-	-	-	-	0
9.0	-	-	-	-	-	-	-	-	-	-	-	-	-	-	-	-	-	0
9.5	-	-	-	-	-	-	-	-	-	-	-	-	-	-	-	-	-	0
10.0	-	-	-	-	-	-	-	-	-	-	-	-	-	-	-	-	-	0
TOT	0	0	0.175	0.995	3.187	5.264	4.212	0.901	0	0	0	0	0	0	0	0	0	14.961

Table A.7: Scatter diagram for H_S and T_p, occurences given in percentage of total number of occurrences for 12-14 m/s. The values for H_S and T_p denotes the highest value for each bin.

Hs\Tp	1	2	3	4	5	6	7	8	9	10	11	12	13	14	15	16	17	TOT
0.5	-	-	0.026	0.002	0.001	0.003	0.001	-	-	-	-	-	-	-	-	-	-	0.033
1.0	-	-	0.010	0.155	0.17	0.026	0.003	0.002	0.003	-	-	-	-	-	-	-	-	0.368
1.5	-	-	-	0.018	0.775	1.49	0.157	0.002	0.001	0.001	0.001	-	-	-	-	-	-	2.444
2.0	-	-	-	-	0.04	1.947	2.571	0.092	0.015	0.006	0.001	-	-	-	-	-	-	4.673
2.5	-	-	-	-	-	0.019	1.777	0.918	0.354	0.105	0.004	-	-	-	-	-	-	3.178
3.0	-	-	-	-	-	-	0.019	0.26	0.332	0.241	0.044	-	-	-	-	-	-	0.896
3.5	-	-	-	-	-	-	-	-	0.008	0.031	0.017	-	-	-	-	-	-	0.056
4.0	-	-	-	-	-	-	-	-	-	-	-	-	-	-	-	-	-	0
4.5	-	-	-	-	-	-	-	-	-	-	-	-	-	-	-	-	-	0
5.0	-	-	-	-	-	-	-	-	-	-	-	-	-	-	-	-	-	0
5.5	-	-	-	-	-	-	-	-	-	-	-	-	-	-	-	-	-	0
6.0	-	-	-	-	-	-	-	-	-	-	-	-	-	-	-	-	-	0
6.5	-	-	-	-	-	-	-	-	-	-	-	-	-	-	-	-	-	0
7.0	-	-	-	-	-	-	-	-	-	-	-	-	-	-	-	-	-	0
7.5	-	-	-	-	-	-	-	-	-	-	-	-	-	-	-	-	-	0
8.0	-	-	-	-	-	-	-	-	-	-	-	-	-	-	-	-	-	0
8.5	-	-	-	-	-	-	-	-	-	-	-	-	-	-	-	-	-	0
9.0	-	-	-	-	-	-	-	-	-	-	-	-	-	-	-	-	-	0
9.5	-	-	-	-	-	-	-	-	-	-	-	-	-	-	-	-	-	0
10.0	-	-	0	0	0	0	0	0	-	-	-	-	-	-	-	-	-	0
TOT	0	0	0.037	0.175	0.987	3.485	4.527	1.274	0.712	0.385	0.067	0	0	0	0	0	0	11.647

Table A.8: Scatter diagram for H_S and T_p, occurences given in percentage of total number of occurrences for 14-16 m/s. The values for H_S and T_p denotes the highest value for each bin.

Hs\Tp	1	2	3	4	5	6	7	8	9	10	11	12	13	14	15	16	17	TOT
0.5	-	-	-	-	-	-	-	-	-	-	-	-	-	-	-	-	-	0
1.0	-	-	0.003	0.024	0.005	0.002	-	-	0.001	0.001	-	-	-	-	-	-	-	0.037
1.5	-	-	-	0.008	0.128	0.132	0.006	0.002	0.001	0.001	-	0.001	-	-	-	-	-	0.279
2.0	-	-	-	-	0.039	1.015	0.608	0.004	0.001	0.001	-	0.001	-	-	-	-	-	1.669
2.5	-	-	-	-	-	0.15	2.653	0.237	0.017	0.006	0.001	0.002	0.001	-	-	-	-	3.066
3.0	-	-	-	-	-	-	0.614	1.008	0.376	0.077	0.025	0.001	-	-	-	-	-	2.100
3.5	-	-	-	-	-	-	-	0.085	0.372	0.294	0.153	0.027	0.001	-	-	-	-	0.932
4.0	-	-	-	-	-	-	-	0.001	0.004	0.055	0.093	0.042	0.003	-	-	-	-	0.198
4.5	-	-	-	-	-	-	-	-	-	-	0.003	0.01	-	-	-	-	-	0.013
5.0	-	-	-	-	-	-	-	-	-	-	-	-	-	-	-	-	-	0
5.5	-	-	-	-	-	-	-	-	-	-	-	-	-	-	-	-	-	0
6.0	-	-	-	-	-	-	-	-	-	-	-	-	-	-	-	-	-	0
6.5	-	-	-	-	-	-	-	-	-	-	-	-	-	-	-	-	-	0
7.0	-	-	-	-	-	-	-	-	-	-	-	-	-	-	-	-	-	0
7.5	-	-	-	-	-	-	-	-	-	-	-	-	-	-	-	-	-	0
8.0	-	-	-	-	-	-	-	-	-	-	-	-	-	-	-	-	-	0
8.5	-	-	-	-	-	-	-	-	-	-	-	-	-	-	-	-	-	0
9.0	-	-	-	-	-	-	-	-	-	-	-	-	-	-	-	-	-	0
9.5	-	-	-	-	-	-	-	-	-	-	-	-	-	-	-	-	-	0
10.0	-	-	-	-	-	-	-	-	-	-	-	-	-	-	-	-	-	0
TOT	0	0	0.003	0.032	0.173	1.299	3.882	1.336	0.773	0.434	0.275	0.082	0.004	0	0	0	0	8.293

Table A.9: Scatter diagram for H_S and T_p, occurences given in percentage of total number of occurrences for 16-18 m/s. The values for H_S and T_p denotes the highest value for each bin.

Hs\Tp	1	2	3	4	5	6	7	8	9	10	11	12	13	14	15	16	17	TOT
0.5	-	-	0.001	-	-	-	-	-	-	-	0.001	-	-	-	-	-	-	0.001
1.0	-	-	-	0.002	-	-	-	-	0.001	0.001	-	-	-	-	-	-	-	0.003
1.5	-	-	-	0.002	0.013	0.004	-	-	0.001	0.001	0.001	-	-	-	-	-	-	0.021
2.0	-	-	-	-	0.016	0.124	0.031	-	-	-	-	-	-	-	-	-	-	0.171
2.5	-	-	-	-	-	0.149	0.880	0.016	0.001	0.001	-	0.001	-	-	-	-	-	1.047
3.0	-	-	-	-	-	0.001	1.291	0.606	0.041	0.002	0.001	0.001	0.001	-	-	-	-	1.942
3.5	-	-	-	-	-	-	0.051	0.681	0.510	0.071	0.015	0.002	0.001	-	-	-	-	1.331
4.0	-	-	-	-	-	-	-	0.005	0.204	0.291	0.114	0.028	0.004	-	-	-	-	0.646
4.5	-	-	-	-	-	-	-	-	-	0.043	0.112	0.084	0.021	0.001	-	-	-	0.261
5.0	-	-	-	-	-	-	-	-	-	-	0.010	0.026	0.015	-	-	-	-	0.051
5.5	-	-	-	-	-	-	-	-	-	-	-	0.001	0.008	0.001	-	-	-	0.010
6.0	-	-	-	-	-	-	-	-	-	-	-	-	0.001	0.001	-	-	-	0.001
6.5	-	-	-	-	-	-	-	-	-	-	-	-	-	-	-	-	-	0
7.0	-	-	-	-	-	-	-	-	-	-	-	-	-	-	-	-	-	0
7.5	-	-	-	-	-	-	-	-	-	-	-	-	-	-	-	-	-	0
8.0	-	-	-	-	-	-	-	-	-	-	-	-	-	-	-	-	-	0
8.5	-	-	-	-	-	-	-	-	-	-	-	-	-	-	-	-	-	0
9.0	-	-	-	-	-	-	-	-	-	-	-	-	-	-	-	-	-	0
9.5	-	-	-	-	-	-	-	-	-	-	-	-	-	-	-	-	-	0
10.0	-	-	-	-	-	-	-	-	-	-	-	-	-	-	-	-	-	0
TOT	0	0	0.001	0.004	0.030	0.277	2.252	1.308	0.757	0.409	0.253	0.142	0.050	0.002	0	0	0	5.485

Table A.10: Scatter diagram for H_S and T_p, occurences given in percentage of total number of occurrences for 18-20 m/s. The values for H_S and T_p denotes the highest value for each bin.

Hs\Tp	1	2	3	4	5	6	7	8	9	10	11	12	13	14	15	16	17	TOT
0.5	-	-	-	-	-	-	-	-	-	-	-	-	-	-	-	-	-	0
1.0	-	-	-	0.001	-	-	-	-	-	-	-	-	-	-	-	-	-	0.001
1.5	-	-	-	0.001	0.003	-	-	-	-	-	-	-	-	-	-	-	-	0.004
2.0	-	-	-	-	0.001	0.008	0.002	-	-	-	-	-	-	-	-	-	-	0.011
2.5	-	-	-	-	-	0.031	0.064	6E-04	-	-	-	-	-	0.001	-	-	-	0.096
3.0	-	-	-	-	-	0.006	0.468	0.083	0.001	0.001	0.001	-	-	-	-	-	-	0.559
3.5	-	-	-	-	-	-	0.214	0.775	0.123	0.001	0.000	-	-	-	-	-	-	1.112
4.0	-	-	-	-	-	-	0.001	0.205	0.484	0.112	0.008	0.001	0.001	-	-	-	-	0.812
4.5	-	-	-	-	-	-	-	-	0.061	0.258	0.095	0.017	0.004	-	-	-	-	0.435
5.0	-	-	-	-	-	-	-	-	-	0.019	0.107	0.067	0.021	0.001	-	-	-	0.215
5.5	-	-	-	-	-	-	-	-	-	-	0.003	0.039	0.031	0.008	-	-	-	0.081
6.0	-	-	-	-	-	-	-	-	-	-	0.001	0.002	0.012	0.010	0.001	-	-	0.025
6.5	-	-	-	-	-	-	-	-	-	-	-	-	0.002	0.004	0.001	-	-	0.007
7.0	-	-	-	-	-	-	-	-	-	-	-	-	-	-	-	-	-	0
7.5	-	-	-	-	-	-	-	-	-	-	-	-	-	-	-	-	-	0
8.0	-	-	-	-	-	-	-	-	-	-	-	-	-	-	-	-	-	0
8.5	-	-	-	-	-	-	-	-	-	-	-	-	-	-	-	-	-	0
9.0	-	-	-	-	-	-	-	-	-	-	-	-	-	-	-	-	-	0
9.5	-	-	-	-	-	-	-	-	-	-	-	-	-	-	-	-	-	0
10.0	-	-	-	-	-	-	-	-	-	-	-	-	-	-	-	-	-	0
TOT	0	0	0	0.003	0.004	0.044	0.748	1.064	0.669	0.390	0.215	0.126	0.071	0.023	0.002	0	0	3.359

Table A.11: Scatter diagram for H_S and T_p, occurences given in percentage of total number of occurrences for 20-22 m/s. The values for H_S and T_p denotes the highest value for each bin.

Hs\Tp	1	2	3	4	5	6	7	8	9	10	11	12	13	14	15	16	17	TOT
0.5	-	-	-	-	-	-	-	-	-	-	-	-	-	-	-	-	-	0
1.0	-	-	-	-	-	-	-	-	-	-	-	-	-	-	-	-	-	0
1.5	-	-	-	0.001	-	0.001	-	-	-	-	-	-	-	-	-	-	-	0.001
2.0	-	-	-	-	-	0.002	0.001	0.001	-	-	-	-	-	-	-	-	-	0.003
2.5	-	-	-	-	-	0.006	0.001	-	-	-	-	-	-	-	-	-	-	0.006
3.0	-	-	-	-	-	0.001	0.047	0.001	-	-	-	-	-	-	-	-	-	0.049
3.5	-	-	-	-	-	-	0.092	0.135	0.007	-	-	-	-	-	-	-	-	0.235
4.0	-	-	-	-	-	-	0.008	0.317	0.248	0.005	0.001	-	-	-	-	-	-	0.578
4.5	-	-	-	-	-	-	-	0.013	0.311	0.142	0.005	-	-	-	-	-	-	0.472
5.0	-	-	-	-	-	-	-	-	0.008	0.132	0.094	0.010	0.001	0.001	-	-	-	0.245
5.5	-	-	-	-	-	-	-	-	-	0.004	0.047	0.045	0.010	-	-	-	-	0.107
6.0	-	-	-	-	-	-	-	-	-	-	-	0.017	0.030	0.003	0.001	-	-	0.052
6.5	-	-	-	-	-	-	-	-	-	-	-	0.001	0.008	0.008	0.001	-	-	0.018
7.0	-	-	-	-	-	-	-	-	-	-	-	-	0.001	0.004	0.001	-	-	0.006
7.5	-	-	-	-	-	-	-	-	-	-	-	-	-	0.001	0.003	-	-	0.003
8.0	-	-	-	-	-	-	-	-	-	-	-	-	-	-	-	-	-	0
8.5	-	-	-	-	-	-	-	-	-	-	-	-	-	-	-	-	-	0
9.0	-	-	-	-	-	-	-	-	-	-	-	-	-	-	-	-	-	0
9.5	-	-	-	-	-	-	-	-	-	-	-	-	-	-	-	-	-	0
10.0	-	-	-	-	-	-	-	-	-	-	-	-	-	-	-	-	-	0
TOT	0	0	0	0.001	0	0.009	0.148	0.467	0.574	0.284	0.147	0.073	0.049	0.017	0.006	0	0	1.775

Table A.12: Scatter diagram for H_S and T_p, occurences given in percentage of total number of occurrences for 22-24 m/s. The values for H_S and T_p denotes the highest value for each bin.

Hs\Tp	1	2	3	4	5	6	7	8	9	10	11	12	13	14	15	16	17	TOT
0.5	-	-	-	-	-	-	-	-	-	-	-	-	-	-	-	-	-	0
1.0	-	-	-	-	-	-	-	-	-	-	-	-	-	-	-	-	-	0
1.5	-	-	-	-	-	-	-	-	-	-	-	-	-	-	-	-	-	0
2.0	-	-	-	-	-	0.001	-	-	-	-	-	-	0.001	-	-	-	-	0.001
2.5	-	-	-	-	-	-	-	-	-	-	-	-	-	0.001	-	-	-	0.001
3.0	-	-	-	-	-	-	0.004	0.002	-	-	-	-	-	-	-	-	-	0.006
3.5	-	-	-	-	-	-	0.012	0.006	0.001	0.001	-	-	-	-	-	-	-	0.019
4.0	-	-	-	-	-	-	0.007	0.060	0.013	-	-	-	-	-	-	-	-	0.080
4.5	-	-	-	-	-	-	-	0.048	0.162	0.016	0.001	-	-	-	-	-	-	0.227
5.0	-	-	-	-	-	-	-	0.001	0.08	0.125	0.006	-	-	-	-	-	-	0.211
5.5	-	-	-	-	-	-	-	-	0.001	0.047	0.056	0.002	0.001	-	-	-	-	0.106
6.0	-	-	-	-	-	-	-	-	-	0.003	0.018	0.02	0.006	-	-	-	-	0.047
6.5	-	-	-	-	-	-	-	-	-	-	-	0.006	0.014	0.001	0.001	-	-	0.022
7.0	-	-	-	-	-	-	-	-	-	-	-	0.003	0.007	0.006	0.001	-	-	0.017
7.5	-	-	-	-	-	-	-	-	-	-	-	-	-	0.004	0.004	-	-	0.008
8.0	-	-	-	-	-	-	-	-	-	-	-	-	-	0.001	0.003	-	-	0.004
8.5	-	-	-	-	-	-	-	-	-	-	-	-	-	-	-	-	-	0
9.0	-	-	-	-	-	-	-	-	-	-	-	-	-	-	-	-	-	0
9.5	-	-	-	-	-	-	-	-	-	-	-	-	-	-	-	-	-	0
10.0	-	-	-	-	-	-	-	-	-	-	-	-	-	-	-	-	-	0
TOT	0	0	0	0	0	0.001	0.023	0.116	0.256	0.192	0.080	0.031	0.029	0.013	0.008	0	0	0.749

Table A.13: Scatter diagram for H_S and T_p, occurences given in percentage of total number of occurrences for 24-26 m/s. The values for H_S and T_p denotes the highest value for each bin.

Hs\Tp	1	2	3	4	5	6	7	8	9	10	11	12	13	14	15	16	17	TOT
0.5	-	-	-	-	-	-	-	-	-	-	-	-	-	-	-	-	-	0
1.0	-	-	-	-	-	-	-	-	-	-	-	-	-	-	-	-	-	0
1.5	-	-	-	-	-	-	-	-	-	-	-	-	-	-	-	-	-	0
2.0	-	-	-	-	-	-	-	-	-	-	-	-	-	-	-	-	-	0
2.5	-	-	-	-	-	-	-	-	-	-	-	-	-	-	-	-	-	0
3.0	-	-	-	-	-	-	0.001	-	-	-	-	-	-	-	-	-	-	0.001
3.5	-	-	-	-	-	0.001	0.001	0.001	-	-	-	-	-	-	-	-	-	0.002
4.0	-	-	-	-	-	-	0.001	0.003	-	0.001	-	-	-	-	-	-	-	0.004
4.5	-	-	-	-	-	-	0.001	0.011	0.013	0.002	-	-	-	-	-	-	-	0.027
5.0	-	-	-	-	-	-	-	0.001	0.039	0.016	-	-	-	-	-	-	-	0.056
5.5	-	-	-	-	-	-	-	-	0.008	0.073	0.008	-	-	-	-	-	-	0.089
6.0	-	-	-	-	-	-	-	-	-	0.012	0.040	0.001	-	-	-	-	-	0.053
6.5	-	-	-	-	-	-	-	-	-	-	0.009	0.013	-	-	-	-	-	0.022
7.0	-	-	-	-	-	-	-	-	-	-	-	0.004	0.008	0.001	-	-	-	0.013
7.5	-	-	-	-	-	-	-	-	-	-	-	0.001	0.004	0.003	-	-	-	0.009
8.0	-	-	-	-	-	-	-	-	-	-	-	-	-	0.003	0.001	-	-	0.004
8.5	-	-	-	-	-	-	-	-	-	-	-	-	-	-	0.001	-	-	0.001
9.0	-	-	-	-	-	-	-	-	-	-	-	-	-	-	-	-	0.001	0.001
9.5	-	-	-	-	-	-	-	-	-	-	-	-	-	-	-	-	-	0
10.0	-	-	-	-	-	-	-	-	-	-	-	-	-	-	-	-	-	0
TOT	0	0	0	0	0	0.001	0.003	0.015	0.060	0.103	0.057	0.021	0.013	0.007	0.003	0	0.001	0.283

Table A.14: Scatter diagram for H_S and T_p, occurences given in percentage of total number of occurrences for 26-28 m/s. The values for H_S and T_p denotes the highest value for each bin.

Hs\Tp	1	2	3	4	5	6	7	8	9	10	11	12	13	14	15	16	17	TOT
0.5	-	-	-	-	-	-	-	-	-	-	-	-	-	-	-	-	-	0
1.0	-	-	-	-	-	-	-	-	-	-	-	-	-	-	-	-	-	0
1.5	-	-	-	-	-	-	-	-	-	-	-	-	-	-	-	-	-	0
2.0	-	-	-	-	-	-	-	-	-	-	-	-	-	-	-	-	-	0
2.5	-	-	-	-	-	-	-	-	-	-	-	-	-	-	-	-	-	0
3.0	-	-	-	-	-	-	-	-	-	-	-	-	-	-	-	-	-	0
3.5	-	-	-	-	-	-	-	-	-	-	-	-	-	-	-	-	-	0
4.0	-	-	-	-	-	-	-	-	0.001	-	-	-	-	-	-	-	-	0.001
4.5	-	-	-	-	-	-	-	0.001	0.001	-	-	-	-	-	-	-	-	0.001
5.0	-	-	-	-	-	-	-	0.001	0.004	0.002	-	-	-	-	-	-	-	0.008
5.5	-	-	-	-	-	-	-	-	0.007	0.013	0.001	-	-	-	-	-	-	0.021
6.0	-	-	-	-	-	-	-	-	-	0.015	0.005	-	-	-	-	-	-	0.021
6.5	-	-	-	-	-	-	-	-	-	0.001	0.012	0.003	-	-	-	-	-	0.017
7.0	-	-	-	-	-	-	-	-	-	-	0.003	0.005	-	-	-	-	-	0.008
7.5	-	-	-	-	-	-	-	-	-	-	-	0.001	0.003	-	-	-	-	0.004
8.0	-	-	-	-	-	-	-	-	-	-	-	0.001	0.001	0.001	-	-	-	0.003
8.5	-	-	-	-	-	-	-	-	-	-	-	-	-	0.001	-	-	-	0.001
9.0	-	-	-	-	-	-	-	-	-	-	-	-	-	-	0.001	-	-	0.001
9.5	-	-	-	-	-	-	-	-	-	-	-	-	-	-	-	-	-	0
10.0	-	-	-	-	-	-	-	-	-	-	-	-	-	-	-	-	0.001	0.001
TOT	0	0	0	0	0	0	0	0.002	0.013	0.032	0.021	0.010	0.004	0.003	0.001	0	0.001	0.088

Table A.15: Scatter diagram for H_S and T_p, occurences given in percentage of total number of occurrences for 28-30 m/s. The values for H_S and T_p denotes the highest value for each bin.

Hs\Tp	1	2	3	4	5	6	7	8	9	10	11	12	13	14	15	16	17	TOT
0.5	-	-	-	-	-	-	-	-	-	-	-	-	-	-	-	-	-	0
1.0	-	-	-	-	-	-	-	-	-	-	-	-	-	-	-	-	-	0
1.5	-	-	-	-	-	-	-	-	-	-	-	-	-	-	-	-	-	0
2.0	-	-	-	-	-	-	-	-	-	-	-	-	-	-	-	-	-	0
2.5	-	-	-	-	-	-	-	-	-	-	-	-	-	-	-	-	-	0
3.0	-	-	-	-	-	-	-	-	-	-	-	-	-	-	-	-	-	0
3.5	-	-	-	-	-	-	-	-	-	-	-	-	-	-	-	-	-	0
4.0	-	-	-	-	-	-	0.001	0.001	-	-	-	-	-	-	-	-	-	0.001
4.5	-	-	-	-	-	-	-	-	-	-	-	-	-	-	-	-	-	0
5.0	-	-	-	-	-	-	-	-	0.001	-	-	-	-	-	-	-	-	0.001
5.5	-	-	-	-	-	-	-	-	0.001	-	-	-	-	-	-	-	-	0.001
6.0	-	-	-	-	-	-	-	-	-	0.003	0.001	-	-	-	-	-	-	0.003
6.5	-	-	-	-	-	-	-	-	-	0.003	0.002	-	-	-	-	-	-	0.005
7.0	-	-	-	-	-	-	-	-	-	-	0.007	-	-	-	-	-	-	0.007
7.5	-	-	-	-	-	-	-	-	-	-	0.001	0.001	-	-	-	-	-	0.003
8.0	-	-	-	-	-	-	-	-	-	-	-	0.001	0.001	-	-	-	-	0.002
8.5	-	-	-	-	-	-	-	-	-	-	-	0.001	-	-	-	-	-	0.001
9.0	-	-	-	-	-	-	-	-	-	-	-	-	-	-	-	-	-	0
9.5	-	-	-	-	-	-	-	-	-	-	-	-	-	-	-	-	-	0
10.0	-	-	-	-	-	-	-	-	-	-	-	-	-	-	-	-	-	0
TOT	0	0	0	0	0	0	0	0.001	0.002	0.006	0.011	0.003	0.001	0	0	0	0.000	0.024

Table A.16: Scatter diagram for H_S and T_p, occurences given in percentage of total number of occurrences for 30-32 m/s. The values for H_S and T_p denotes the highest value for each bin.

Hs\Tp	1	2	3	4	5	6	7	8	9	10	11	12	13	14	15	16	17	TOT
0.5	-	-	-	-	-	-	-	-	-	-	-	-	-	-	-	-	-	0
1.0	-	-	-	-	-	-	-	-	-	-	-	-	-	-	-	-	-	0
1.5	-	-	-	-	-	-	-	-	-	-	-	-	-	-	-	-	-	0
2.0	-	-	-	-	-	-	-	-	-	-	-	-	-	-	-	-	-	0
2.5	-	-	-	-	-	-	-	-	-	-	-	-	-	-	-	-	-	0
3.0	-	-	-	-	-	-	-	-	-	-	-	-	-	-	-	-	-	0
3.5	-	-	-	-	-	-	-	-	-	-	-	-	-	-	-	-	-	0
4.0	-	-	-	-	-	-	-	-	-	-	-	-	-	-	-	-	-	0
4.5	-	-	-	-	-	-	-	-	-	-	-	-	-	-	-	-	-	0
5.0	-	-	-	-	-	-	-	-	-	-	-	-	-	-	-	-	-	0
5.5	-	-	-	-	-	-	-	-	-	-	-	-	-	-	-	-	-	0
6.0	-	-	-	-	-	-	-	-	-	-	-	-	-	-	-	-	-	0
6.5	-	-	-	-	-	-	-	-	-	-	-	-	-	-	-	-	-	0
7.0	-	-	-	-	-	-	-	-	-	0.001	0.002	-	-	-	-	-	-	0.003
7.5	-	-	-	-	-	-	-	-	-	-	0.003	-	-	-	-	-	-	0.003
8.0	-	-	-	-	-	-	-	-	-	-	-	0.001	-	-	-	-	-	0.001
8.5	-	-	-	-	-	-	-	-	-	-	-	-	-	-	-	-	-	0
9.0	-	-	-	-	-	-	-	-	-	-	-	-	-	-	-	-	-	0
9.5	-	-	-	-	-	-	-	-	-	-	-	-	-	-	-	-	-	0
10.0	-	-	-	-	-	-	-	-	-	-	-	-	-	-	-	-	-	0
TOT	0	0	0	0	0	0	0	0	0	0.001	0.005	0.001	0	0	0	0	0	0.007

Table A.17: Scatter diagram for H_S and T_p, occurences given in percentage of total number of occurrences for 32-34 m/s. The values for H_S and T_p denotes the highest value for each bin.

Hs\Tp	1	2	3	4	5	6	7	8	9	10	11	12	13	14	15	16	17	TOT
0.5	-	-	-	-	-	-	-	-	-	-	-	-	-	-	-	-	-	0
1.0	-	-	-	-	-	-	-	-	-	-	-	-	-	-	-	-	-	0
1.5	-	-	-	-	-	-	-	-	-	-	-	-	-	-	-	-	-	0
2.0	-	-	-	-	-	-	-	-	-	-	-	-	-	-	-	-	-	0
2.5	-	-	-	-	-	-	-	-	-	-	-	-	-	-	-	-	-	0
3.0	-	-	-	-	-	-	-	-	-	-	-	-	-	-	-	-	-	0
3.5	-	-	-	-	-	-	-	-	-	-	-	-	-	-	-	-	-	0
4.0	-	-	-	-	-	-	-	-	-	-	-	-	-	-	-	-	-	0
4.5	-	-	-	-	-	-	-	-	-	-	-	-	-	-	-	-	-	0
5.0	-	-	-	-	-	-	-	-	-	-	-	-	-	-	-	-	-	0
5.5	-	-	-	-	-	-	-	-	-	-	-	-	-	-	-	-	-	0
6.0	-	-	-	-	-	-	-	-	-	-	-	-	-	-	-	-	-	0
6.5	-	-	-	-	-	-	-	-	-	-	-	-	-	-	-	-	-	0
7.0	-	-	-	-	-	-	-	-	-	-	-	-	-	-	-	-	-	0
7.5	-	-	-	-	-	-	-	-	-	-	0.002	-	-	-	-	-	-	0.002
8.0	-	-	-	-	-	-	-	-	-	-	-	-	-	-	-	-	-	0
8.5	-	-	-	-	-	-	-	-	-	-	-	0.001	-	-	-	-	-	0.001
9.0	-	-	-	-	-	-	-	-	-	-	-	-	-	-	-	-	-	0
9.5	-	-	-	-	-	-	-	-	-	-	-	-	-	-	-	-	-	0
10.0	-	-	-	-	-	-	-	-	-	-	-	-	-	-	-	-	-	0
TOT	0	0	0	0	0	0	0	0	0	0	0.002	0.001	0	0	0	0	0	0.003

A.2 Scatter Diagrams for Each Direction Bin

Scatter diagrams have also been computed for each direction bin in order to determine the probability of the misaligned load cases. The probabilities in the scatter digrams are the probability of occurrence of total occurrences, and the total probability of each direction bin is given in the lower right corner cell of the diagram. Each direction bin has a span of 15° and is denoted by the mean value of each bin.

Table A.18: Scatter diagram for H_S and T_p, occurences given in percentage of total number of occurrences for 0°. The values for H_S and T_p denotes the highest value for each bin.

Hs\Tp	1	2	3	4	5	6	7	8	9	10	11	12	13	14	15	16	17	TOT
0-0-5	0.495	-	3.744	3.758	0.107	0.009	0.004	-	-	-	-	-	-	-	-	-	-	8.117
0.5-1.0	-	-	0.039	2.533	4.722	1.405	0.010	0.001	0.001	-	-	-	-	-	-	-	-	8.710
1.0-1.5	-	-	-	0.009	0.895	3.126	1.267	0.013	0.002	0.001	-	-	-	-	-	-	-	5.311
1.5-2.0	-	-	-	-	0.032	1.051	1.882	0.316	0.026	0.004	-	0.001	0.001	-	-	-	-	3.313
2.0-2.5	-	-	-	-	-	0.090	1.469	0.425	0.193	0.043	0.003	-	0.001	0.001	-	-	-	2.224
2.5-3.0	-	-	-	-	-	0.003	0.597	0.470	0.205	0.126	0.026	0.001	-	-	-	-	-	1.428
3.0-3.5	-	-	-	-	-	-	0.095	0.379	0.220	0.117	0.056	0.011	0.001	-	-	-	-	0.879
3.5-4.0	-	-	-	-	-	-	0.004	0.151	0.175	0.103	0.063	0.022	0.004	-	-	-	-	0.522
4.0-4.5	-	-	-	-	-	-	0.001	0.026	0.114	0.098	0.050	0.030	0.010	0.001	-	-	-	0.329
4.5-5.0	-	-	-	-	-	-	-	-	0.032	0.046	0.046	0.021	0.010	0.001	-	-	-	0.157
5.0-5.5	-	-	-	-	-	-	-	-	0.004	0.025	0.017	0.021	0.009	0.004	-	-	-	0.081
5.5-6.0	-	-	-	-	-	-	-	-	-	0.008	0.008	0.010	0.009	0.005	0.001	-	-	0.040
6.0-6.5	-	-	-	-	-	-	-	-	-	0.001	0.003	0.004	0.006	0.004	0.001	-	-	0.017
6.5-7.0	-	-	-	-	-	-	-	-	-	0.001	0.004	0.002	0.003	0.003	0.001	-	-	0.013
7.0-7.5	-	-	-	-	-	-	-	-	-	-	0.002	0.001	0.001	0.002	0.004	-	-	0.010
7.5-8.0	-	-	-	-	-	-	-	-	-	-	-	-	0.001	0.002	0.001	-	-	0.003
8.0-8.5	-	-	-	-	-	-	-	-	-	-	-	0.001	-	0.001	-	-	-	0.003
8.5-9.0	-	-	-	-	-	-	-	-	-	-	-	-	-	-	-	-	0.001	0.001
9.0-9.5	-	-	-	-	-	-	-	-	-	-	-	-	-	-	-	-	-	0
9.5-10.0	-	-	-	-	-	-	-	-	-	-	-	-	-	-	-	-	-	0
TOT	0.495	0	3.783	6.300	5.755	5.684	5.329	1.781	0.972	0.572	0.279	0.124	0.053	0.024	0.006	0	0.001	31.158

Table A.19: Scatter diagram for H_S and T_p, occurences given in percentage of total number of occurrences for 15°. The values for H_S and T_p denotes the highest value for each bin.

Hs\Tp	1	2	3	4	5	6	7	8	9	10	11	12	13	14	15	16	17	TOT
0-0-5	0.948	-	4.438	3.968	0.118	0.021	0.003	-	-	-	-	-	-	-	-	-	-	9.497
0.5-1.0	-	-	0.084	3.255	4.969	1.382	0.025	0.004	0.003	0.001	-	-	-	-	-	-	-	9.722
1.0-1.5	-	-	-	0.019	1.737	4.699	1.395	0.010	0.003	0.001	0.001	0.001	-	-	-	-	-	7.866
1.5-2.0	-	-	-	-	0.049	2.132	3.314	0.365	0.042	0.004	-	-	-	-	-	-	-	5.906
2.0-2.5	-	-	-	-	-	0.216	3.139	0.754	0.290	0.065	0.003	0.001	-	-	-	-	-	4.466
2.5-3.0	-	-	-	-	-	0.003	1.483	1.039	0.385	0.166	0.039	0.001	0.001	-	-	-	-	3.115
3.0-3.5	-	-	-	-	-	-	0.236	1.009	0.558	0.191	0.116	0.015	0.001	-	-	-	-	2.124
3.5-4.0	-	-	-	-	-	-	0.010	0.372	0.556	0.247	0.118	0.045	0.003	-	-	-	-	1.351
4.0-4.5	-	-	-	-	-	-	-	0.041	0.336	0.253	0.117	0.065	0.013	-	-	-	-	0.825
4.5-5.0	-	-	-	-	-	-	-	0.002	0.082	0.164	0.116	0.058	0.022	0.001	-	-	-	0.445
5.0-5.5	-	-	-	-	-	-	-	-	0.012	0.084	0.056	0.047	0.028	0.004	-	-	-	0.232
5.5-6.0	-	-	-	-	-	-	-	-	-	0.021	0.033	0.022	0.031	0.008	0.001	-	-	0.114
6.0-6.5	-	-	-	-	-	-	-	-	-	0.003	0.016	0.009	0.015	0.006	0.002	-	-	0.051
6.5-7.0	-	-	-	-	-	-	-	-	-	0.001	0.005	0.009	0.008	0.007	0.001	-	-	0.030
7.0-7.5	-	-	-	-	-	-	-	-	-	-	0.004	0.003	0.003	0.004	0.002	-	-	0.015
7.5-8.0	-	-	-	-	-	-	-	-	-	-	-	0.003	0.001	0.003	0.002	-	-	0.008
8.0-8.5	-	-	-	-	-	-	-	-	-	-	-	0.001	-	-	0.001	-	-	0.002
8.5-9.0	-	-	-	-	-	-	-	-	-	-	-	-	-	-	0.001	-	-	0.001
9.0-9.5	-	-	-	-	-	-	-	-	-	-	-	-	-	-	-	-	-	0
9.5-10.0	-	-	-	-	-	-	-	-	-	-	-	-	-	-	-	-	-	0
TOT	0.948	0	4.523	7.242	6.873	8.453	9.605	3.595	2.267	1.200	0.622	0.279	0.125	0.032	0.010	0	0.001	45.773

Table A.20: Scatter diagram for H_S and T_p, occurences given in percentage of total number of occurrences for 30°. The values for H_S and T_p denotes the highest value for each bin.

Hs\Tp	1	2	3	4	5	6	7	8	9	10	11	12	13	14	15	16	17	TOT
0-0-5	0.900	-	2.205	1.108	0.035	0.015	0.003	-	-	-	0.001	-	-	-	-	-	-	4.267
0.5-1.0	-	-	0.051	1.080	1.067	0.134	0.005	0.002	0.001	0.001	-	-	-	-	-	-	-	2.340
1.0-1.5	-	-	-	0.011	0.592	1.126	0.145	0.006	0.003	0.001	-	-	-	-	-	-	-	1.883
1.5-2.0	-	-	-	-	0.016	0.594	0.903	0.025	0.007	0.002	0.001	-	-	-	-	-	-	1.548
2.0-2.5	-	-	-	-	-	0.048	0.843	0.250	0.038	0.009	0.001	0.001	-	0.001	-	-	-	1.190
2.5-3.0	-	-	-	-	-	0.001	0.355	0.430	0.158	0.030	0.006	0.000	-	-	-	-	-	0.981
3.0-3.5	-	-	-	-	-	-	0.040	0.294	0.225	0.089	0.013	0.003	0.001	-	-	-	-	0.664
3.5-4.0	-	-	-	-	-	-	0.002	0.068	0.221	0.109	0.034	0.003	0.001	-	-	-	-	0.438
4.0-4.5	-	-	-	-	-	-	-	0.006	0.096	0.106	0.048	0.015	0.003	-	-	-	-	0.274
4.5-5.0	-	-	-	-	-	-	-	0.001	0.018	0.080	0.049	0.023	0.005	-	-	-	-	0.176
5.0-5.5	-	-	-	-	-	-	-	-	0.001	0.028	0.040	0.017	0.012	-	-	-	-	0.099
5.5-6.0	-	-	-	-	-	-	-	-	-	0.005	0.022	0.009	0.010	0.001	0.001	-	-	0.047
6.0-6.5	-	-	-	-	-	-	-	-	-	0.001	0.004	0.011	0.003	0.003	0.001	-	-	0.021
6.5-7.0	-	-	-	-	-	-	-	-	-	-	0.003	0.001	0.006	0.002	-	-	-	0.012
7.0-7.5	-	-	-	-	-	-	-	-	-	-	0.001	0.001	0.003	0.003	0.001	-	-	0.008
7.5-8.0	-	-	-	-	-	-	-	-	-	-	-	-	0.001	0.001	0.001	-	-	0.003
8.0-8.5	-	-	-	-	-	-	-	-	-	-	-	-	-	-	-	-	-	0.000
8.5-9.0	-	-	-	-	-	-	-	-	-	-	-	-	-	-	-	-	-	0.000
9.0-9.5	-	-	-	-	-	-	-	-	-	-	-	-	-	-	-	-	-	0.000
9.5-10.0	-	-	-	-	-	-	-	-	-	-	-	-	-	-	-	-	0.001	0.001
TOT	0.900	0.000	2.256	2.199	1.710	1.917	2.297	1.081	0.768	0.460	0.222	0.084	0.042	0.009	0.003	0.000	0.001	13.950

Table A.21: Scatter diagram for H_S and T_p, occurences given in percentage of total number of occurrences for 45°. The values for H_S and T_p denotes the highest value for each bin.

Hs\Tp	1	2	3	4	5	6	7	8	9	10	11	12	13	14	15	16	17	TOT
0-0-5	0.891	-	0.716	0.195	0.012	0.003	-	-	-	-	-	-	-	-	-	-	-	1.818
0.5-1.0	-	-	0.023	0.125	0.058	0.012	0.003	0.001	0.001	0.001	-	-	-	-	-	-	-	0.223
1.0-1.5	-	-	-	0.003	0.046	0.054	0.009	-	-	-	0.001	-	-	-	-	-	-	0.112
1.5-2.0	-	-	-	-	0.004	0.041	0.040	-	0.001	-	-	-	-	-	-	-	-	0.086
2.0-2.5	-	-	-	-	-	0.002	0.045	0.009	-	-	-	0.001	-	-	-	-	-	0.057
2.5-3.0	-	-	-	-	-	-	0.009	0.022	0.005	-	-	-	-	-	-	-	-	0.035
3.0-3.5	-	-	-	-	-	0.001	-	0.002	0.017	0.001	0.001	0.001	-	-	-	-	-	0.022
3.5-4.0	-	-	-	-	-	-	0.001	0.001	0.004	0.005	0.001	-	-	-	-	-	-	0.011
4.0-4.5	-	-	-	-	-	-	-	-	0.001	0.005	0.001	-	-	-	-	-	-	0.008
4.5-5.0	-	-	-	-	-	-	-	-	-	0.003	0.005	0.001	-	-	-	-	-	0.008
5.0-5.5	-	-	-	-	-	-	-	-	-	-	0.001	0.001	-	-	-	-	-	0.002
5.5-6.0	-	-	-	-	-	-	-	-	-	-	0.001	-	-	-	-	-	-	0.001
6.0-6.5	-	-	-	-	-	-	-	-	-	-	0.001	-	0.001	-	-	-	-	0.001
6.5-7.0	-	-	-	-	-	-	-	-	-	-	-	-	-	-	-	-	-	0
7.0-7.5	-	-	-	-	-	-	-	-	-	-	-	-	-	-	-	-	-	0
7.5-8.0	-	-	-	-	-	-	-	-	-	-	-	-	-	-	-	-	-	0
8.0-8.5	-	-	-	-	-	-	-	-	-	-	-	-	-	-	-	-	-	0
8.5-9.0	-	-	-	-	-	-	-	-	-	-	-	-	-	-	-	-	-	0
9.0-9.5	-	-	-	-	-	-	-	-	-	-	-	-	-	-	-	-	-	0
9.5-10.0	-	-	-	-	-	-	-	-	-	-	-	-	-	-	-	-	-	0
TOT	0.891	0	0.739	0.323	0.120	0.114	0.107	0.035	0.028	0.014	0.012	0.003	0.001	0	0	0	0	2.386

Table A.22: Scatter diagram for H_S and T_p, occurences given in percentage of total number of occurrences for 60°. The values for H_S and T_p denotes the highest value for each bin.

Hs\Tp	1	2	3	4	5	6	7	8	9	10	11	12	13	14	15	16	17	TOT
0-0-5	0.889	-	0.128	0.012	0.001	-	-	-	-	-	-	-	-	-	-	-	-	1.030
0.5-1.0	-	-	0.006	0.004	0.001	0.001	-	-	-	-	-	-	-	-	-	-	-	0.012
1.0-1.5	-	-	-	-	0.001	0.001	-	-	-	0.001	-	-	-	-	-	-	-	0.003
1.5-2.0	-	-	-	-	-	0.003	0.002	-	-	-	-	-	-	-	-	-	-	0.005
2.0-2.5	-	-	-	-	-	-	0.001	-	-	-	-	-	-	-	-	-	-	0.001
2.5-3.0	-	-	-	-	-	-	-	-	-	-	-	-	-	-	-	-	-	0
3.0-3.5	-	-	-	-	-	-	-	-	-	-	-	-	-	-	-	-	-	0
3.5-4.0	-	-	-	-	-	-	-	-	-	-	-	-	-	-	-	-	-	0
4.0-4.5	-	-	-	-	-	-	-	-	-	-	-	-	-	-	-	-	-	0
4.5-5.0	-	-	-	-	-	-	-	-	-	-	-	-	-	-	-	-	-	0
5.0-5.5	-	-	-	-	-	-	-	-	-	-	-	-	-	-	-	-	-	0
5.5-6.0	-	-	-	-	-	-	-	-	-	-	-	-	-	-	-	-	-	0
6.0-6.5	-	-	-	-	-	-	-	-	-	-	-	-	-	-	-	-	-	0
6.5-7.0	-	-	-	-	-	-	-	-	-	-	-	-	-	-	-	-	-	0
7.0-7.5	-	-	-	-	-	-	-	-	-	-	-	-	-	-	-	-	-	0
7.5-8.0	-	-	-	-	-	-	-	-	-	-	-	-	-	-	-	-	-	0
8.0-8.5	-	-	-	-	-	-	-	-	-	-	-	-	-	-	-	-	-	0
8.5-9.0	-	-	-	-	-	-	-	-	-	-	-	-	-	-	-	-	-	0
9.0-9.5	-	-	-	-	-	-	-	-	-	-	-	-	-	-	-	-	-	0
9.5-10.0	-	-	-	-	-	-	-	-	-	-	-	-	-	-	-	-	-	0
TOT	0.889	0	0.134	0.016	0.003	0.005	0.003	0	0	0.001	0	0	0	0	0	0	0	1.051

Table A.23: Scatter diagram for H_S and T_p, occurences given in percentage of total number of occurrences for 75°. The values for H_S and T_p denotes the highest value for each bin.

Hs\Tp	1	2	3	4	5	6	7	8	9	10	11	12	13	14	15	16	17	TOT
0-0-5	0.820	-	0.004	-	-	-	-	-	-	-	-	-	-	-	-	-	-	0.824
0.5-1.0	-	-	-	-	0.001	-	-	-	-	-	-	-	-	-	-	-	-	0.001
1.0-1.5	-	-	-	-	-	-	-	-	-	-	-	-	-	-	-	-	-	0
1.5-2.0	-	-	-	-	-	-	-	-	-	-	-	-	-	-	-	-	-	0
2.0-2.5	-	-	-	-	-	-	-	-	-	-	-	-	-	-	-	-	-	0
2.5-3.0	-	-	-	-	-	-	-	-	-	-	-	-	-	-	-	-	-	0
3.0-3.5	-	-	-	-	-	-	-	-	-	-	-	-	-	-	-	-	-	0
3.5-4.0	-	-	-	-	-	-	-	-	-	-	-	-	-	-	-	-	-	0
4.0-4.5	-	-	-	-	-	-	-	-	-	-	-	-	-	-	-	-	-	0
4.5-5.0	-	-	-	-	-	-	-	-	-	-	-	-	-	-	-	-	-	0
5.0-5.5	-	-	-	-	-	-	-	-	-	-	-	-	-	-	-	-	-	0
5.5-6.0	-	-	-	-	-	-	-	-	-	-	-	-	-	-	-	-	-	0
6.0-6.5	-	-	-	-	-	-	-	-	-	-	-	-	-	-	-	-	-	0
6.5-7.0	-	-	-	-	-	-	-	-	-	-	-	-	-	-	-	-	-	0
7.0-7.5	-	-	-	-	-	-	-	-	-	-	-	-	-	-	-	-	-	0
7.5-8.0	-	-	-	-	-	-	-	-	-	-	-	-	-	-	-	-	-	0
8.0-8.5	-	-	-	-	-	-	-	-	-	-	-	-	-	-	-	-	-	0
8.5-9.0	-	-	-	-	-	-	-	-	-	-	-	-	-	-	-	-	-	0
9.0-9.5	-	-	-	-	-	-	-	-	-	-	-	-	-	-	-	-	-	0
9.5-10.0	-	-	-	-	-	-	-	-	-	-	-	-	-	-	-	-	-	0
TOT	0.820	0	0.004	0	0.001	0	0	0	0	0	0	0	0	0	0	0	0	0.825

Table A.24: Scatter diagram for H_S and T_p, occurences given in percentage of total number of occurrences for 90°. The values for H_S and T_p denotes the highest value for each bin.

Hs\Tp	1	2	3	4	5	6	7	8	9	10	11	12	13	14	15	16	17	TOT
0.5	0.846	-	-	-	-	-	-	-	-	-	-	-	-	-	-	-	-	0.846
1.0	-	-	-	-	-	-	-	-	-	-	-	-	-	-	-	-	-	0
1.5	-	-	-	-	-	-	-	-	-	-	-	-	-	-	-	-	-	0
2.0	-	-	-	-	-	-	-	-	-	-	-	-	-	-	-	-	-	0
2.5	-	-	-	-	-	-	-	-	-	-	-	-	-	-	-	-	-	0
3.0	-	-	-	-	-	-	-	-	-	-	-	-	-	-	-	-	-	0
3.5	-	-	-	-	-	-	-	-	-	-	-	-	-	-	-	-	-	0
4.0	-	-	-	-	-	-	-	-	-	-	-	-	-	-	-	-	-	0
4.5	-	-	-	-	-	-	-	-	-	-	-	-	-	-	-	-	-	0
5.0	-	-	-	-	-	-	-	-	-	-	-	-	-	-	-	-	-	0
5.5	-	-	-	-	-	-	-	-	-	-	-	-	-	-	-	-	-	0
6.0	-	-	-	-	-	-	-	-	-	-	-	-	-	-	-	-	-	0
6.5	-	-	-	-	-	-	-	-	-	-	-	-	-	-	-	-	-	0
7.0	-	-	-	-	-	-	-	-	-	-	-	-	-	-	-	-	-	0
7.5	-	-	-	-	-	-	-	-	-	-	-	-	-	-	-	-	-	0
8.0	-	-	-	-	-	-	-	-	-	-	-	-	-	-	-	-	-	0
8.5	-	-	-	-	-	-	-	-	-	-	-	-	-	-	-	-	-	0
9.0	-	-	-	-	-	-	-	-	-	-	-	-	-	-	-	-	-	0
9.5	-	-	-	-	-	-	-	-	-	-	-	-	-	-	-	-	-	0
10.0	-	-	-	-	-	-	-	-	-	-	-	-	-	-	-	-	-	0
TOT	0.846	0	0	0	0	0	0	0	0	0	0	0	0	0	0	0	0	0.846

Appendix B

Aerodynamic damping

In order to determine the aerodynamic damping an analysis of the free vibrations in the tower top, and the decay of the amplitude for each cycle is performed. The plots in Figure B.1 to B.9 present the time series of the vibrations from 100 seconds, when the step pulse load is set to zero, to 250 seconds. The green curve respresents the unfiltered deterministic vibrations and the red curve represents the filtered vibrations.

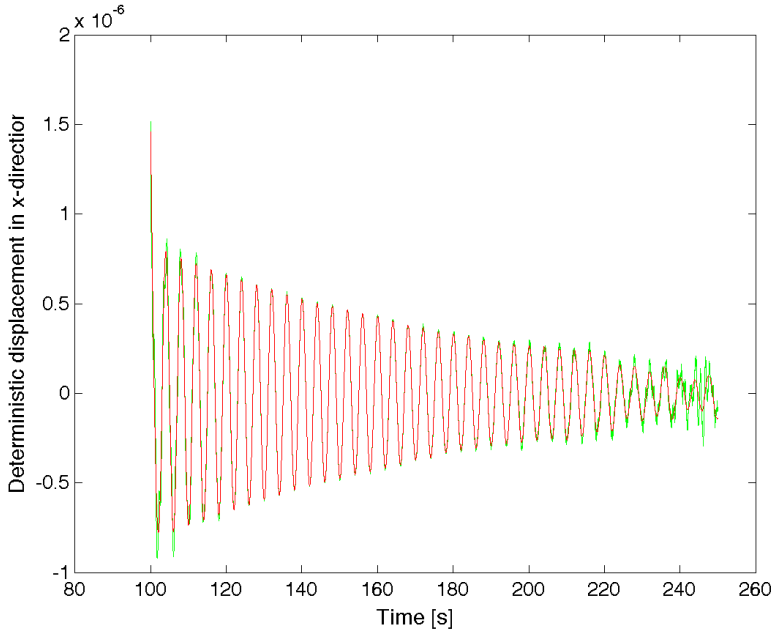

Figure B.1: Time series of the unfiltered (green curve) and filtered (red curve) deterministic part of free vibrations of the tower top in the x-direction for a mean wind speed at the hub of 2.7 m/s.

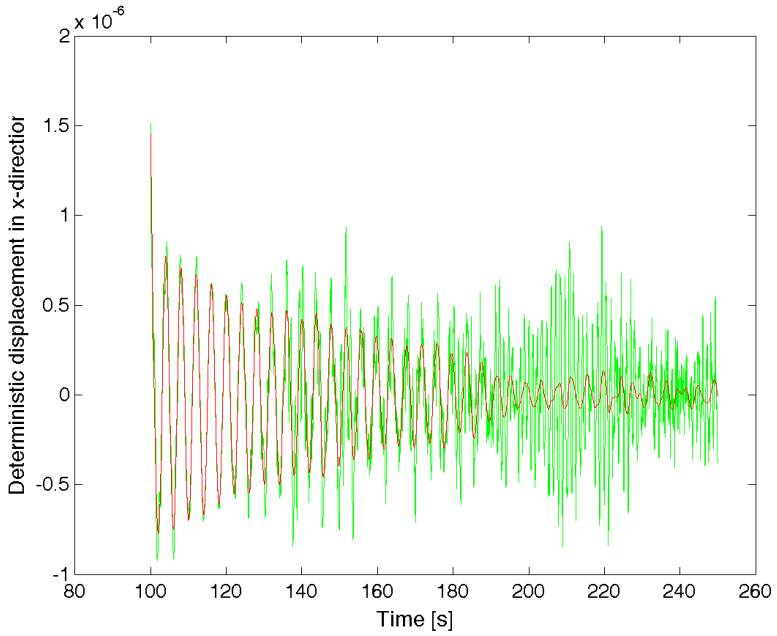

Figure B.2: Time series of the unfiltered (green curve) and filtered (red curve) deterministic part of free vibrations of the tower top in the x-direction for a mean wind speed at the hub of 5.5 m/s.

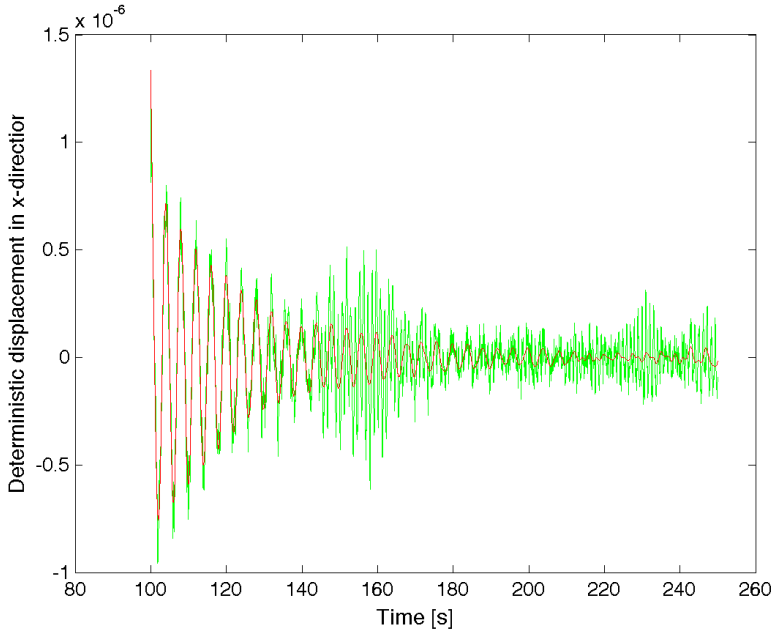

Figure B.3: Time series of the unfiltered (green curve) and filtered (red curve) deterministic part of free vibrations of the tower top in the x-direction for a mean wind speed at the hub of 8.3 m/s.

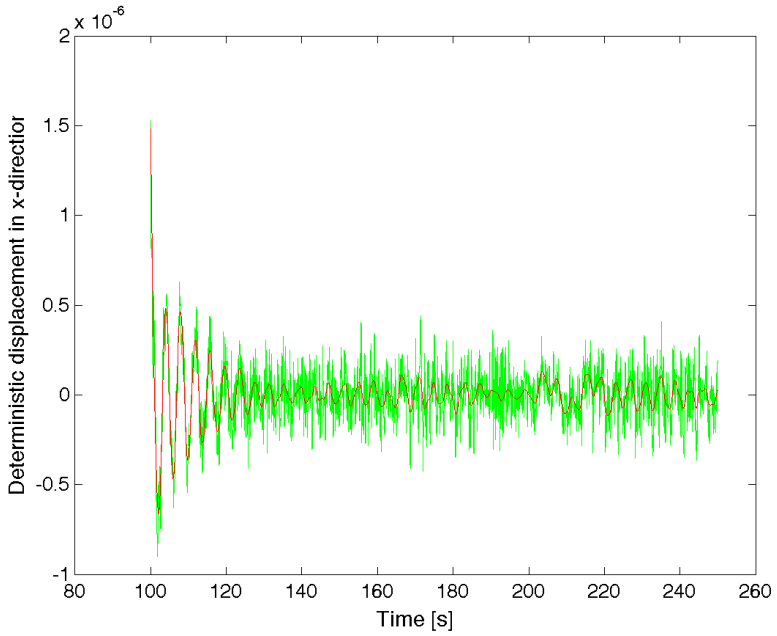

Figure B.4: Time series of the unfiltered (green curve) and filtered (red curve) deterministic part of free vibrations of the tower top in the x-direction for a mean wind speed at the hub of 11.1 m/s.

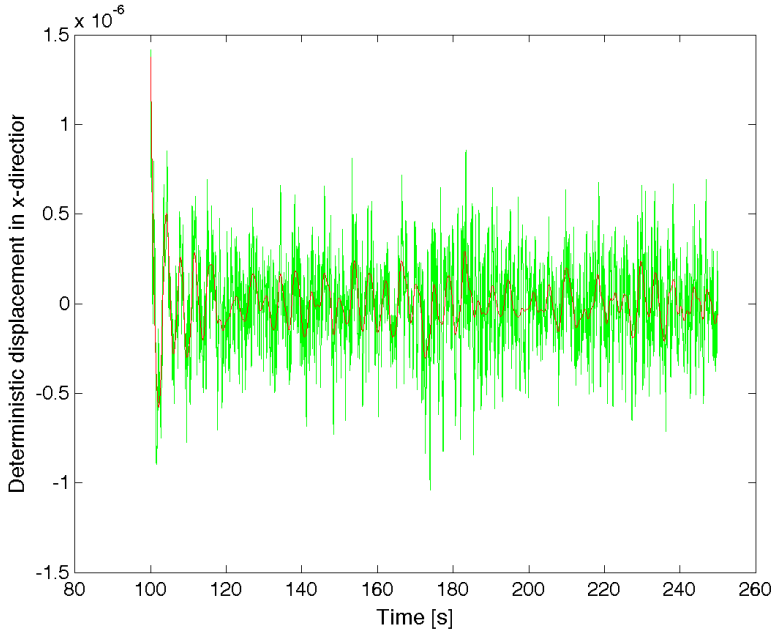

Figure B.5: Time series of the unfiltered (green curve) and filtered (red curve) deterministic part of free vibrations of the tower top in the x-direction for a mean wind speed at the hub of 13.9 m/s.

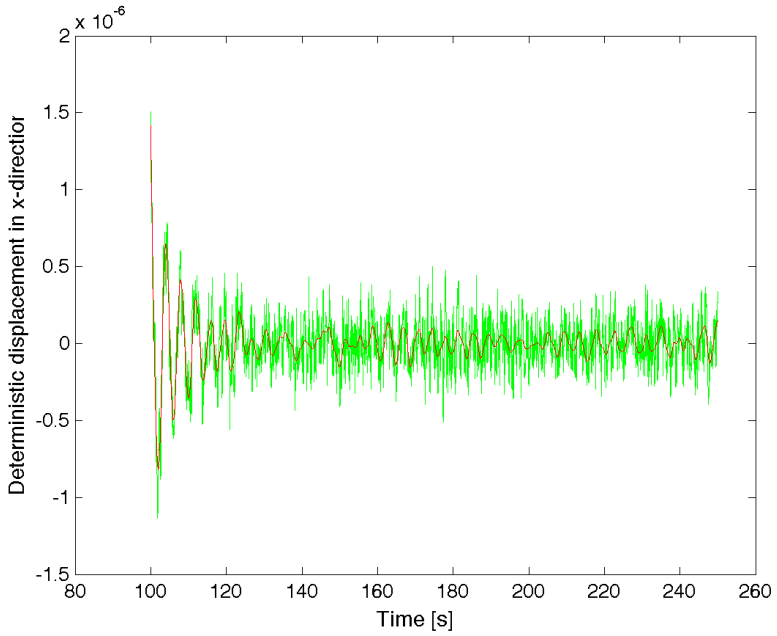

Figure B.6: Time series of the unfiltered (green curve) and filtered (red curve) deterministic part of free vibrations of the tower top in the x-direction for a mean wind speed at the hub of 16.7 m/s.

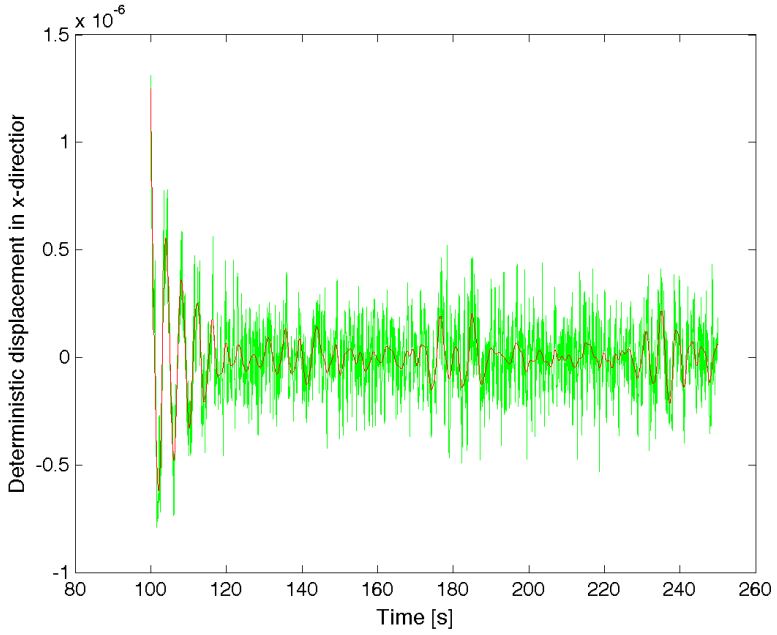

Figure B.7: Time series of the unfiltered (green curve) and filtered (red curve) deterministic part of free vibrations of the tower top in the x-direction for a mean wind speed at the hub of 19.5 m/s.

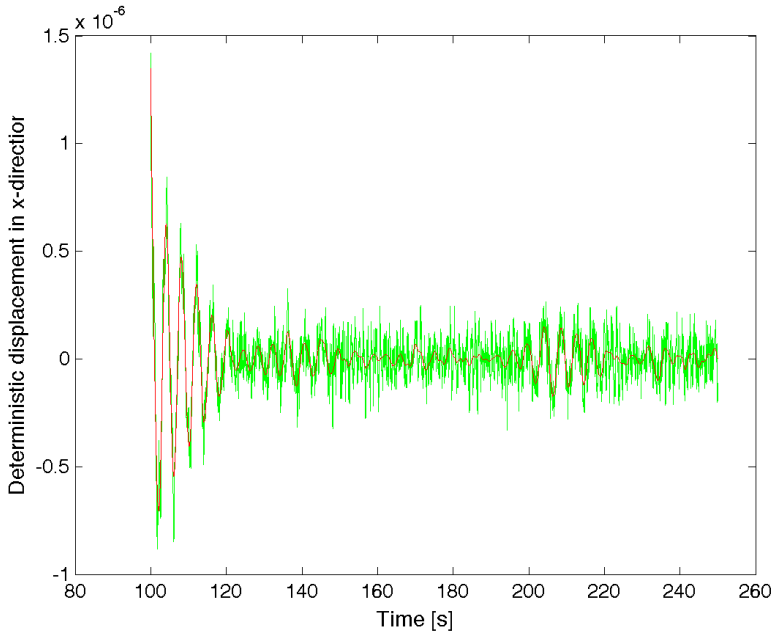

Figure B.8: Time series of the unfiltered (green curve) and filtered (red curve) deterministic part of free vibrations of the tower top in the x-direction for a mean wind speed at the hub of 22.3 m/s.

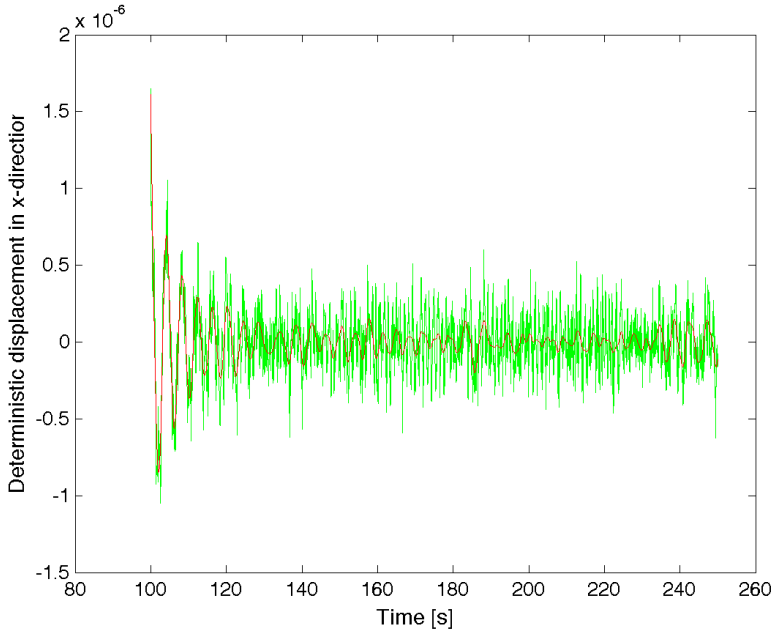

Figure B.9: Time series of the unfiltered (green curve) and filtered (red curve) deterministic part of free vibrations of the tower top in the x-direction for a mean wind speed at the hub of 25.1 m/s.